Development of a Novel Fibre-Reinforced Polymer (FRP) Wall Panel System for Thermally Efficient Residential Construction in New Zealand

Thesis for Master of Engineering with Endorsement in Civil Engineering

The University of Waikato

CHONG FENG

2025

Abstract

This thesis investigates the viability of a novel Fibre Reinforced Polymer (FRP) wall panel system as an alternative to conventional lightweight timber-framed construction for residential buildings in New Zealand. This study is motivated by the widening gap between the thermal performance assumed at the building consent stage and the significantly lower as-built performance delivered by traditional timber-framed envelopes. Despite the existing insulation requirements under the New Zealand Building Code, timber-framed walls routinely fail to meet the minimum thermal thresholds because of systemic thermal bridging, discontinuous insulation, and high framing percentages arising from structural, weathertightness, and regulatory constraints. These factors collectively undermine compliance with Clauses H1 (Energy Efficiency) and E3 (Internal Moisture), indicating the need for alternative construction systems capable of delivering verifiable thermal performance.

The FRP wall panel system evaluated in this study was first implemented in two full-scale duplex dwellings (the case-study building) completed in Hamilton in 2024, providing an opportunity for a comprehensive structural and thermal assessment. The system comprises factory-produced FRP composite panels with integrated phenolic foam insulation, tongue-and-groove joints, and a cavity air layer, yielding an inherently continuous thermal envelope. A multi-method research framework was employed, integrating (1) a comparative literature review, (2) NZS 4214 isothermal-planes thermal-bridging analysis, (3) laboratory thermal conductivity testing, (4) BRANZ P21 structural verification of wall and lintel specimens, and (5) in-field heat-flux and U-value monitoring undertaken in both summer and spring across two units of the case-study building.

The experimental results confirmed that the FRP wall panel system exhibited markedly reduced thermal bridging compared to timber framing. Laboratory characterisation established an FRP skin thermal conductivity of 0.248 W/m·K, enabling accurate construction-level thermal resistance (R-value) calculation. When applying NZS 4214 isothermal planes method, the FRP wall panel system achieved a conservative construction R-value of R2.84 $m^2·K/W$ representing a 70.1% improvement over a typical timber-framed wall with a 30.95% framing fraction (R1.67), and a 77.5% improvement over a 34.12% framing fraction scenario (R1.60). These findings demonstrate that the FRP wall panel system comfortably exceeds the current H1/AS1 requirement of R2.0 for external walls without relying on the thermal-mitigation strategies

required in timber framing. Structural testing further confirmed that the FRP walls and lintel configurations met or exceeded the NZBC Clause B1 performance when assessed against the AS/NZS 1170 load combinations and BRANZ P21 cyclic racking criteria.

In-field monitoring corroborated the analytical results. Continuous heat flux measurements recorded stable in-situ U-values consistent with theoretical modelling, while cavity and indoor temperatures remained resilient to outdoor fluctuations. The system effectively mitigates localised thermal bridging at corners, junctions, and lintels, where timber-framed envelopes typically experience significant insulation discontinuities. The analysis produced 12 representative U-value measurements over different diurnal periods. The individual values ranged from 0.060 to 0.387 W/m²K, while the average U-value across the study period was 0.206 W/m²K with typical indoor and outdoor temperatures of 22 °C and 17 °C, respectively. When compared with the theoretically derived U-value of 0.352 W/m²K (equivalent to R2.84 m²·K/W), the in-field results show that, on average, the measured U-value was 41% lower than the theoretical value, corresponding to an in-situ R-value of approximately R4.85 m²·K/W, which is approximately 70.8% higher than the analytical R2.84 value.

Collectively, these findings provide strong and defensible evidence that the FRP wall panel system offers a credible, high-performance alternative to conventional timber-framed construction. Through integrated structural and thermal functionality, the system addresses longstanding deficiencies associated with timber-framed envelopes, simplifies compliance pathways across Clauses H1, E2, and B1, and delivers a more thermally reliable building envelope under real New Zealand Zone 2 climatic conditions. Therefore, this study establishes the FRP wall panel system as a technically robust and practically viable construction methodology capable of supporting the delivery of warmer, drier, healthier, and more energy-efficient housing in New Zealand.

Acknowledgements

I would like to express my deepest gratitude to my primary supervisor, Dr Zhiyuan (Arthur) Fang, whose guidance, insight, and unwavering support have been instrumental throughout every stage of this research. His expertise, patience, and commitment to academic excellence have shaped the direction and quality of this thesis in immeasurable ways. I am equally grateful to Professor James Lim and Professor Mike Duke for their invaluable support, constructive feedback, and encouragement, each of which has significantly enriched the development of this work.

My sincere appreciation also extends to Mr Puviyarasann Velayudham, whose professional assistance, technical knowledge, and willingness to engage closely with the experimental procedures greatly contributed to the successful execution of the research programme. I am further indebted to Mr Peter Jefferies, Mr Louie Tong, and the entire team for their continuous support, trust, and commitment to advancing this project. Their encouragement and practical assistance have been foundational to the progress achieved.

I also wish to acknowledge Ms Kelly Zhou and KZEL Holdings Ltd for generously providing access to the case-study building, without which the in-field monitoring and applied investigations central to this research would not have been possible.

Finally, and most importantly, I extend my heartfelt thanks to my family. To my mother, my parents-in-law, my wife Lili Niu, and my three beautiful children, Tianyi Feng, Tianxiang Feng, and Tianjiao Feng. Your unconditional love, patience, and steadfast support have sustained me through every challenge and milestone of this journey. This thesis would not have been completed without your belief in me and your constant presence by my side. This achievement is as much yours as it is mine.

Table of Contents

List of figures

List of tables

Definitions

Air Gap

A narrow cavity within the wall assembly that contributes to thermal resistance by reducing conductive heat transfer. In the FRP system, typically 25–27 mm.

AS/NZS 1170

A suite of standards specifying structural design actions (dead, live, wind, earthquake loads) referenced by NZBC B1/VM1.

AS/NZS 4859.1

The standard governing the thermal performance of insulation materials, including declared thermal conductivity.

Beacon Pathway Study

A two-stage research programme (2020–2021) in partnership with BRANZ that quantified as-built thermal bridging, framing percentages, and insulation deficiencies in New Zealand homes.

BRANZ P21 Test

A cyclic racking test method used to determine bracing capacity of wall systems under earthquake and wind actions.

Cavity Batten

Vertical or horizontal timber or composite battens used to form a drained and ventilated cavity required under E2/AS1.

Clauses H1, E2, E3 (NZBC)

H1 regulates energy efficiency; E2 regulates external moisture; E3 regulates internal moisture and mould prevention.

Construction R-value (RT)

Total thermal resistance of a building element including internal and external surface resistances.

Dwangs / Nogs

Horizontal framing members between studs providing fixing support and cavity restraint—significant contributors to thermal bridging.

E2/AS1

Acceptable Solution for External Moisture, introducing mandatory drained cavities and influencing contemporary framing intensification.

Effective Emittance (ε)

A property of a surface indicating its ability to emit radiant heat; aluminium foil facings ($\varepsilon \approx 0.05$) reduce radiative transfer.

FRP (Fibre Reinforced Polymer)

A composite material of polymer resin reinforced with fibres, used in the proposed wall panel system to provide combined structural and thermal performance.

FRP Rib

Internal vertical FRP webs forming the subdivisions of each FRP panel, acting as stiffeners and localised thermal bridges.

FRP Tongue-and-Groove Joint

Interlocking panel connection ensuring insulation continuity while reducing air infiltration pathways.

H1/AS1 and H1/VM1

Thermal-performance compliance pathways for housing; amended in 2022 to increase wall, roof, and window insulation requirements.

Insulation Continuity

The degree to which thermal insulation forms an uninterrupted layer across an assembly; often disrupted in timber framing but maintained in FRP panels.

Isothermal Planes Method (NZS 4214)

The prescribed calculation method for determining construction R-values, accounting for parallel heat-flow regions and thermal bridges.

Lambda Meter

Laboratory instrument for measuring material thermal conductivity under steady-state conditions (ASTM C177).

Lintel

Structural beam spanning openings in wall framing. A major source of thermal bridging in timber structures; thermally continuous in FRP design.

NZBC (New Zealand Building Code)

Performance-based national code specifying minimum building requirements for safety, durability, energy efficiency, and moisture management.

NZS 3604

The primary standard governing the design of light timber-framed buildings without specific engineering design.

NZS 4214

The standard that defines methods for calculating the thermal resistance of building envelope components.

NZS 4218

Standard for the energy efficiency of residential buildings; defines framed-wall assumptions for thermal calculations.

Phenolic Foam

A high-performance rigid insulation used within FRP panel cavities; low thermal conductivity (~0.020 W/m·K) and low moisture absorption.

R-value

A measure of thermal resistance ($m^2 \cdot K/W$). Higher values indicate greater insulating performance.

Thermal Bridging

Heat flow bypassing insulation through high-conductivity elements such as studs, plates, nogs, lintels, or FRP ribs.

Thermal Conductivity (k-value)

A material property defining the rate of heat transfer; inversely related to R-value.

Under-stud / Trimmer Stud

Supporting studs adjacent to lintels in timber framing; contribute significantly to localised thermal bridging.

U-value

The inverse of total thermal resistance (1/R), representing overall heat-transfer rate of a building element.

Weathertightness

The ability of a building envelope to resist water ingress under NZBC Clause E2.

Glossary

A Cross-sectional area.

BU Bracing units (NZS 3604 measure of lateral resistance).

C Average residual displacement measured after the first 8 mm cycle in P21 testing (mm).

Δ Deflection at a given displacement level (e.g., 8 mm serviceability displacement in P21 testing).

ΔT Temperature difference across a building element.

ε Surface emittance (dimensionless); used for determining air-gap R-values (e.g., $\varepsilon = 0.05$ for foil facings).

EQ Earthquake action in AS/NZS 1170 load combinations.

f_x Area fraction of region *x* bounded by the isothermal planes (NZS 4214).

G Dead load in AS/NZS 1170 load combinations.

K Thermal conductivity of a material (W/m·K).

K_1 Displacement-recovery factor in BRANZ P21; assesses residual deformation after the 8 mm displacement cycle (acceptable result $K_1 \geq 0.8$).

K_2 Systems factor in BRANZ P21; accounts for structural redundancy in typical wall layouts and affects serviceability bracing capacities.

K_4 Ductility-modification factor in BRANZ P21 / TR10; derived from measured ductility μ and applied to ultimate bracing capacity.

λ Alternative notation for thermal conductivity (used in laboratory thermal-conductivity equipment).

L Thickness of a material layer (m).

M Displacement ductility factor; ratio of ultimate displacement to effective yield displacement, used to determine K_4.

P Applied lateral load (kN) in BRANZ P21 racking tests.

Q Live load in AS/NZS 1170 load combinations.

R Thermal resistance (general symbol).

R_x Thermal resistance of region *x* if considered alone (NZS 4214 isothermal planes method).

Rb Thermal resistance of the thermally bridged portion of the wall assembly.

R1, R2, R3 Thermal resistances of individual layers in the NZS 4214 construction R-value equation.

Rsi Internal surface thermal resistance (0.09 $m^2 \cdot K/W$ under NZS 4214).

Rse External surface thermal resistance (0.03 $m^2 \cdot K/W$ under NZS 4214).

RT Total construction R-value of a building element ($m^2 \cdot K/W$).

T Temperature (°C or K).

U Overall thermal transmittance ($W/m^2 \cdot K$), defined as 1/RT.

W Wind action in AS/NZS 1170 load combinations.

1 Introduction

1.1 Timber Framed Construction Dominated Residential Building Section

In New Zealand, timber framing has long been the overwhelmingly dominant construction method, accounting for approximately 90% of residential buildings between 2010 and 2019, far exceeding the uptake of steel and concrete alternatives [1]. This proportion has remained consistently high in more recent years. By 2021, it was estimated that more than 95% of residential structures in New Zealand were constructed using timber frames manufactured offsite in frame-and-truss production facilities, with representatives of the Frame and Truss Manufacturers Association indicating that the proportion may be as high as 96% [2].

Within this context, NZS 3604 serves as the primary standard for the design and construction of light timber-framed buildings that do not require specific engineering designs, offering prescriptive structural methods and details for low rise residential structures [3]. This standard is extensively utilised across the industry by builders, architects, engineers, designers, and students, acting as a fundamental reference for demonstrating code compliance with the performance-based requirements of the New Zealand Building Code (the "NZBC") during the building consent process [3, 49]. Additionally, it provides crucial guidance for building consent authorities, such as councils, when evaluating documentation and approving construction methods, and is an essential teaching resource in tertiary and trade training programs [3, 49].

The NZBC and its associated documents, along with the Building Act 2004 (the "Act"), are the primary regulatory frameworks governing building works [4]. The Act adopts a performance-based regulatory model, under which the NZBC sets out mandatory minimum standards for construction [17, 19]. All new building works must comply with the NZBC to the extent required by the Act. Regarding thermal insulation, the primary applicable clause under the building code is H1 (Energy Efficiency) [5,20]. Appropriate insulation reduces uncontrolled heat loss in winter and limits heat ingress in summer to decrease the energy required for heating and cooling [5]. Therefore, ensuring that the building envelope provides the right amount of insulation is critical not only for maintaining occupant comfort and well-being but also for supporting nationwide objectives for reduced energy consumption and improved environmental performance [5,28].

1.2 The Tension Between Building Code Compliance and Performance Excellence

The findings of research conducted by the Building Research Association of New Zealand, Inc. (BRANZ) in 2024 indicated that compliance with the NZBC is perceived as representing only a minimum standard, which fails to incentivise the sector to pursue higher levels of quality or excellence [16]. Many industry participants report that housing is generally built only to meet the minimum standards required under the NZBC [16]. Compliance with the NZBC is often treated as the endpoint rather than the baseline, particularly in the lower cost segment of the market [16]. As a result, features related to sustainability and energy efficiency are frequently omitted, considered luxuries rather than necessities [16]. The notion of "going beyond the code" has become central to the sector's discourse in recent years. Many industry stakeholders acknowledge that houses are often constructed to meet only the lowest legally permissible standards, which does little to incentivise excellence or innovation [18]. This industry mindset provides a critical backdrop for understanding contemporary challenges in thermal performance, prompting a detailed examination of thermal design compliance and the performance deficiencies commonly observed in timber-framed building envelopes.

1.3 Thermal Design Compliance and As-Built Deficiency in Timber-Framed Construction

Thermal Transmittance (U-value) and Thermal Resistance (R-value) have long been key metrics for designing low-energy and passive houses, with a primary focus on improving insulation [36]. For example, better insulation (lower U-value or higher R-value) can reduce seasonal energy consumption [37]. The 2022 amendments of H1/AS1 and H1/VM1 aim to make new housing and small buildings warmer, drier, healthier, and more energy efficient by raising the minimum insulation R-value requirements for roofs, windows, walls, and floors [15]. The required R-value for the external walls in the 2022 H1/AS1 and H1/VM is 2.0 [6,7].

However, a growing body of research indicates that achieving even the minimum H1 R-value compliance requirements for external walls in real construction practice is often difficult and, in many cases, impossible. The principal factors causing as-built R-values to diverge from their idealised design values are consistently identified as the well-known and often overlooked trio of thermal bridging, insulation gaps, and the presence of moisture [27]. One of the most comprehensive New Zealand research programmes demonstrating this gap is a two-stage study undertaken between 2020 and 2021 by Beacon Pathway ("Beacon") and BRANZ. Ryan et al. demonstrated that the design R-values recorded at the building consent stage are often not realised upon the completion of building construction [2, 20]. The research found that the nominal thermal resistance assumed for compliance is systematically eroded by real-world factors, including higher-than-assumed framing percentages, discontinuous insulation, poorly detailed junctions, and the additional thermal bridging introduced by structural elements such as lintels [2,20]. Accordingly, the problem is not simply that H1 sets only a low benchmark, but also that the light-weight timber-framed building method in New Zealand is unable to deliver even this minimum thermal performance under real-world building conditions [2,20].

Furthermore, the industry's response to the leaky-building crisis seems to have exacerbated this imbalance. In practice, designers, builders, and councils have generally prioritised compliance with E2 concerning External Moisture [42] over H1, opting for conservative detailing choices that maximize assurance of weathertightness [20]. These choices, however, often lead to an increase in framing content and exacerbate thermal bridging. While these practices reduce moisture risk, they also increase the quantity and complexity of timber framing, therefore intensifying thermal bridging. This pattern reflects a broader issue of siloed regulatory development, in which amendments to one clause proceed without fully considering their implications for the performance requirements of others.

1.4 Inherent Engineering Constraints of External Walls in Framed Structures

Heat transfer occurs through multiple elements of the building envelope, with external walls accounting for approximately 35% of total heat loss and a further 25% occurring through the roof, windows, and doors [74]. It shows, the external walls play a significant role in provide the effective thermal resistance barrier to maintain the stability of the temperate and control heat loss. Although the enhanced 2022 version of the H1 provisions of the NZBC is generally perceived as improving the thermal performance of newly constructed housing, the upgraded requirements for the external walls was only uplifted by 0.1 from R1.9 to R2.0, which still constitute only a minimum regulatory threshold rather than a benchmark for the best thermal performance [19].

Ryan et al. [2] suggested that within the confines of current standards, building code clauses, and common variations in cladding systems, wind zones, and construction requirements, simply optimising the percentage of timber framing designs in standard 90mm walls cannot sufficiently reduce thermal bridging to achieve the intended construction R-value minimums set by the NZBC. This limitation is reflected in the most recent H1/AS (Sixth Edition), which requires designers to assume a minimum wall-framing fraction of 38% unless a lower value can be rigorously justified, and stipulates that the construction R-value for walls forming part of the thermal envelope may be as low as R1.0 under the calculation or thermal modelling methods[75]. While this adjustment offers a compliance pathway for conventional timber-framed construction, it achieves this by reducing the required performance threshold within the regulatory framework solely for compliance purposes. This approach does not address the fundamental engineering issue that the actual thermal performance of external walls is compromised by the structural and weathertightness requirements inherent in the timber-framed system. The revised provisions further indicate that traditional timber-framed construction remains limited by inherent engineering constraints, specifically related to structural integrity, weathertightness, and thermal insulation capabilities.

1.5 The Need for Viable Alternative Building Solutions

This systemic performance gap also corresponds to broader concerns regarding the overall quality of New Zealand's residential construction industry. Both system leaders and industry practitioners across major housing-related disciplines argue that the current construction standards are insufficient to mitigate long-term performance risks [18]. In practice, many homes remain too cold and damp, poorly oriented to the sun, and inadequately insulated [21]. About 30% of homes in New Zealand remain poorly insulated, and approximately one-quarter of homeowners, along with nearly half of renters, continue to face persistent issues with dampness or mould [22, 23]. Each year, approximately 6,000 children are hospitalised due to housing-related illnesses, while almost 30% of households experience energy hardship [23, 24]. A 2021 survey of 2,000 New Zealand children reported that approximately 60% were living in homes with temperatures and humidity levels outside the World Health Organization's recommended range[25,26]. More than half of these children slept in bedrooms that were too cold and subsequently reported poor overall health outcomes [25, 26].

Given that New Zealand is engaged in a large-scale residential building programme that will continue for decades, it is imperative that new dwellings meet NZBC requirements for energy efficiency, thermal resistance, and moisture management, rather than perpetuating a systemic performance deficit that will impose long-term social and economic costs [20]. In this context, there is a clear need to explore innovative building methodologies and alternative construction solutions that can be empirically proven not to carry the inherent thermal limitations embedded in conventional framed systems.

1.6 Novelty, Research Aim and Hypothesis

Although the proposed FRP wall panel system represents a purpose-designed innovation intended to offer an alternative construction option for the New Zealand residential sector, its suitability cannot be assumed without rigorous evaluation. Prior to this research, the system had not been implemented in residential constructions in New Zealand. Its first full-scale application completed in 2024 with the construction of two duplex dwellings in Hamilton, Waikato. This pilot project has provided a critical opportunity to examine the system's practical integration into a real building project. The introduction of such a novel system therefore necessitates a comprehensive research programme to verify its performance across all relevant domains.

The primary aim of this research is to evaluate the viability of the novel FRP wall panel system as an alternative to conventional lightweight timber-framed construction for residential buildings in New Zealand. This evaluation focuses on determining whether the FRP wall panel system can deliver both structural and thermal performance that meets or exceeds the requirements of the NZBC, while also mitigating the inherent limitations of timber-framed construction and ensuring that thermal performance is not compromised by structural or weathertightness requirements. Through a combination of theoretical calculations, structural verification, and in-field performance monitoring, the study seeks to establish whether the FRP wall panel system can provide a genuinely unified and synergistic performance by combining structural capacity, insulation continuity, and weathertightness within a single integrated envelope system for the New Zealand residential building sector.

It is hypothesised that the FRP wall panel system will demonstrate superior thermal efficiency and comparable or enhanced structural performance relative to conventional timber-framed construction. Specifically, it is proposed that:

- Thermal Hypothesis**:** The integrated insulation continuity and reduced thermal-bridging pathways within the FRP wall panel system will result in higher construction R-values and more stable in-situ thermal performance, therefore lowering the discrepancy between designed and as-built thermal outcomes commonly observed in timber-framed buildings.

- Structural Hypothesis**:** The dual-function FRP wall panel system including the lintel configuration will provide sufficient bracing capacity and load-carrying performance to satisfy the structural requirements of NZBC Clause B1 and the AS/NZS 1170 suite of structural actions.

- System-Level Hypothesis: By integrating structural and thermal functionality within a single componentised system, the FRP wall panel system will offer a synergistic dual-performance advantage, simplifying compliance pathways, reducing the need for additional thermal-bridging mitigation measures.

Collectively, these hypotheses posit that the FRP wall panel system represents a credible and potentially superior alternative to conventional timber-framed construction for achieving high-performance, energy-efficient residential buildings in New Zealand.

2 Development of an Innovative Fibre Reinforced Polymer (FRP) Wall Panel System as a Pathway to Thermally Efficient Housing

2.1 The First FRP Wall Panel System Building Project in New Zealand

Fibre reinforced polymer (FRP) composites have been widely adopted for structural applications internationally. Beyond their mechanical performance, several studies highlight the thermal advantages of FRP systems, including reduced thermal bridging, enhanced moisture resistance, and improved suitability for damp-prone environments [29-31]. Research also indicates that FRP assemblies demonstrate adaptive energy behaviour across seasonal and regional climate variations, supporting their applicability in areas with fluctuating temperatures [29, 31,32,33]. In the United States, experimental evaluation of FRP sandwich panel building envelopes, comprising pultruded fibreglass skins with tongue and groove joints surrounding a foam core, demonstrated reduced air infiltration and diminished heat loss at interface locations, achieving thermal resistances of approximately R2.0 for a 75 mm panel. [29]. These panels were reported to outperform several conventional envelope systems commonly used in the United States [29]. However, the findings were limited to laboratory testing of panel specimens rather than in-situ evaluation of completed buildings, and therefore do not fully reflect real-world conditions.

Marston's 2007 study [30] similarly identified the potential of FRP for New Zealand's residential construction sector, highlighting the substantial opportunities for innovation within the local building industry. However, due to the variability in FRP material types, which arises from differences in reinforcement composition, fibre arrangement, polymer matrices, and manufacturing processes, the preparation of succinct codes and standards is going to be more difficult than it has been for conventional materials [30].

2.2 The Proposed FRP Wall Panel System Evaluated

The FRP wall panel incorporated in the building system evaluated in this thesis is an internationally manufactured product utilising globally patented composite technology. A range of material testing was undertaken on the FRP wall panels to verify their suitability for residential building applications and to characterise the material properties relevant to long-term performance [34]. Comparative durability testing under 500-hour condensation-cycle conditions showed that timber absorbed 88–91% moisture, indicating a high risk of biological decay, while uncoated steel exhibited pronounced corrosion [34]. In contrast, the FRP panels demonstrated substantially greater hygrothermal stability, with minimal water absorption (0.37% mass gain) and no condensation-related risks [34]. Further durability assessment using a 1000-hour neutral salt-spray test revealed no observable physical deterioration, and three-point bending tests conducted on field-aged specimens exposed for 16 months recorded only a modest mechanical reduction of 5–9% [34]. Collectively, these results affirm the FRP panels' robust resistance to moisture ingress and environmental degradation, supporting their applicability and reliability in New Zealand residential construction.

The FRP wall panel system comprises two primary components: the standard 450 mm × 100 mm FRP wall panels and the 150 mm × 120 mm FRP corner panels. The dimensions and configurations of these elements are illustrated in Figures 1 and 2.

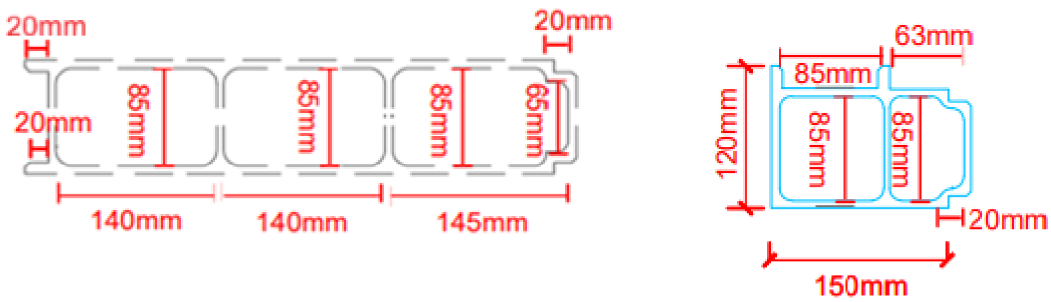

(a) FRP wall panel (b) FRP corner panel

Figure 1-Dimensions of the FRP panels

During the last 8 year of research and development of the particular type of FRP wall panel system, a comprehensive suite of experimental tests has verified that the FRP wall panel system meets the key performance requirements of the current regulatory framework, including the NZBC and NZS 3604. These assessments confirm compliance across critical domains such as structural capacity, seismic performance, air-infiltration control, and durability. The system incorporates a tongue-and-groove jointing mechanism and is capped with capped with light-gauge galvanised U-channels (approximately 101 mm × 90 mm × 1.2 mm) at both the top and bottom, providing enhanced structural continuity and stability (Figure 1-2).

The system has since been implemented in practice, with construction of two duplex dwellings in Hamilton commencing in 2023 and reaching completion in 2024 (Figure 3-4).

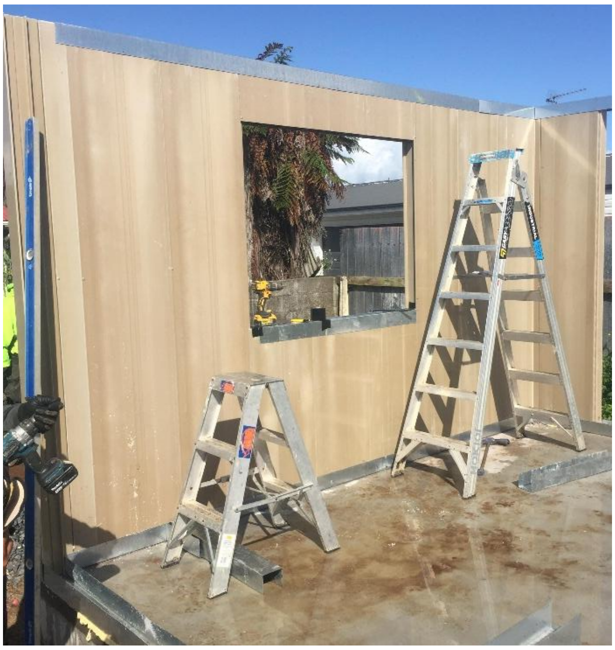

a) FRP panel walls (internal view) b) FRP panel walls (corner view)

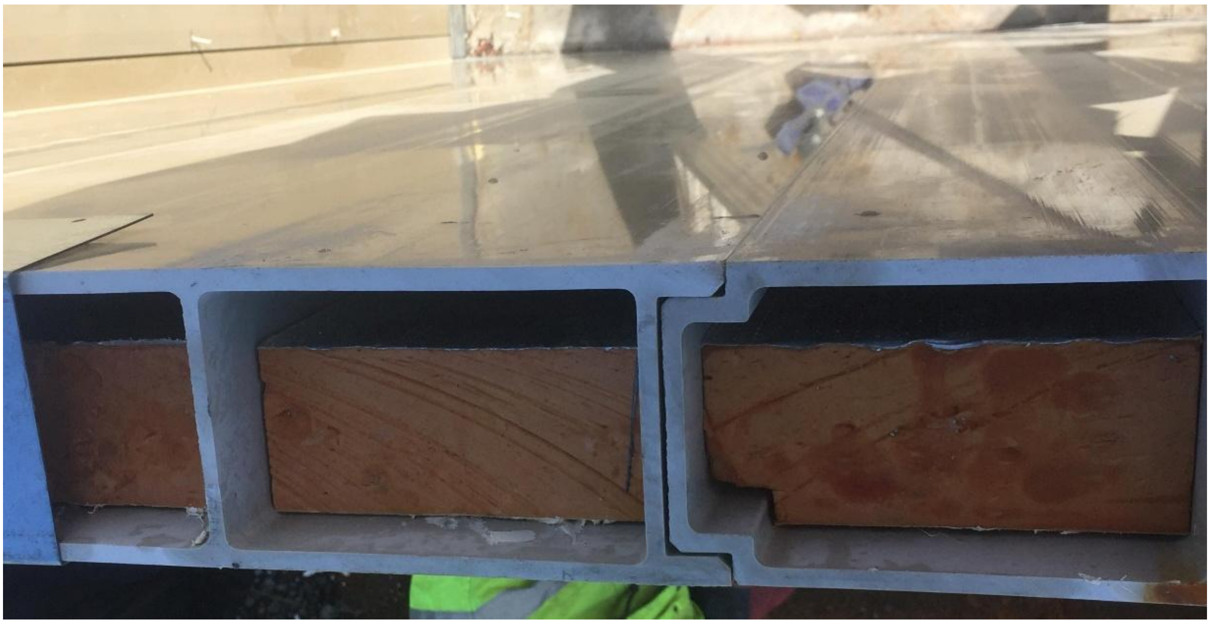

c) FRP wall panel system (top view) showing the tongue-and-groove joints.

Figure 2- FRP Wall panel system installation details

2.3 Two Duplex Dwelling House in Hamilton

The two duplex dwellings obtained full Code Compliance Certificate from Hamilton City Council upon completion, establishing the first verified track record of the FRP wall panel system as a fully compliant building solution within the New Zealand construction industry.

Figure 3-The completed duplexes built with FRP wall panel system (front view)

Figure 4-The completed duplexes built with FRP wall panel system (back view)

2.4 The Initial Infield Investigation to the Thermal Performance of Building System

The initial field-based performance evaluation of these duplexes was conducted between 2023 and 2024, beginning at the construction stage and continuing through to completion. This evaluation aimed to assess the thermal behaviour of the FRP wall panel system, which incorporates cavity insulation and an air gap, under peak summer conditions [34]. The study analysed outdoor climate effects, indoor temperatures, airflow characteristics, heat-transfer dynamics, and energy behaviour of the investigated building. The study evaluates the suitability of the FRP enclosure system for New Zealand Climate Zone 2 through both experimental monitoring and Integrated Environmental Solutions: Virtual Environment (IES-VE) simulation. The findings offer the first empirical, real-world evidence supporting the FRP wall panel system's potential as a climate-resilient, energy-efficient alternative for residential building in New Zealand [34].

2.5 Key Finding of the Field-based Thermal Performance Study

Field measurements indicate that, despite the absence of mechanical cooling systems, the indoor temperatures of the tested units remained within the World Health Organisation's recommended comfort range of 18–24 °C for 67.6% of the observation period [34]. This represents an approximate 10% improvement over older timber-framed houses, where indoor temperatures commonly exceed the 24 °C threshold 57% of the time during summer [34,73]. The enhanced performance of the FRP wall panel system is primarily attributed to its hybrid thermal configuration, which combines a phenolic foam-insulated cavity with a 26 mm air gap, collectively acting as a dynamic thermal buffer [34]. Cavity temperatures were consistently maintained between 17–22 °C, substantially moderating the influence of outdoor temperatures, which ranged from 5.8–32.9 °C during the monitoring period.

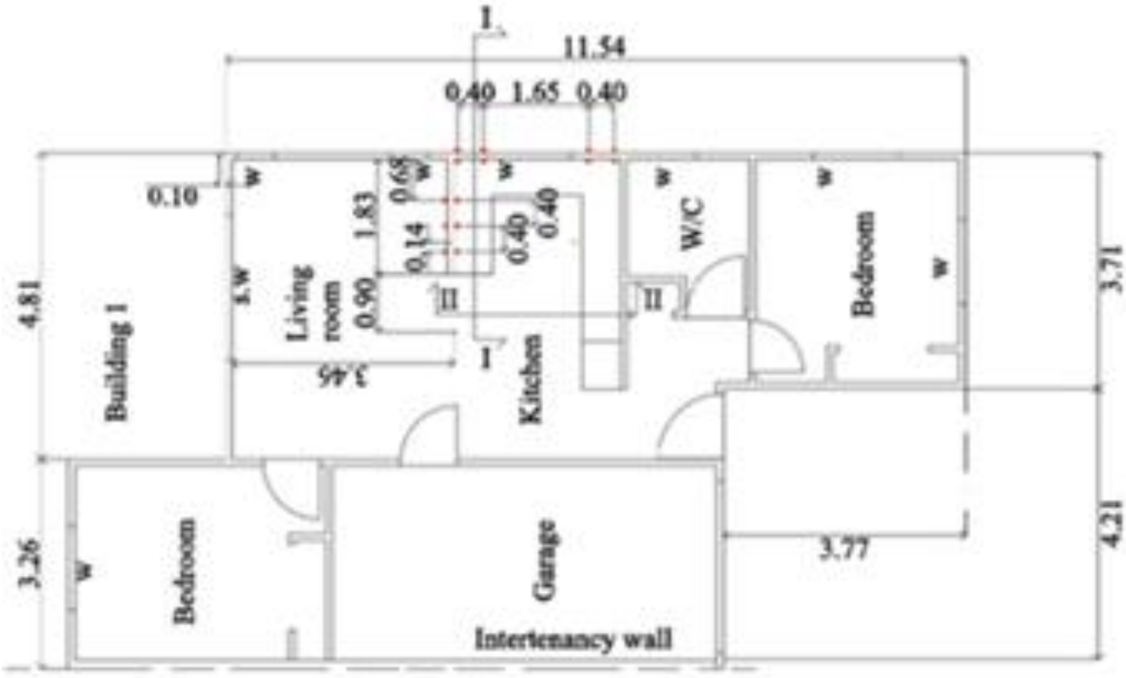

Figure 5- Floor plan of the evaluated unit within the investigated building [34]

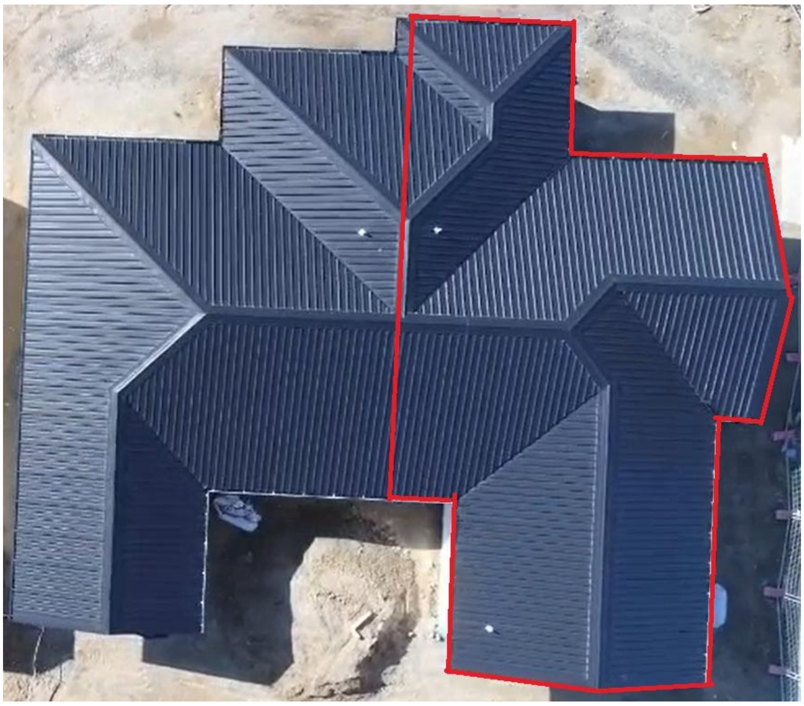

Figure 6-Aerial view of the investigated building with the red outlined the tested unit

Heat transfer calculations for February, the peak summer month, indicated modest heat gains (maximum 3.86 W/m²) and heat losses (maximum 1.01 W/m²), therefore demonstrating the system's capacity to mitigate extreme internal fluctuations [34]. Importantly, the wall assembly exhibited a recoverable heat-storage effect, gradually releasing accumulated heat during cooler periods, which further contributed to the stabilization of indoor conditions [34]. Complementary airflow monitoring (0.08–0.12 m/s) revealed that even low natural ventilation rates were adequate to maintain indoor comfort, thereby reinforcing the system's passive thermal regulation capability [34].

Heat-loss modelling further demonstrated that the investigated building exceeded the 2022 H1 (effective in 2023) [6,7] performance requirements by 4%, even under conditions of limited ventilation and the absence of mechanical climate control. Collectively, the findings highlight FRP wall panel system's potential as a climate-resilient building envelope solution that can support national goals for healthy, energy-efficient housing [34]. The FRP wall panel system incorporates an air-gap configuration that reduces thermal bridging by decoupling primary conductive pathways [34], complemented by interlocking joints that minimise air infiltration and further enhance thermal bridge resistance, as elaborated by Abdou et al. [29]. These collective features improve overall thermal efficiency by simultaneously addressing conductive heat transfer through insulation and convective heat transfer through improved airtightness.

The experimental findings indicate that the superior thermal performance of the FRP wall panel system, in comparison with conventional framed construction, arises from three interrelated mechanisms [34]. 1) The system's internal air cavity functions as a dynamic thermal buffer, moderating the transfer of external temperature variations into the indoor environment. Monitoring showed that cavity air temperatures remained within a relatively narrow range of approximately 17–22 °C, providing around 5 °C of thermal stabilisation despite wider outdoor fluctuations. 2) The integration of low thermal mass FRP components with a continuous insulation layer creates a hybrid assembly that operates both as an effective air barrier and a limited thermal storage medium. This configuration facilitates rapid thermal response while simultaneously delaying heat transmission, outperforming conventional wall systems that typically depend on either high or low thermal mass in isolation. 3) The FRP wall panel system enables passive heat redistribution, whereby heat accumulated within the cavity during warmer periods is gradually released during cooler nighttime conditions, contributing to enhanced indoor thermal stability without reliance on mechanical heating or cooling systems.

2.6 Further Infield Investigation in this Study

While the mechanisms outlined above describe the overall thermal behaviour of the FRP wall panel system, the investigation by Velayudham et al. [34] primarily assessed its global thermal performance and did not undertake a detailed examination of localised thermal bridging effects. That initial in-field monitoring was carried out in the two-bedroom unit at the rear of the duplex during the summer period from November 2023 to March 2024, with particular emphasis on the data collected between January and March 2024. Although this work demonstrated stable and superior thermal performance, it did not isolate or quantify the specific contribution of the FRP system's junction configurations to mitigating thermal bridging, nor did it evaluate how these thermal behaviours interact with or are influenced by the system's correlated structural design and weathertightness requirements. Building on this foundation, the present thesis conducts a targeted in-field assessment in the master bedroom of the three-bedroom unit in the front duplex, with heat-flux and U-value measurements undertaken during the moderate spring conditions of October to December 2024. This subsequent investigation aims to validate the theoretically calculated R-value of the FRP wall panel system and to provide a more granular evaluation of how the system's inherent configuration counteracts thermal bridging.

3 Research Methodology and Comparative Analytical Framework

3.1 Research Methodology

Given the critical role of envelope level mechanisms in enhancing thermal performance, the issue of thermal bridging constitutes an important part of the detailed analysis presented in the subsequent chapters of this thesis.

Each section of this thesis begins with a critical literature review contrasting the performance characteristics of conventional timber-framed construction with those of FRP wall panel system. This establishes the theoretical and empirical basis for the comparative evaluation and identifies gaps in current knowledge that the subsequent analyses seek to address. As established in the preceding introduction, conventional lightweight timber-framed construction, which dominates local residential building practice in New Zealand, frequently faces persistent challenges in achieving the key NZBC requirements relating to thermal resistance and indoor environmental stability. Thermal bridging and construction related variability contribute to significant discrepancies between designed and as-built performance. These deficiencies undermine compliance with key requirements relating to thermal resistance and indoor environmental stability, and collectively limit the capacity of timber-framed buildings to achieve durable, healthy, and energy-efficient outcomes under New Zealand's climatic conditions.

3.2 Comparative Analytical Framework

On this basis, the present thesis evaluates the viability and suitability of the FRP wall panel system as a thermally efficient alternative to conventional timber-framed construction, with specific regard to New Zealand's regulatory framework, design standards, climatic conditions, and residential performance requirements. To determine whether the proposed FRP system offers a credible response to the longstanding deficiencies associated with timber-framed constructions, a comparative, multi-dimensional analytical framework is implemented with reference to the front duplex dwelling of the two duplex dwellings built in Hamilton ("the case study building"). This framework integrates a critical review of existing literature, verified numerical calculation methods, experimental investigations conducted under controlled laboratory conditions, and infield environmental studies.

3.3 Thermal Bridging Analysis and Structural Verification

Central to this investigation is the analysis of thermal bridging, which is undertaken through a synthesis of published research and the verification of numerical modelling. Thermal-bridge calculations are performed using the isothermal-planes method prescribed in NZS 4214:2006 ("4214"), as cited in H1/AS1 and H1/VM1. This approach enables the quantification of conductive heat losses at framing elements and junctions, thereby allowing direct comparison between conventional timber-framed assemblies and the case-study building constructed using the FRP wall panel system. These analytical findings are further supported by structural and thermal experimental testing on representative FRP wall and lintel specimens, providing empirical evidence of the extent to which the system mitigates thermal bridging when compared with traditional timber framing.

3.4 Infield Heatflux and U-value Investigation

In addition, an infield investigation conducted the moisture behaviour of each construction system under New Zealand's high-humidity, mixed-climate conditions. The inherent susceptibility of timber framing to interstitial condensation and biological degradation is contrasted with the moisture-resistant characteristics of FRP composite skins [71]. To further evaluate the real-world thermal performance of the FRP wall panel system, an in-field heat flux assessment was undertaken on the case study building. The purpose of the testing was to determine the actual in-situ U-value and R-value of the FRP wall system under occupied environmental conditions, and to compare the measured performance with the theoretical calculations derived from the isothermal planes method under NZS 4214.

3.5 Emphasising Thermal Efficiency and Practical Viability

Collectively, these performance dimensions constitute a comprehensive and integrated evaluative framework for determining whether the FRP wall-panel system serves as a thermally efficient and practically viable alternative to traditional timber-framed housing in New Zealand. Through the combined application of literature review, numerical analysis, laboratory testing, on-site monitoring, and real-world construction experience, the thesis provides an evidence-based assessment of the FRP wall panel system's potential to enhance building envelope performance and contribute to higher quality and more thermally efficient residential construction outcomes.

4 Inherent Thermal Limitations in Conventional Framing Structure

4.1 What is Thermal Bridging in Conventional Timber Framing Constructions

Assessing the performance of constructed houses compared to their intended designs remains a persistent challenge in the construction industry [38]. Adding an insulation product with a specified R-value to a wall assembly does not typically result in an equivalent increase in the overall thermal resistance of the wall [10]. A portion of the intended thermal benefit is commonly lost due to thermal bridging, which effectively creates parallel heat-flow paths that bypass the insulation layer and reduce the realised R-value of the assembly [39]. Moreover, an excessive insulation thickness can lead to high costs for households and may increase the risk of overheating, offering only marginal benefits [10, 37, 72].

Thermal bridges are building materials or elements with comparatively high thermal conductivity, allowing heat to transfer more readily through them than through surrounding components [40]. They provide preferential pathways for heat to flow from the warmer interior of a building to the colder exterior [35, 41]. As illustrated in Figure 7, structural framing members in conventional timber-framed construction act as significant thermal bridges [39]. Functioning much like a thermal “tunnel,” these elements provide a substantially easier pathway for heat flow compared with the surrounding insulation [40]. The thermal conductivity of timber is approximately double that of most conventional insulation products and can be up to seven times higher than high-performance rigid foam insulations such as phenolic foam [35,39]. When insulation is placed between framing elements rather than externally as in continuous exterior insulation systems, the framing provides conductive pathways that allow additional heat transfer through the wall [39]. Consequently, even when nominal insulation levels appear adequate, the presence of framing-induced thermal bridges can significantly compromise the effective thermal performance of the building envelope [12]. The magnitude of this reduction depends on the proportion of the thermal bridge area relative to the total wall area. [41] Dwellings with a high proportion of thermal bridges consequently require greater purchased energy to maintain comfortable indoor temperatures for occupants. [41]

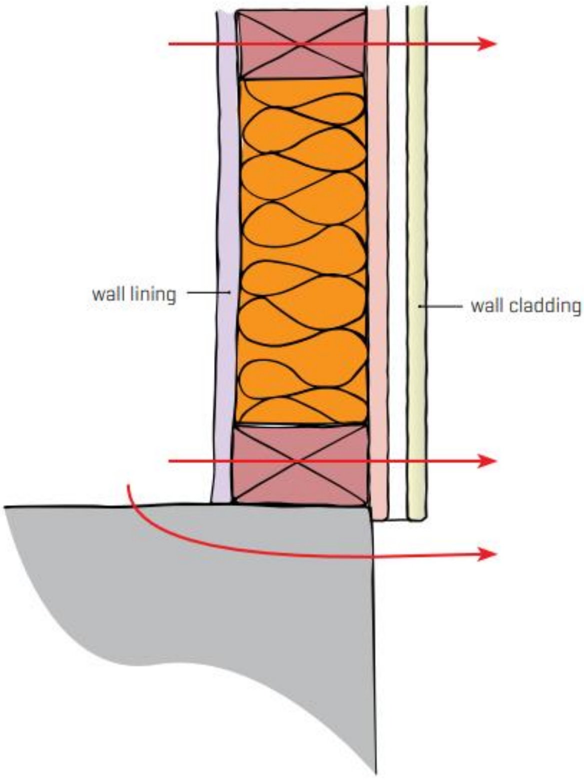

Figure 7-Typical thermal bridges through the wall and the concrete slab [41]

As the industry shifts toward constructing homes with higher thermal performance, it has become increasingly important for designers and builders to understand the nature of thermal bridges and the strategies available to mitigate their effects [41]. Although the investigation of the adverse effects of thermal bridging on housing performance is not a novel concept, emerging evidence in recent years suggests that the proportion of timber framing in external walls of new residential constructions has risen to such an extent that it compromises the requirements outlined in Clauses H1 and E3 of the NZBC [20]. In response to these concerns, Beacon and BRANZ conducted the two-stage study between 2020 and 2021 to quantify the scale of the issue more clearly. This research examined 47 residential dwellings under construction across Auckland, Hamilton, Wellington, and Christchurch, with the primary objective of determining the actual percentage of framing present in external walls of timber-framed houses and assessing whether as-built conditions now typically exceed the framing assumptions embedded in H1 and E3 calculation methods. Furthermore, the study seeks to elucidate whether high framing percentages constitute a significant and definitive issue and to identify the underlying causes of elevated framing percentages in New Zealand [20].

4.2 Stage One: Thermal Bridging Drivers and As-Built Framing Percentages

Beacon's Stage One investigation provides an evidence-based account of how contemporary regulatory settings, structural demands, and construction practices contribute to elevated thermal bridging in New Zealand's new residential buildings. The study conducted a comprehensive analysis of 47 residential structures, facilitating a systematic evaluation of the as-built framing content and the processes by which design intentions deviate from actual thermal performance outcomes in timber-framed buildings.

4.2.1 Regulatory and Technical Drivers: External Moisture, Structural Requirements

The study delineates a series of interconnected regulatory modifications, particularly those originating from Clause E2 of the NZBC and NZS 3604, which have significantly contributed to an increase in timber framing density. Following the leaky-building crisis, amendments to E2/AS1[42] introduced stringent weathertightness requirements that reshaped the geometric configuration of external walls. The compulsory implementation of drained and vented cavities has resulted in detailing practices that inherently require an increased use of timber components. For example, cavity battens typically necessitate nogging at 800 mm centres rather than the 1200 mm centres previously permitted under NZS 3604, effectively adding an extra line of nogs across standard-height walls and reducing the area available for insulation. Junction details also became more conservative: internal corners that were formerly framed with three studs are now commonly constructed with five, even for direct-fix claddings, to ensure adequate fixing and support for flashings and weatherproofing elements.

This situation is further compounded by the fact that, although H1 was amended in 2007 after the major E2/AS1 revisions, the standard framing percentage embedded in the H1 compliance pathways does not appear to have been recalibrated to reflect the substantial increase in timber content driven by Clause E2 of the NZBC and NZS 3604. As a result, the deemed-to-comply methods in H1/AS1 and E3/AS1 may no longer reliably achieve the minimum R-values they assign. At a minimum, E3/AS1 requires external walls to achieve an R-value above R1.5 [43], yet the methods used to assess compliance have not kept pace with the design and construction changes embedded in more recent amendments to other Code clauses.

Moreover, the industry's response to the leaky-building crisis appears to have contributed to this imbalance. In practice, designers, builders, and councils have generally prioritised compliance with E2 over H1, opting for conservative detailing choices that maximize assurance of weathertightness [20]. These choices, however, often lead to an increase in framing content and exacerbate thermal bridging. This type of siloed regulatory development, where amendments to one clause occur independently of the thermal performance requirements in another, has unintentionally amplified framing ratios in modern residential dwellings [20]. The combined consequence is a construction environment in which nearly all framing elements now serve legitimate functional purposes, yet the thermal assumptions embedded in the NZBC performance pathways have not been updated to reflect this evolved structural reality [14].

Moreover, the industry's response to the leaky-building crisis appears to have reinforced this regulatory imbalance. In practice, designers, builders, and territorial authorities have tended to prioritise E2 compliance over the thermal-performance obligations of H1, often adopting highly conservative detailing to ensure robust weathertightness. While these practices reduce moisture risk, they also increase the quantity and complexity of timber framing, thereby intensifying thermal bridging. This pattern reflects a broader issue of siloed regulatory development, in which amendments to one clause proceed without fully considering their implications for the performance requirements of others.

4.2.2 As-Built Framing Percentages and the Magnitude of Thermal Bridging

The primary quantitative outcome of Stage One is the significant discrepancy between the anticipated and actual framing percentages [20]. When expressed as the ratio of framing area to net wall area (excluding openings), the 47 houses exhibited an average framing percentage of just over 34%. Individual levels ranged from 24% to 57%, and some individual wall panels exceeded 70% framing, with isolated panels approaching 100% framing coverage. The majority of observed panels lay within the range of twenty to 50%, well above the fourteen to eighteen percent typically assumed in H1/AS1 calculations. The study also assessed the extent of site-added framing [20]. Approximately one-quarter of wall frame panels contained some form of additional full-depth timber. Most site-added timber was associated with practical construction needs, such as lining support in kitchens and bathrooms, service accommodation, flashings, stair construction, and fit-out requirements. More consequential for thermal performance was the presence of uninsulated or partially insulated areas. Such areas, created by complex framing geometries and inaccessibility during insulation installation, represent direct thermal losses that compound the systematic impact of high framing percentages.

Importantly, analysis of contemporary detailing practices indicates that very little timber within modern wall frames can be considered "unnecessary" [20]. Each 90 × 45 mm member is typically included to satisfy legitimate structural, weathertightness, or fixings-related requirements, providing essential support for claddings, linings, services, and building hardware. The research further demonstrates that attempts to optimise or marginally reduce framing content in standard 90 mm walls are unlikely to produce a meaningful reduction in overall framing percentage or the associated thermal bridging [20].

4.2.3 Implications for H1, E3, and the Design–As-Built Performance Gap

The definition of "framed walls" in NZS 4218 [13] explicitly excludes lintels, supporting studs, and studs located at corners and junctions. When these elements are omitted from the total calculation, the resulting construction R-value represents a simplified and idealised version of the wall, and therefore appears significantly higher than the actual thermal performance of the as-built assembly. Figure 8 illustrates this discrepancy by contrasting the actual framing installed on site for a single case-study wall panel with the framing configuration permitted under the NZS 4218 definition. The standard allows the exclusion of lintels, trimming studs, double studs, and other structural elements that, in practice, form a substantial portion of the framing system and contribute meaningfully to thermal bridging.

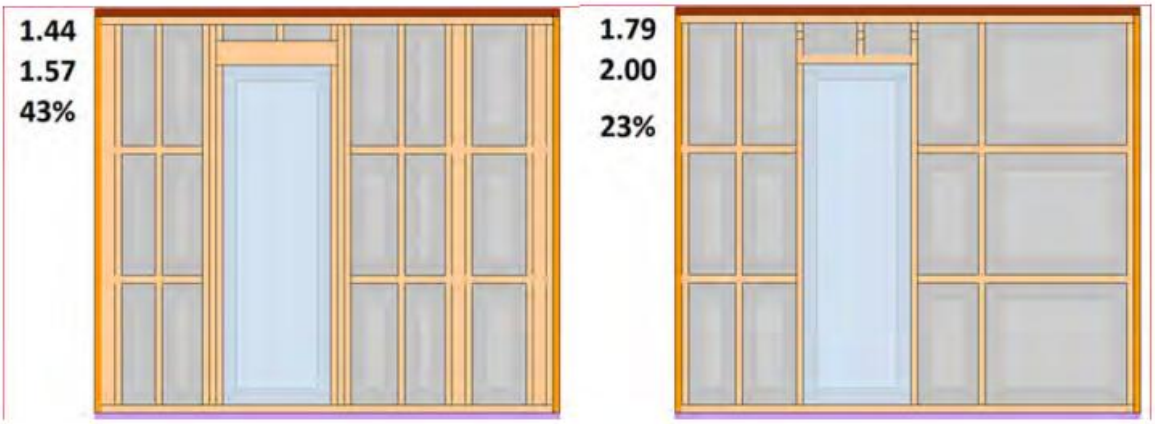

Figure 8-Actual Timber Framing (left) compared to definitions under NZS4218 (right) [20]

For each illustrated panel, Figure 8 presents in the top-left corner indicate: (1) the construction R-value achieved with R2.0 insulation in the cavities, (2) the construction R-value achieved with R2.8 insulation which is the maximum practicable for a 90 mm stud wall, and (3) the percentage of framing within the panel.

In the first illustration (left-hand side), which reflects the actual wall as constructed on site, the net framing content is 43% (excluding the window opening from the calculation). With R2.0

insulation, the wall achieves a construction R-value of only R1.44, demonstrating the substantial reduction caused by thermal bridging. Even with higher-performance R2.8 insulation, the construction R-value only marginally exceeds the minimum R1.5 requirement specified under Clause E3 of the NZBC. The second illustration (right-hand side) depicts the same wall panel but includes only those framing elements mandated for inclusion under the NZS 4218 definition for R-value calculations. This encompasses studs, dwangs, top plates, and bottom plates, while excluding lintels, additional studs supporting lintels, and supplementary studs at corners and junctions. By omitting these essential structural components, the simplified NZS 4218 approach produces a more favourable, yet significantly less representative construction R-value.

4.2.4 Weak Points in Timber Framing

The first phase study has identified six weak points in conventional practice that materially diminish the as-built thermal performance of residential buildings [20]. (1) Voids in external corners (Figure 9); (2) Poorly insulated or voids in internal corners; (3) Voids in internal to external wall junctions (Figure 10); (4) No insulation over the top plate; (5) No mid-floor perimeter insulation; (6) No insulation on slab vertical edge.

Light coming through from an un-clad external corner – this results in a significant uninsulated cold spot in the thermal envelope (on every corner of most dwellings surveyed)

An external corner junction (uninsulated) showing the light coming through the external wrap

Uninsulated corner – note that in the lower section of this gap insulation offcuts have been inserted into this difficult to access space.

Uninsulated corner showing mixture of 140mm and 90mm framing

Figure 9-Uninsulated external corners in timber framing structure [20]

	
Two internal wall junctions required to support this cupboard (and the wall between the two bedrooms). Both full height and wide gaps in the thermal envelope that will remain uninsulated	Light can be seen shining through the building paper at the left hand side of the image where the internal wall meets the external wall
	
A small internal wall for a cupboard opening intersects with the external wall – timing of the insulation install means that this void is now impossible to insulate	The internal to external wall junction showing the absence of insulation and also the poor seal which may lead to heat loss and moisture ingress through condensation

Figure 10-Uninsulated internal to external wall junctions [20]

4.3 Stage Two: Understanding and Addressing High Framing Ratios

The second phase of the research sought to deepen understanding of why timber-framed residential buildings in New Zealand exhibit such high percentages of framing and to identify which specific regulatory, structural, and practical drivers have the greatest influence on additional timber being incorporated into wall assemblies. A further objective was to examine whether, within the constraints of existing standards and common construction practices, there is realistic scope to optimise design to achieve lower framing ratios [2].

The second phase adopts a more focused analytical approach, examining the causes, consequences, and potential amelioration strategies associated with elevated framing content. The research comprises three interconnected components [2]. The first investigates the drivers of current framing percentages to understand how regulatory requirements, structural loading demands, fixings, construction sequencing, and industry conventions contribute to the proliferation of timber elements. The second component involves a detailed thermal modelling analysis to quantify the impacts of elevated framing content, as well as the weak points and blind spots identified in Stage One. This modelling quantifies the reduction in construction R-values attributable to excessive thermal bridging and insulation voids, thereby clarifying the extent to which actual performance diverges from values assumed in H1 calculations. The third component considers potential solutions by identifying advanced framing and insulation strategies, followed by an industry workshop to evaluate whether such strategies could feasibly be adapted for use within existing New Zealand framing practices.

A key technical constraint examined during this stage relates to the use of dwangs or nogs, which play a significant role in dictating timber density within external walls. When cavity construction was first introduced in 2005, E2/AS1 required nogs at 800 mm centres, illustrating the long-standing regulatory reliance on intermediate blocking and the resulting constraints on reducing framing density [2]. In practice, frame-and-truss manufacturing has largely shifted to full-depth timber for nogs due to safety concerns associated with nailing smaller end sections in factory environments [2]. Consequently, all optimisation scenarios modelled in this study employed full-depth nogs. The application of nogs remains mandatory under E2/AS1 clause 9.1.8.5 when studs exceed 450 mm centres and there is no external sheathing, as an intermediate batten or restraint is required to prevent insulation from being displaced into the cavity [42].

To explore the effects of these constraints on thermal performance, the second phase utilises detailed data from five representative houses selected from the 47 dwellings examined in Stage One [2]. These five houses include three single-storey dwellings in Auckland, Wellington, and Christchurch and two additional houses of modest complexity, are broadly representative in terms of materials and configuration. Their average framing percentage of 32% (ranging from 26% to 36%) is slightly lower than the overall first phase average of 34% yet remains characteristic of contemporary New Zealand construction. Each dwelling was modelled to determine its as-built construction R-values, to quantify the impact of the identified weak points on thermal performance, and to assess the implications of reducing framing to an aspirational 25%.

The modelling results show that, even under highly favourable conditions involving a simple single-storey dwelling and multiple expert optimisation techniques, the framing percentage remained constrained to no less than approximately 27% [2]. Achieving a framing ratio below 27% proved challenging even for an experienced detailer operating under idealised conditions, reflecting the structural, regulatory, and practical limitations embedded within current construction practice [2]. These findings underscore that within the present confines of NZS 3604, the NZBC, and common construction specifications, it is not feasible to reduce framing content in standard 90 mm walls to a level that would significantly decrease thermal bridging or reliably achieve the construction R-value minimums intended by Clause H1.

5 Thermal Bridging Comparison Between Conventional Structure and FRP Wall Panel System

This section evaluates the extent to which the FRP wall panel system, as implemented in the case study building, provides a viable acceptable or alternative solution capable of overcoming the thermal shortcomings observed in standard 90mm timber framing construction. To establish a robust basis for comparison in thesis, the analysis draws on the baseline dwelling modelled in Stage Two of the Beacon study, which was developed by an expert detailer for a representative single-storey timber-framed house in Auckland. The thermal-bridging calculation applies the NZS 4214 isothermal planes method to the Stage Two sample house, re-specified with the FRP wall panel system, to quantify its construction R-value and compare it with the timber-framed baseline.

5.1 Thermal Bridging Calculation-Isothermal Planes Method

Thermal performance assessment of building envelope components in New Zealand is underpinned by NZS 4214, which prescribes the isothermal planes method as the principal analytical framework for calculating construction R-values [46]. Applying the isothermal planes method offers a consistent and replicable means of evaluating the thermal performance of conventional wall and establishes a robust baseline for comparative analysis in subsequent sections of this study. Thermal bridges shall be determined by the isothermal planes method [46]. The isothermal planes method requires first selecting two planes parallel to the wall that enclose the portion of the structure where thermal bridging occurs, and then subdividing this portion into regions such that each contains only one set of stacked layers, with each region numbered accordingly. For each region, the area fraction (f_x) and the thermal resistance that would apply if that region existed alone are calculated. Using these values, the thermal resistance of the selected portion is determined in accordance with Equations 1 and 2 below, after which the resistances of any layers outside the selected portion are added to obtain the total thermal resistance.

$$\frac{1}{R_b} = \frac{f_1}{R_1} + \frac{f_2}{R_2} + \frac{f_3}{R_3} + \cdots \qquad \text{(Eq. 1)}$$

And then applying equation 2 to work out the total construction R-value.

$$R_b = \frac{1}{\left[\frac{1}{R_b}\right]} \qquad \text{(Eq. 2)}$$

where

f_x is the fraction of the cross-section at right angles to the direction of heat flow occupied by each region, and where x=1,2,3 etc.

R_x is the thermal resistance through the region corresponding to f_x

R_b is the thermal resistance through the bridged portion of the structure

5.2 Construction R-Value Calculation-Timber-Framed Sample House

A single-storey detached dwelling was selected as the reference case in the second phase of the Beacon research to enable a detailed examination of framing percentages within a representative residential building scenario that reflects prevailing construction norms in New Zealand. As illustrated in Figures 11 and 12, the sample house featured a 116 m² floor area, a 25-degree hip roof, 600 mm soffits, and nominal 2400 mm wall heights [2]. The construction assumptions incorporated widely established industry practices, including the use of 90 × 45 mm SG8 radiata pine studs, three-stud configurations at external corners and at internal-to-external wall junctions, nogs installed at 800 mm centres, and cladding fixed over a drained and ventilated cavity [2].

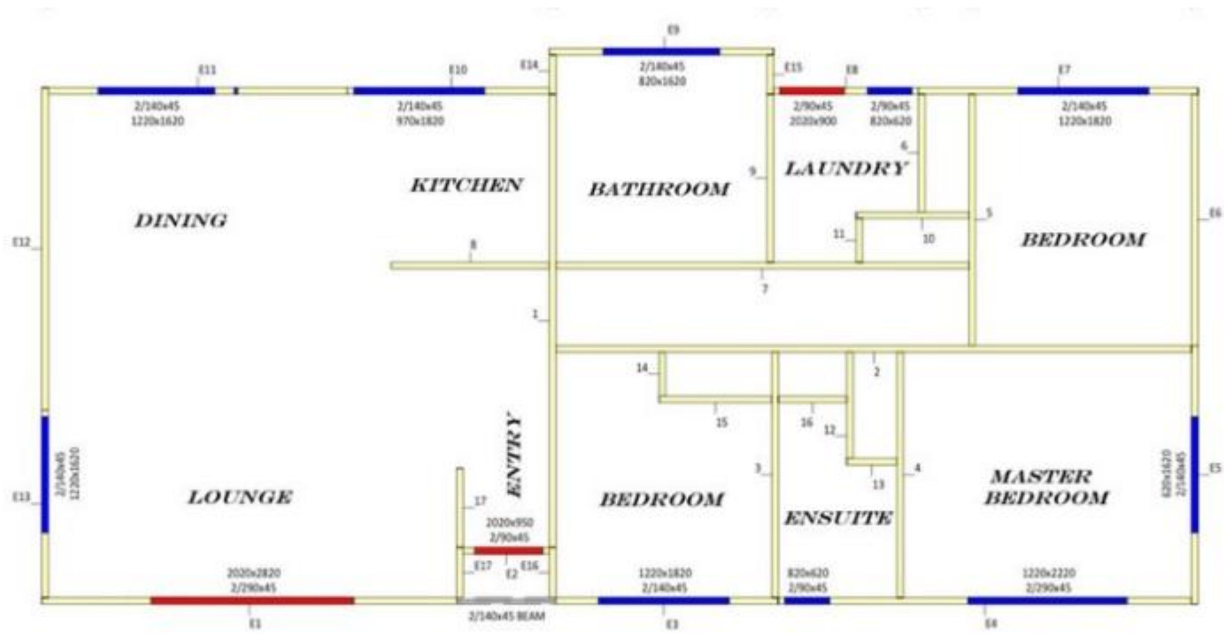

Figure 11-Simplified house plan design for use in detailing analysis [2]

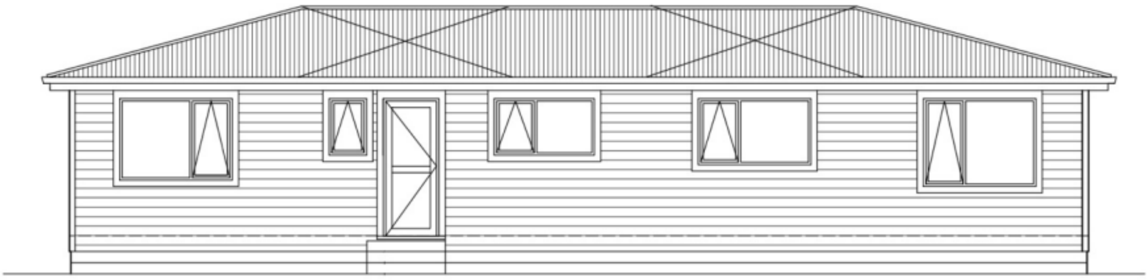

Figure 12-Simplified house plan design for use in detailing analysis [2]

Based on the sample house plan, the expert detailer developed a full set of working drawings representing a range of wind and cladding scenarios for a typical Auckland location. Using timber quantity outputs generated by the detailing software, the detailer was able to determine the actual cubic volume of timber used in each framing configuration [2]. The detailer developed 13 different cladding scenarios, applying 90 × 45 mm studs at 600 mm centres for High wind zones and 400 mm centres for Extra High wind zones, as well as 140 × 45 mm studs at 600 mm centres [2, 45]. These configurations were used to calculate the timber framing percentage, which directly influences the extent of thermal bridging and therefore affects the actual construction R-value. To facilitate comparison with the thermal-bridging calculations conducted for the FRP wall panel system, it is practical to reference the standardized set of framing assumptions: 600 mm stud spacing and nogs at 800 mm centres for horizontal weatherboard cladding (Figure 13), and nogs at 480 mm centres for vertical shiplap weatherboard cladding (Figure 14).This consistent approach ensures that differences in thermal bridging could be attributed to the wall system itself, rather than to variations in cladding or framing layout.

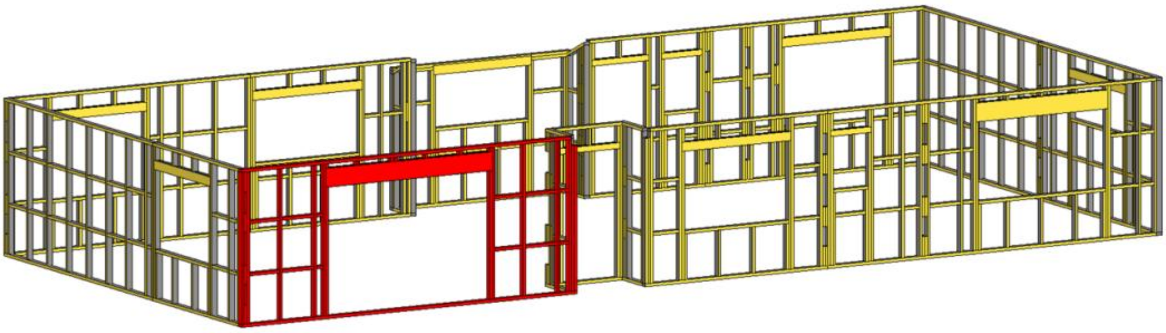

Figure 13-Typical scenario showing studs at 600mm centres and nogs at 800mm [2]

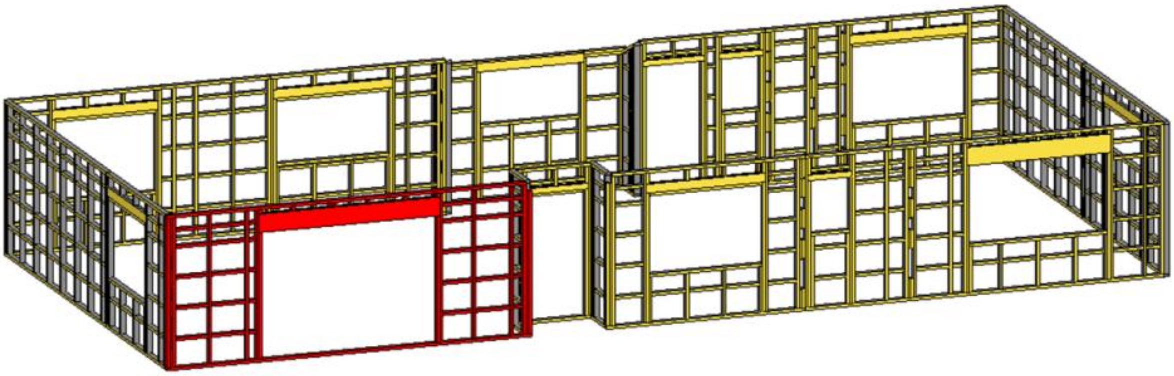

Figure 14-Typical scenario showing studs at 600mm centres and nogs at 480mm [2]

Table 1 Summary of the detailing results based on the sample house design

Scenario number	Cladding	Details	Percentages of framing		
			90mm x 45mm 600mm centres	90mm x 45mm 400mm centres	140mm x 45mm 600mm centres
1 SH#A	Brick	2 rows nogs @800mm	29.29%	31.99%	29.86%
2 SH#ADO2	SH#A brick Stud-saver** external corners only	2 rows nogs @800mm	28.63%	30.12%	29.13%*
3 SH#ADO3	SH#A Brick Stud-saver** external corners and partition walls	2 rows nogs @800mm	27.37%	29.02%	27.87%*
4 SH#ADO1	Detailer editing of SH#A	2 rows nogs @800mm	29.29 n/c	30.83	29.86%*
5 SH#K	Brick	1 row nogs @1350mm max	27.75%	30.30%	28.25%*
6 SH#KDO1	Detailer editing of SH#K brick	1 row nogs @1350mm max	27.75 n/c	29.20	28.25%*
7 SH#B	Horizontal w/bd SH#B	2 rows nogs @800mm + soffit nog	30.95%	33.82%	31.45%
8 SH#C	Horizontal w/bd SH#C	1 row nogs @ 1350mm max + soffit nog	29.35%	32.49%	29.75%
9 SH#E	Vertical shiplap w/bd	4 rows nogs @480 + soffit nog	34.12%	37.18%	34.95%
10 SH#E-M1	Vertical shiplap w/bd	4 rows nogs @480 + soffit nog + double sills	34.72%	37.78*	35.55*
11 SH#D	Plywood or fibre cement sheathing	2 rows nogs @ 800	30.44%	34.10%	30.88%
12 SH#H	Plywood or fibre cement sheathing	1 row nogs @ 1350 max	28.74%	32.48%	29.24*
13 SH#J	Plywood or fibre cement sheathing	No nogs ***	27.40%	31.01%	27.90*

Table 1. above summarises the key results for each scenario derived from variations of the standard simple house design. The first column identifies the scenario number alongside its research label (with SH denoting Simple House) [2]. The second column specifies the cladding type, while the third column outlines the framing variable applied in that scenario [2].

The timber percentages detailed in the highlighted scenarios 7 and 9 of Table 1 are the main reference values used to calculate the actual construction R-value of the sample dwelling. These scenarios represent the most relevant framing configurations for conventional timber-framed houses. By applying the isothermal planes method to the framing percentages observed in these timber-framed cases, the reference sets a baseline for evaluating the thermal performance of a comparable dwelling built with the FRP system. This approach enables a direct evaluation of the extent to which the FRP wall panel system may enhance the overall as-built R-value relative to conventional timber framing.

It is recommended to refer to Table E1(c) of NZS4214, [46] where the R-value for 94mm timber framing is conveniently listed as 0.78 $m^2 \cdot K/W$. The R2.8 insulation represents the highest level of insulation that can feasibly fit within 90mm timber framing cavities. To apply Equation 1 and Equation 2, the construction R-values with timber framing for the sample house in scenarios 7 and 9 are as follows:

#7: R_1 = R 2.8 $m^2 \cdot K/W$ (insulation product)

R_2 = R 0.78 $m^2 \cdot K/W$ (94mmx45mm Timber Framing)

f_2 = 0.3095

f_1 = 1- 0.3095 = 0.6905

$$\frac{1}{R_b} = \frac{f_1}{R_1} + \frac{f_2}{R_2} = \frac{0.6905}{2.8} + \frac{0.3095}{0.78} = 0.6434$$

$$R_b = \frac{1}{[\frac{1}{R_b}]} = \frac{1}{0.6434} = 1.55 \ m^2 \cdot K/W$$

#9: R_1 = R 2.8 (insulation product)

R_2 = R 0.78 (94mmx45mm Timber Framing)

f_2 = 0.3412

f_1 = 1- 0.3412 = 0.6588

$$\frac{1}{R_b} = \frac{f_1}{R_1} + \frac{f_2}{R_2} = \frac{0.6588}{2.8} + \frac{0.3412}{0.78} = 0.6727$$

$$R_b = \frac{1}{[\frac{1}{R_b}]} = \frac{1}{0.6727} = 1.48\ \text{m}^2\cdot\text{K/W}$$

The total R-value of the timber-framed building elements is calculated using the equation 3 provided in NZS 4214 [46] as follows,

$$R_T = R_{si} + R_1 + R_2 + \cdots + R_{Se} \qquad \text{(Eq. 3)}$$

R_T = total thermal resistance,

R_{si} = internal surface resistance: 0.09 $m^2 \cdot K/W$,

R_{se} = external surface resistance:0.03 $m^2 \cdot K/W$,

$R_{1,2,3}$= thermal resistance of each layer

Therefore,

- #7 Insulated Timber Framing: R_T = 0.09+1.55+0.03= 1.67 $m^2 \cdot K/W$
- #9 Insulated Timber Framing: R_T = 0.09+1.48+0.03= 1.60 $m^2 \cdot K/W$

The calculation of construction R-values for Scenarios 7 and 9 of the Stage Two sample house design demonstrates the significant influence of framing percentage on overall thermal performance. In Scenario 7, where the framing fraction is 30.95%, the application of the isothermal planes method yields a overall construction thermal resistance of R1.67 $m^2 \cdot K/W$. In contrast, Scenario 9 incorporates a higher framing fraction of 34.12%, resulting in a reduced construction R-value of R 1.60 $m^2 \cdot K/W$. These results illustrate the inverse relationship between framing intensity and wall thermal performance. The comparison between the two scenarios provides a clear baseline for evaluating the potential performance gains achievable through alternative systems such as the FRP wall panel system. The results of the thermal-bridging calculations indicate that, once the actual framing percentages observed in the Stage Two study are accounted for, both scenarios evaluated only marginally achieve the minimum construction R-value of R1.5 required under E3/AS1. Incorporating the realistic extent of thermal bridging into the analysis reveals that neither scenario can achieve the previous H1/AS1 compliance threshold of R1.9 nor the current H1/AS1 requirement of R2.0 for external walls.

5.3 Three Weak points of Thermal Bridging in the FRP Wall Panel System

In contrast to traditional timber-framed buildings, the FRP wall panel system does not display the typical insulation deficiencies commonly associated with voids that frequently occur at external and internal corners, as well as at the junctions between internal and external walls. In comparing the thermal-insulation performance of conventional timber-framed construction with that of the FRP wall panel system, three recurrent weak points in timber framing are identified as the focus of analysis: (1) voids that occur in external corners due to framing congestion and inaccessible cavities, (2) poorly insulated or uninsulated pockets within internal corners where construction geometry restricts full insulation placement, and (3) voids at internal-to-external wall junctions.

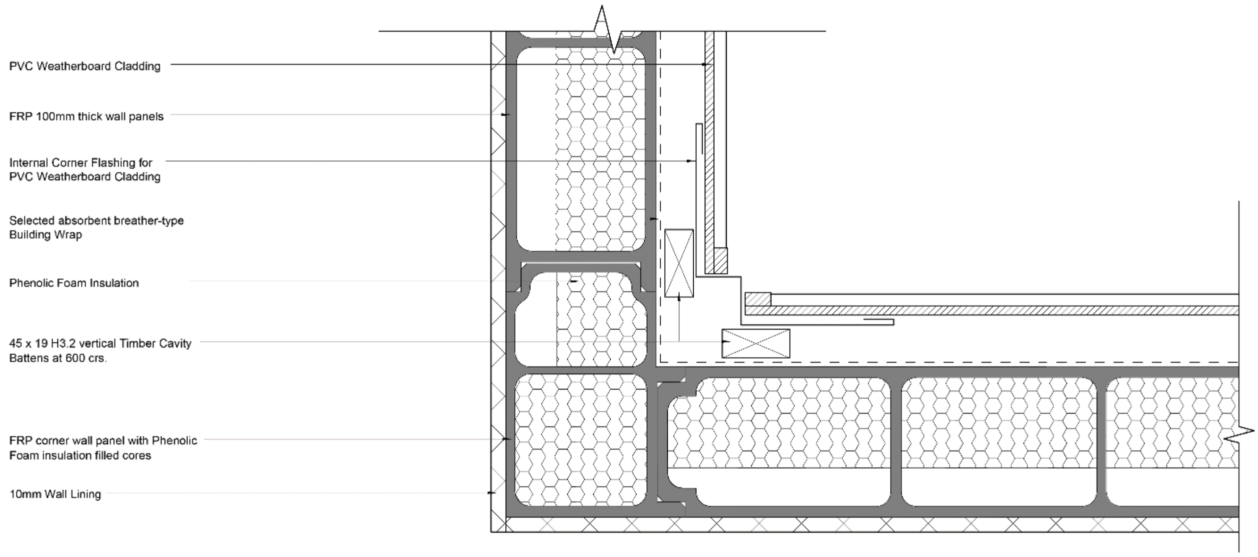

Figure 15-FRP wall panel system-internal corner filled with phenolic foam insulation

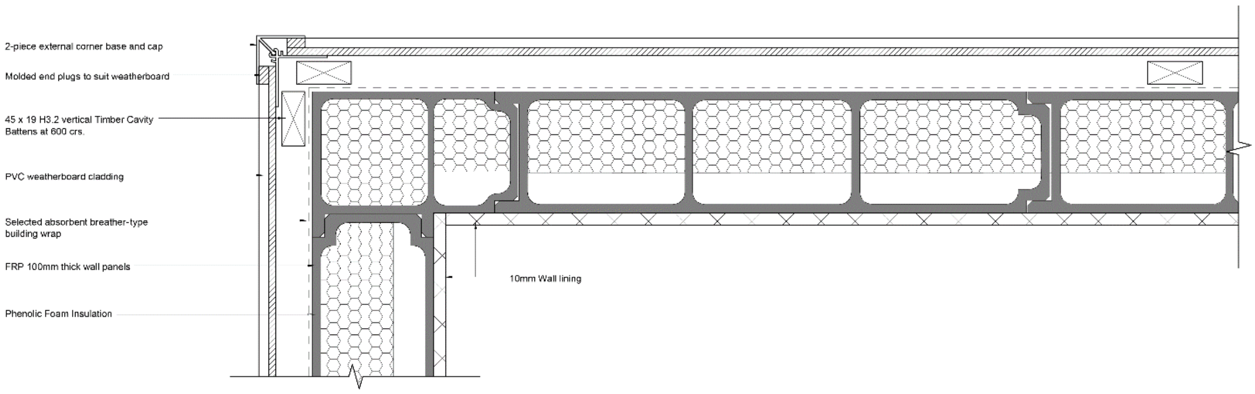

Figure 16-FRP wall panel system-external corner filled with phenolic foam insulation

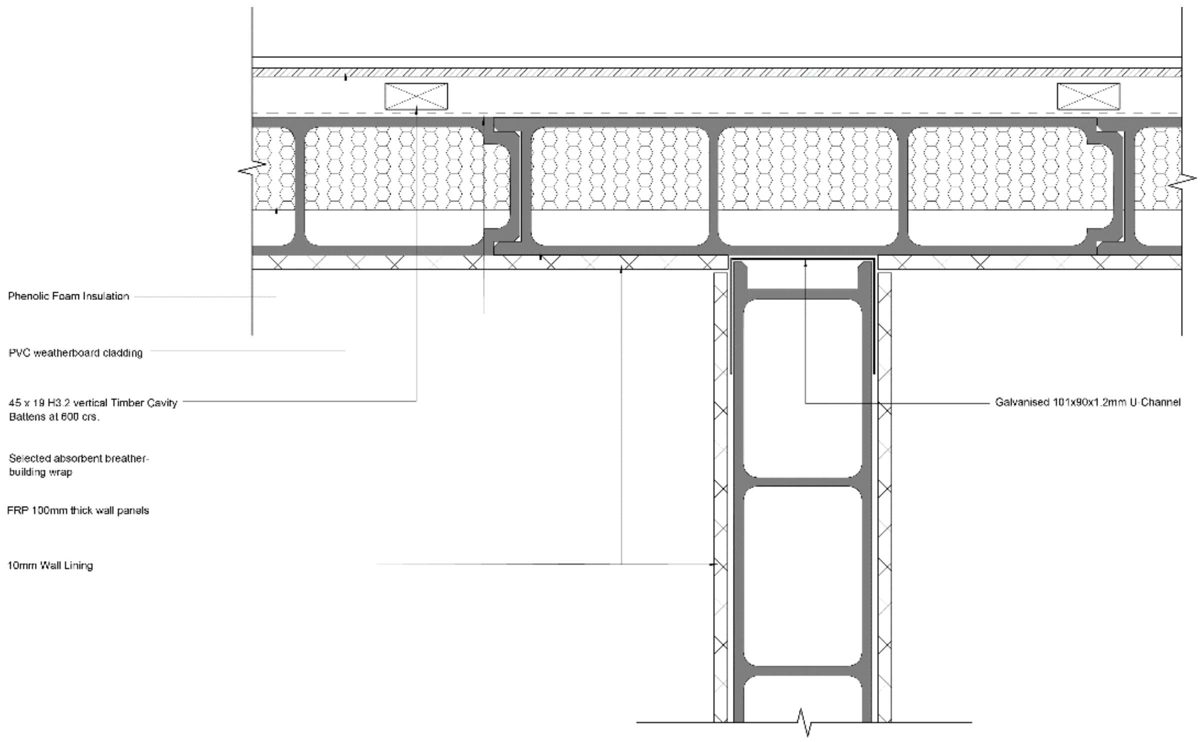

Figure 17-FRP wall panel system-typical joint between internal wall and external wall

As illustrated in Figures 15,16,17, the FRP wall panel system, which combines phenolic-foam insulation pre-inserted into the panel cavities with an interlocking connection method that ensures continuity of the insulated envelope, obviously avoids the three insulation deficiencies commonly observed in conventional timber-framed buildings. Consequently, the FRP system substantially reduces the proportion of thermal bridging within the building envelope and has the potential to achieve a higher overall construction R-value than conventional timber framing.

5.4 Thermal Bridging and Construction R-Value of the FRP Wall Panel System

The NZS 4214 isothermal planes method is applied to calculate the thermal bridging of the FRP wall panel system and to determine its construction R-value using the Stage Two sample house specifications. This enables a direct comparison with the timber-framed baseline and provides a basis for evaluating the extent of thermal performance that could be achieved if the sample house were constructed with the innovative FRP system. This integrated insulation and rib configuration (Figure 18) produces a uniform, predictable thermal profile across the wall panel, enhancing the system's overall construction R-value and improving its thermal reliability compared with conventional timber-framed wall assemblies.

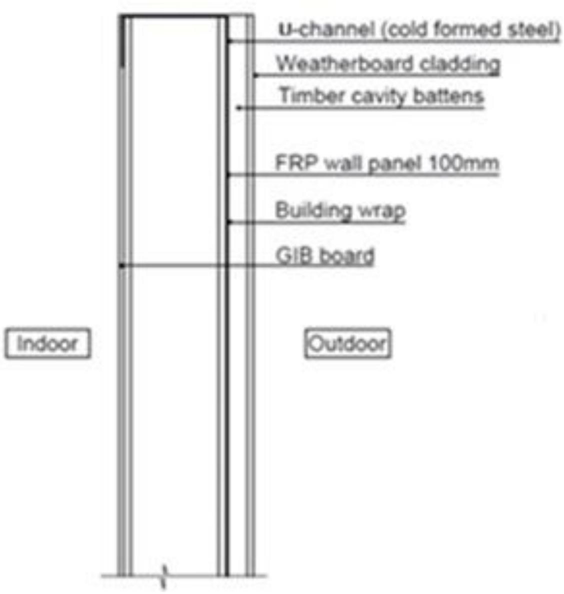

Figure 18-FRP wall panel system wall assembly details

The procedure for determining the overall construction R-value of the FRP wall panel system differs fundamentally from that applied to conventional timber-framed wall assemblies. Unlike timber framing, where thermal performance can be derived from prescribed material properties and framing fractions stated in NZS 4214, the standard does not provide any indicative R-value, thermal conductivity, or equivalent thermal property for FRP composite material. Consequently, the first necessary step in evaluating the thermal performance of the FRP wall system is to experimentally establish the thermal conductivity of the FRP material itself.

5.5 Calculation of R-values Based on Thermal Conductivity Testing of FRP Layers

To achieve this, representative FRP specimens were extracted from the surface layer of sample panels and prepared as 200 mm × 200 mm coupons, as shown in Figure 19 (a). The specimens were assessed utilising a lambda thermal conductivity meter, as depicted in Figure 19 (b), which adheres to the instrumentation standards outlined in ASTM C177 [44]. The testing procedure followed the methodology specified in AS/NZS 4859.1:2002 [47] to determine the steady-state thermal transmission properties of insulation materials. This controlled laboratory characterisation establishes the essential thermal property needed for subsequent construction-level heat-flow calculations. The experimental testing resulted in a measured thermal conductivity (k) of 0.248 W/m·K, confirming the fundamental material-level thermal property required for further analysis.

(a) FRP layer samples

(b) lambda thermal conductivity meter

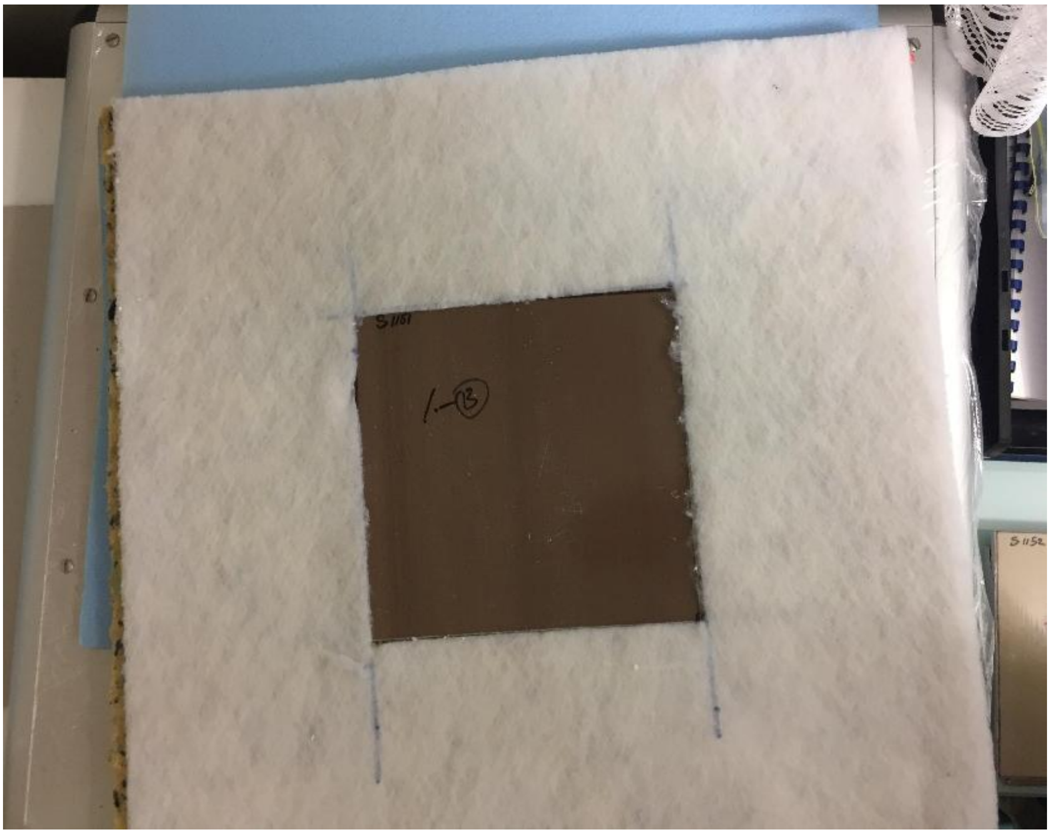

(c) The FRP layer sample is positioned within a pre-cut opening and secured in place by the surrounding white non-woven insulating outer layer.

Figure 19-Thermal conductivity testing of FRP wall panel

Thermal conductivity (k) is defined as the rate of heat transfer through a unit area of a homogeneous material of unit thickness under a unit temperature difference between its two faces, expressed in watts per metre kelvin (W/m·K) [46]. It represents an intrinsic material property governing steady-state conductive heat flow. The thermal conductivity is directly related to the material thermal resistance, such that for a material of thickness l, the thermal resistance R is given by the following equation [46]:

$$k = \frac{l}{R_m} \text{ (conversely, } R_{\mathrm{m}} = \frac{l}{k}\text{)} \qquad \text{(Eq. 4)}$$

The thickness of the FRP specimens tested ranged between 6 mm and 7 mm, and an average nominal thickness of 6.5 mm was adopted for the thermal conductivity assessment and thermal resistance calculations. To apply equation 4, the R-value for the FRP wall panel surface layer is calculated as follow,

$$R_{FRP} = \frac{0.065}{0.248} = 0.026 \text{ m}^2\cdot\text{K/W}$$

5.6 Thermal Properties of FRP Wall Panel Components

The insulation material installed within the cavities of the FRP wall panel system comprises a rigid thermoset phenolic foam core, selected for its high thermal efficiency and dimensional stability. The foam core is manufactured with a dual-facing configuration, consisting of an upper tissue-based facing and a lower aluminium-foil facing that is integrally bonded to the foam during production to enhance durability and thermal performance [48]. The aluminium-foil skin facing the cavities has a low emittance value of E0.05 [48], contributing to reduced radiative heat transfer within the cavity. The product used in this study has a nominal thickness of 60 mm and a declared thermal conductivity (k) of 0.020 W/m·K [48]. Therefore, applying Equation 4, the R-value of 60mm thick phenolic foam core is 3.0 $\text{m}^2\cdot\text{K/W}$.

In addition to its thermal resistance, phenolic foam exhibits several characteristics that render it highly suitable for use in closed-panel FRP wall panel system constructions [48]. Its low moisture absorption substantially mitigates the risk of long-term degradation or loss of insulating performance, which is essential for maintaining the integrity of a wall assembly with high thermal resistance.

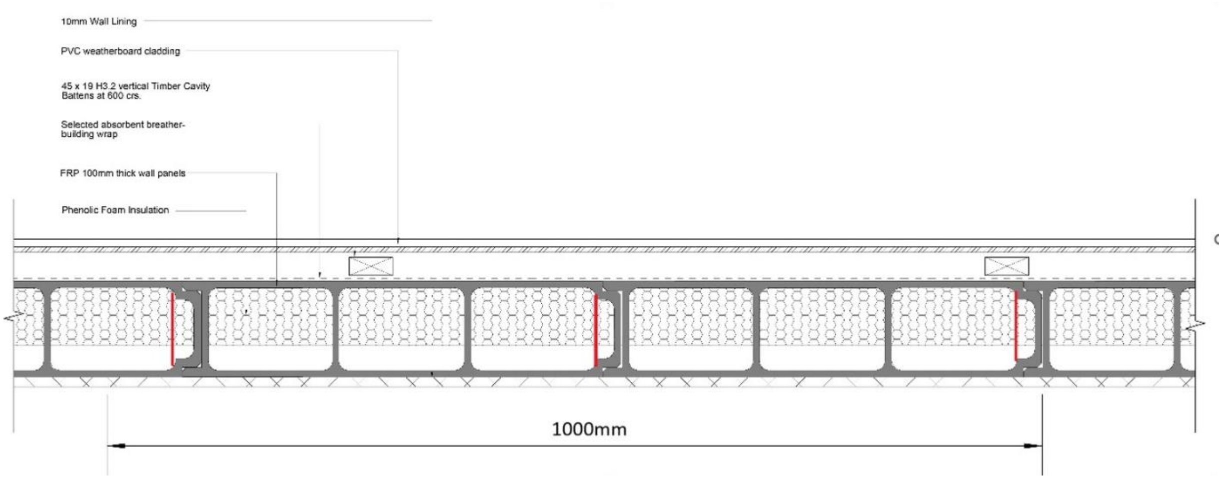

Figure 20-FRP wall panel system 1m length interconnection configuration

Figure 20 illustrates the full 1 metre configuration of the FRP wall panel system. Each individual panel has a nominal width of 450 mm. Therefore, a one metre wall segment consists of two full-width panels. The figure demonstrates that there are 9 internal FRP ribs, each with a width of approximate 6 mm, which divide the cavities and display a consistent and repetitive pattern along each meter of wall length. These ribs, together with the inter-panel joints, act as thermal bridges due to their inability to be filled with phenolic-foam insulation.

In addition to the rib-induced thermal bridges, Figure 20 highlights three joint locations (shown in red) within the 1 metre segment where the insulation thickness is reduced. These occur at the tongue-and-groove connections between adjacent panels. Each panel tongue extends approximately 20 mm in length and 15 mm in depth, reducing the available insulation thickness from the full 60 mm to approximately 45 mm in these regions. As a result, the phenolic foam core in the tongue zones provides a lower thermal resistance than the surrounding fully insulated cavities.

Applying Equation 4, the R-value of the 45 mm thick phenolic foam core is calculated to be 2.25 $m^2 \cdot K/W$. Given these conditions, the ribs and the reduced-thickness insulation zones at the panel joints shall be explicitly incorporated into the isothermal-planes calculation when determining the overall construction R-value of the FRP wall panel system. Their inclusion ensures an accurate representation of the localised thermal bridging effects.

A further factor that should be incorporated into the calculation of the overall construction R-value of the FRP wall panel system is the presence of the internal air gap within the insulated cavities. The nominal thickness of the FRP wall panel is 100 mm. As shown in Figure 21 after subtracting the 60 mm phenolic-foam core and considering the FRP skins, each with a thickness of 6.5 mm, the resultant space provides an approximate air gap of 25 mm. To calculate a representative thermal resistance for this air space, an interpolated value is derived using the tabulated thermal resistances for air gaps as provided in Table E3 of NZS 4214 [46]. The 12 K temperature difference represents a realistic and moderate indoor–outdoor thermal gradient characteristic of typical New Zealand winter conditions during the heating season. The thermal resistance of a 20 mm air space, under a temperature differential of 12 K with horizontal heat flow and surfaces characterised by E0.05 effective emittance, is approximately 0.53 m²·K/W, as determined by the R-value. This air-gap contribution should be included in the isothermal-planes calculation alongside the insulation core and thermal-bridge components to ensure an accurate determination of the overall construction R-value for the FRP wall panel system.

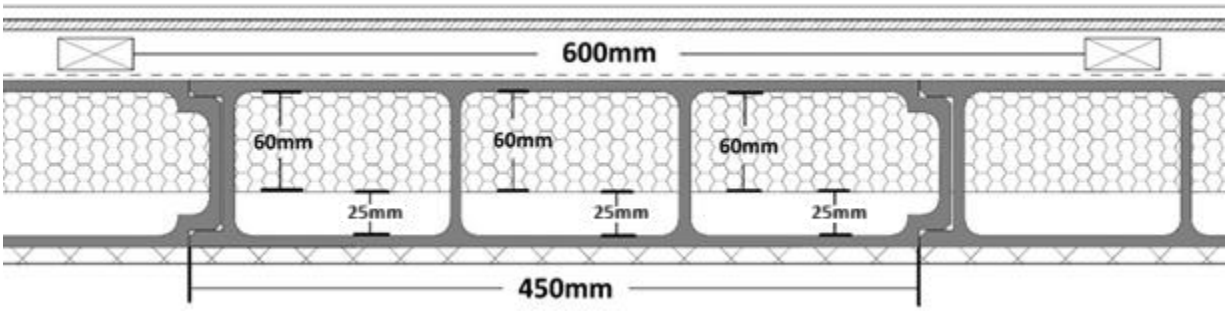

Figure 21-FRP wall panel system dimensions

5.7 Determination of Localised Thermal Resistances for FRP Wall Panel System

Prior to employing the isothermal planes method to ascertain the overall construction R-value of the sample house as outlined in Beacon's Stage Two report, utilising the FRP wall panel system, it is imperative to first determine the R-value of the individual components that contribute to thermal bridging within the system. The R-value of the 100 mm deep FRP ribs, which subdivide the cavities within the FRP panels and function as localised thermal bridges, can be initially quantified. In addition, the reduced thermal resistance associated with the insulation reduced tongue region at each panel joint shall be calculated. These component-level values serve as essential inputs for the subsequent isothermal planes analysis, ensuring that the calculated construction R-value accurately reflects the true thermal behaviour of the FRP wall panel system.

Based on the measured thermal conductivity of the FRP material, the R-value of a 6.5 mm thick FRP skin layer is approximately 0.026 m²·K/W. This corresponds to an approximate thermal resistance of 0.004 m²·K/W per millimetre of FRP thickness. Applying this value, the thermal resistance of a 100 mm deep FRP rib is therefore estimated at 0.40 m²·K/W.

The overall R-value at the panel joints, as depicted in the enlarged detail in Figure 22, is determined by accounting for the combined contributions of the FRP layers, the diminished air gap, and the locally thinned phenolic foam insulation. The tongue section of the joint comprises four FRP layers, with a total combined thickness of approximately 30 mm (15 mm on each side of the joints). Using the per-millimetre R-value established above, these FRP layers contribute approximately 0.12 m²·K/W to the joint's thermal resistance.

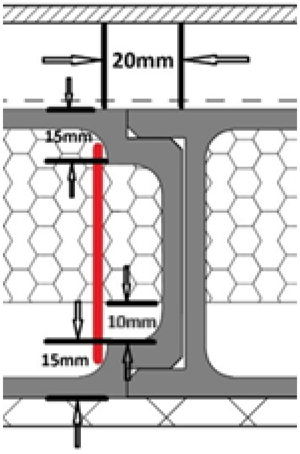

Figure 22-Enlarged Detail of the FRP Wall Panel Joint

To establish a representative approach for assessing the thermal resistance of the narrow cavity air layer within the FRP wall panel system, reference is made to Table E3 of NZS 4214 [46], which provides tabulated air-space R-values only down to a minimum thickness of 13 mm. Because the standard does not specify values for air gaps smaller than 13 mm, the 10 mm cavity present in the FRP panels cannot be directly assessed or reliably interpolated from the available data. In this context, and to maintain a conservative and defensible methodology, it is reasonable to disregard the thermal contribution of this reduced air space altogether and exclude any associated R-value from the overall construction R-value calculation for the FRP wall panel system. This approach ensures that the resulting performance assessment does not overestimate the thermal benefit of the cavity and remains fully aligned with established NZS 4214 calculation principles.

Finally, the tongue region contains a reduced thickness phenolic-foam core of 45 mm. Applying Equation 4, this insulation contributes an R-value of approximately 2.25 m²·K/W. By summing the contributions of the FRP layers and the 45 mm phenolic-foam core, while disregarding the reduced air gap, the total thermal resistance R-value for the insulated tongue region is approximately 2.37 m²·K/W.

5.8 Calculation of the Overall Construction R-Value for FRP Wall Panel System

To apply Equation 1 and Equation 2, the construction R-value of FRP wall panel is as follows:

R_1 = R3.0 (60 mm phenolic foam core insulation) + R0.53(27mm air gap) + R0.052 (two 6.5mm R0.026 FRP layers on each side of the panel) = 3.582 m²·K/W

R_2 = 0.40 m²·K/W (100 mm deep FRP rib)

R_3 = R2.25 (45 mm phenolic foam insulated FRP panel tongue) + R 0.12 (30mm FRP panel layers at the joints, two layer on each side) = 2.37 m²·K/W

f_3 = 6 × 0.006 = 0.036

f_2 = 3 × 0.02 = 0.06

f_1 = 1 – 0.036 – 0.06 = 0.904

$$\frac{1}{R_b} = \frac{f_1}{R_1} + \frac{f_2}{R_2} + \frac{f_3}{R_3} = \frac{0.904}{3.582} + \frac{0.06}{2.37} + \frac{0.036}{0{,}4} = 0.367$$

$$R_b = \frac{1}{[\frac{1}{R_b}]} = \frac{1}{0.367} = 2.72$$

The total R-value of the FRP wall panel system is determined using Equation 3 as specified in NZS 4214 [46], expressed as $R_T = R_{si} + R_{se}$ = 0.09 + 2.72 + 0.03 = 2.84 m²·K/W.

This represents a conservative estimate of the construction R-value of the FRP wall panel system. In addition to disregarding the reduced air gap on the tongue side in the overall R-value calculation, the estimate also excludes the supplementary thermal contribution of the 80 mm, R4.0 phenolic foam core [48] incorporated within the corner panels. Accordingly, the value presented here should be understood as the baseline thermal performance delivered by the FRP wall panel system for the case study building, ensuring that subsequent analyses are grounded in a deliberately understated and defensible assessment.

5.9 Comparison of Construction R-value between the timber-framed scenarios and the FRP wall panel system

The results of the construction R-value calculations demonstrate that, even under conservative assumptions, the FRP wall panel system delivers a substantially higher thermal performance than either of the two representative timber-framed scenarios derived from the Beacon Stage Two study. Whereas the timber-framed Scenarios #7 and #9 achieve construction R-values of R1.67 m²·K/W and R1.60 m²·K/W respectively, the FRP wall panel system attains an overall construction R-value of R2.84 m²·K/W, reflecting the combined effect of reduced thermal bridging area and higher insulation continuity. Figure 23 illustrates the corresponding effect size, showing the percentage increase in construction R-value achieved by the FRP wall panel system relative to each timber-framed scenario. The FRP wall panel system exhibits an improvement of approximately 70.1% over Scenario #7 and 77.5% over Scenario #9, highlighting the substantial thermal-performance advantage inherent in the FRP building envelope.

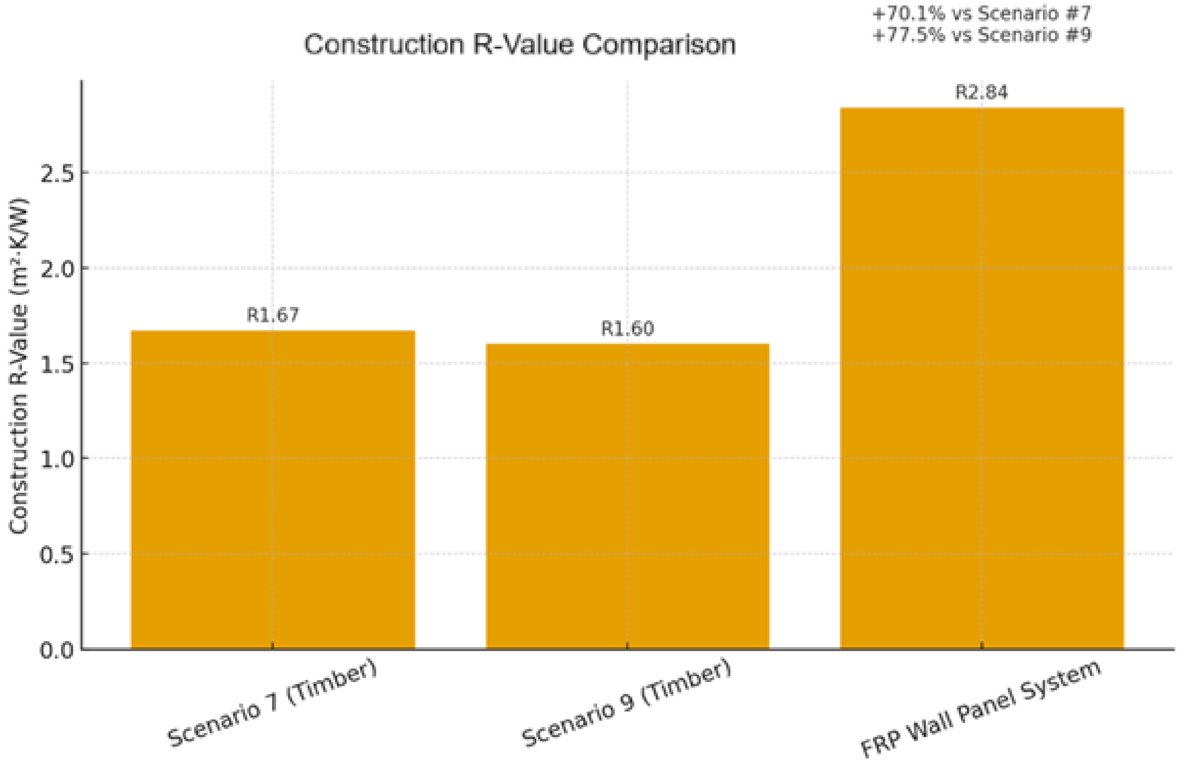

Figure 23-Comparative Construction R-Values and Percentage Improvements

Table 2 summarises the comparative construction R-values for Scenario #7, Scenario #9, and the FRP wall panel system, providing a clear numerical basis for evaluating the magnitude of performance improvement resulting from the FRP configuration.

Table 2-Comprehensive Comparison of Timber-Framed vs FRP Wall Panel System

Parameter	Scenario #7 – Timber Frame	Scenario #9 – Timber Frame	FRP Wall Panel System
Wall System Type	90 × 45 mm timber framing	90 × 45 mm timber framing	FRP composite panels with phenolic foam core
Thermal Bridging Percentage	30.95% timber framing fraction	34.12% timber framing fraction	Minimal – only FRP ribs & joints, approximately 9.6%
Dominant Bridging Mechanism	Studs, plates, nogs, corner clusters, lintels	Increased studs, plates, nogs, lintels	FRP ribs & inter-panel junctions
Insulation Type	R2.8 fibrous bulk insulation	R2.8 fibrous bulk insulation	60 mm phenolic foam + air gaps
Theoretical Maximum insulation R-value	R2.8	R2.8	R3.0 + cavity effects
Construction R-value (core only)	R1.55	R1.48	R2.72 (bridged section)
Internal surface resistance (Rsi)	0.09	0.09	0.09
External surface resistance (Rse)	0.03	0.03	0.03
Final Construction R-value (RT)	1.67 m²·K/W	1.60 m²·K/W	2.84 m²·K/W
Meets E3/AS1 minimum (R1.5)	Yes (marginal)	Yes (marginal)	Yes (well above)
Meets current H1/AS1 (R2.0)	No	No	Yes
Margin above R2.0	−0.33	−0.40	+0.84

Parameter	Scenario #7 – Timber Frame	Scenario #9 – Timber Frame	FRP Wall Panel System
Likelihood of voids / gaps	High (corners, junctions)	Very high	Negligible
Thermal continuity	Disrupted	Highly disrupted	Continuous
Overall thermal bridging risk	**High**	**Very high**	**Low**

If the Stage Two sample house were designed and constructed using the FRP wall panel system, it would readily achieve an external wall construction R-value of approximately R2.84 without the need to address thermal bridging effects. This performance level would comfortably exceed the H1/AS1 minimum thermal-performance requirement of R2.0 for external walls, demonstrating the system's inherent capacity to deliver higher thermal efficiency than conventional timber-framed construction.

In Scenario #7, the timber-framed wall assembly incorporates studs at 600 mm centres, with nogs installed at 800 mm centres for horizontal weatherboard cladding and at 480 mm centres for vertical shiplap weatherboards. These additional framing elements are necessitated by cladding-fixing requirements and result in increased timber density within the wall, thereby elevating thermal bridging. In contrast, as demonstrated in Figures 61 and 62 of the duplex case study building during construction, the FRP wall panel system does not necessitate any specific framing configurations for the installation of either horizontal or vertical cladding. Cavity battens can be fixed directly to the FRP panels at 600 mm centres in accordance with E2/AS1 [42], irrespective of cladding orientation. This avoids the need for additional nogs or intermediate timber elements, therefore preventing the increase in thermal bridging typically associated with conventional timber-framed construction.

6 FRP Wall Panel System Structural Verification against Timber Framing Standards

Clause B1 of the NZBC requires that buildings "withstand likely loads including wind, earthquake, live, and dead loads (people and building contents)" [45]. Compliance with B1 is commonly demonstrated through NZS 3604 which is cited as an Acceptable Solution [2]. Wall framing designed and braced in accordance with NZS 3604 is therefore deemed to comply with B1 of the NZBC. In traditional timber construction, the arrangement of framing around openings, including the sizing of lintels, their support, and the requirements for trimming studs, is determined by several structural parameters: the weight of the roof, the distance between the lintel and the top plate, the clear span of the window or door opening, and any concentrated loads from the structure above [2].

NZS 3604 translates live and dead loads into wall-framing requirements through a series of tables that size framing components based on timber grade. These structural settings were held constant across all scenarios examined in Stage Two of the Beacon study, which serves as the reference baseline for the research in this thesis. The Beacon study quantified the amount of timber in the external walls of a simplified single-storey house with studs at both 600 mm and 400 mm centres. The model house adopted a hip roof, meaning all exterior walls were load-bearing, and each scenario utilised an understud to support the lintel. Given that the structural parameters influencing lintel loads, opening spans, and roof geometry remained constant across scenarios, the Beacon dataset offers a controlled environment for analysing how framing requirements inherently generate thermal vulnerabilities, particularly around lintels, trimming studs, and junctions within conventional timber-framed construction. This controlled scenario thus offers a robust basis for comparison with alternative wall systems that seek to reduce or eliminate thermal bridging at these locations.

Using the Beacon Stage Two scenario as the structural reference condition, the following section introduces the structural verification of the FRP wall panel system. This verification is fundamental to demonstrating whether the FRP system can meet the same structural performance requirements as NZS 3604 compliant timber framing while simultaneously maintaining full insulation continuity in areas that typically represent unavoidable thermal weak points in timber framing. The case study building constructed using the FRP wall panel system provides the practical basis for this verification. Its design closely aligns with the Beacon reference scenario, incorporating a 2.4 m wall height, a 25 degree roof pitch, and engineering provisions for a High Wind Zone and a High Earthquake Zone. The case study building offers a valid and directly comparable model for assessing whether the FRP system can satisfy structural demands under NZBC Clause B1 while mitigating the thermal weakness caused by framing intensification in conventional timber construction.

Base on the parameters of the case study building, the structural verification of the proposed FRP wall panel system is undertaken through two complementary and interrelated lines of evaluation: walls and lintels. First, the in-plane bracing capacity of the wall system is evaluated to determine its ability to resist lateral actions arising from both wind and earthquake loading. This component of the verification process focuses on the FRP wall's load displacement behaviour, ductility characteristics, energy dissipation capacity, and overall stability under cyclic racking forces, as established through BRANZ P21 testing and subsequent NZBC capacity–demand comparisons in accordance with NZS 3604 and NZS 1170.

In conventional timber-framed construction, lintels often represent a significant source of thermal bridging due to the presence of high conductivity structural elements and reduced insulation. By contrast, the FRP lintel configuration is designed to preserve the integrity of the continuous insulation envelope while still satisfying strength, stiffness, and serviceability requirements. In the latter part of this section, the FRP lintel system is evaluated to confirm its ability to transfer both gravity and lateral loads across openings while preserving the continuity of the insulation layer. This dual structural–thermal verification seeks to demonstrate that the FRP lintel system can provide sufficient load-bearing capacity at window and door openings, which typically represent pronounced thermal weak points in conventional timber framing structures, while simultaneously preserving the effectiveness of the thermal insulation layer.

6.1 Case Study Context: FRP Wall Panel System and Duplex Configuration

As illustrated in Figure 6, the case study buildings utilising the FRP wall panel system consist of two adjacent single-storey duplex units located in Hamilton, Waikato. Previous research by Velayudham et al. [34] concentrated on the in-field evaluation of the overall thermal performance of the two-bedroom unit situated in the rear duplex, providing empirical evidence of the system's thermal behaviour under real operating conditions. Building on this foundation, the present thesis focuses on the front duplex. This duplex serves as the basis for the structural verification of the

FRP wall panel system and for the subsequent assessment of in-field thermal performance in the front three-bedroom unit of the duplex. Using the front unit as the primary case study enables a detailed examination of the structural adequacy of the FRP wall panel system. Figure 24 illustrates the floor plan of the case study building, detailing the internal layout of both units and the respective floor areas allocated to each unit. Figure 26 illustrates a three-dimensional representation of the FRP wall panel system, showing how readily the complete wall structure can be modelled during the design phase. This contrasts with the timber-framed system, which relies on considerably more complex and component-intensive framing configurations, as shown in Figures 13 and 14. The case study building provides the spatial framework necessary for understanding its geometric configuration and serves as the basis for the structural and thermal analyses of the FRP wall panel system presented in this thesis.

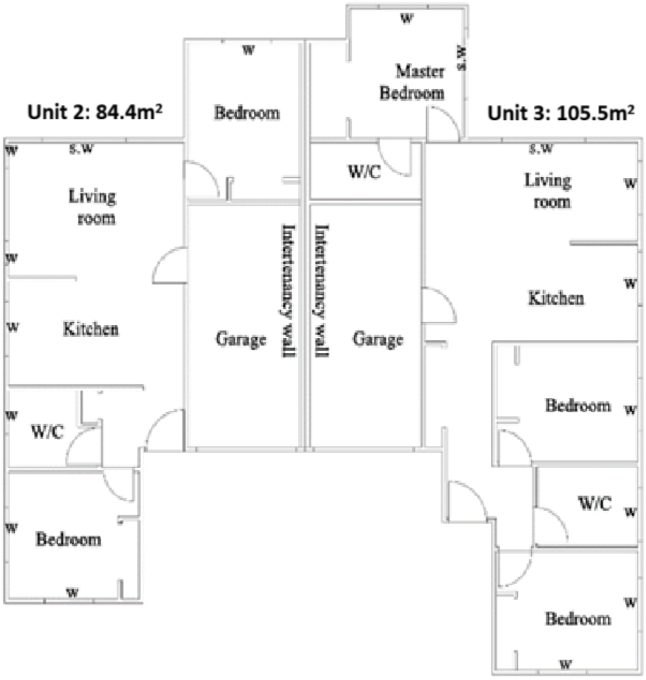

Figure 24-The floor plan of the case study building

6.2 Applicability of NZS 3604 and P21 Bracing Units to the FRP Wall Panel System

NZS 3604 provides the primary prescriptive framework for the structural wall design of most houses and other low-rise, timber-framed buildings in New Zealand. New Zealand's load combinations are governed by the AS/NZS 1170 suite of structural design actions, as formally required by B1/VM1 of the NZBC [45]. The 2011 revision of NZS 3604 was undertaken to ensure alignment with the AS/NZS 1170 loadings suite, particularly in relation to updated wind, earthquake, and snow actions [3].

NZS 3604 requires that the wall system at each storey form an integrated bracing system capable of resisting horizontal actions arising from wind and earthquake loads [3]. The bracing capacity of wall bracing elements must be established in accordance with the BRANZ Technical Paper P21 test procedure [3]. Bracing capacity determined through the P21 test is subsequently expressed in bracing units (“BU"), which represent the mean ultimate load recorded from three identical test specimens [3]. These bracing units provide a standardised means of quantifying both the bracing demand acting on the building and bracing capacity provided by individual structural elements, with 1kN of horizontal load being equivalent to 20 bracing units [3]. Bracing elements are required to extend continuously from the bottom plate at floor level to the top plate at ceiling level and must be incorporated within external and internal walls located along designated bracing lines [3]. The primary design objective is to ensure that the total bracing capacity within the building envelope, intended to resist wind and earthquake forces, exceeds the calculated bracing demand. This is essential to guarantee adequate lateral stability under ultimate limit state loading conditions.[3].

Bracing Units derived from the BRANZ P21 [51] test were originally intended for use in light timber framed residential buildings that fall fully within the scope and assumptions of NZS 3604. Therefore, outside this scope, these BU values are not considered characteristic strengths, but rather average peak test results from limited specimens [50]. Consequently, the direct application of the BU derived from a P21 test for structural brace capacity verification in Specific Engineering Design (“SED”) is not generally permitted. However, in certain circumstances, P21 test-based BU values may still be applied to buildings or materials outside NZS 3604 when the engineer can demonstrate that the structure behaves in a similar way to an NZS 3604 standards building [50]. Experimental testing of NZS 3604 type structures, together with observations from recent earthquakes, indicates that the assumptions regarding structural redundancy are generally valid for relatively simple timber framed buildings [50]. This redundancy arises from several contributory factors, including the following [50],

- the relatively high number of walls;
- partial height windows;
- lintels over doors providing some portal frame action;
- secondary effects from skirting boards and scotias and occasionally from secondary walls not identified as ‘bracing’ walls;
- load-sharing takes place through non-structural connections such as plasterboard stopping.

Pratchett et al. [50] also provides an example of a building configuration that satisfies the intent of NZS 3604. The intent of NZS 3604 is reflected in building configurations that exhibit a high wall to window ratio, the presence of multiple internal walls, and regular bracing lines with well-distributed bracing elements [50]. Such buildings are typically limited to two storeys in height and incorporate multiple layers of redundancy [50]. Accordingly, a design that satisfies these characteristics can be considered to comply with the intent of NZS 3604.

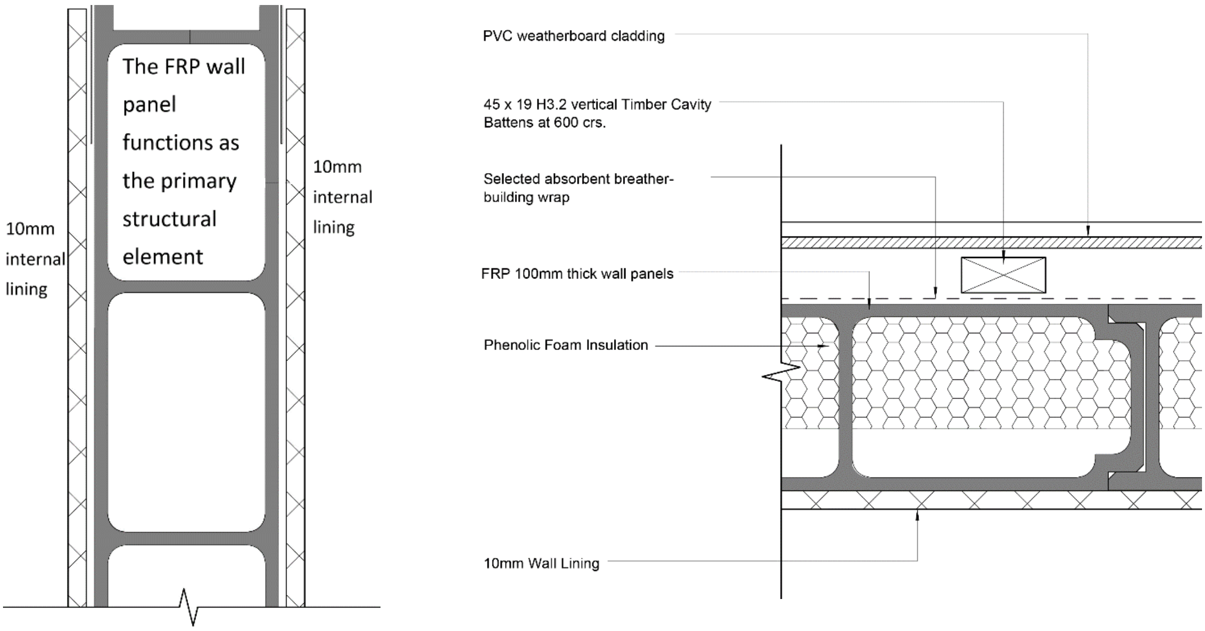

(a) FRP wall panel system (internal wall)

(b) FRP panel wall system (external wall)

Figure 25-The composition of the FRP wall panel system

In the context of structural design in New Zealand, the FRP wall panel system does not fall within the prescriptive scope of NZS 3604, as it is not a conventional timber framing structure. However, notwithstanding the substitution of timber framing with FRP wall panels, the system exhibits comparable layers of structural redundancy. Figure 25 illustrates the composite configuration of the FRP wall, which comprises multiple material layers, including a 10 mm internal lining, 20 mm cavity battens, and PVC weatherboard cladding. Furthermore, the architectural design of the case study building, as depicted in Figure 26, exhibits a substantial ratio of walls to windows and numerous internal walls. On this basis, it is reasonable to infer that the configuration of the FRP case study building aligns with the fundamental intent of NZS 3604, particularly in terms of simplicity, regularity, and redundancy.

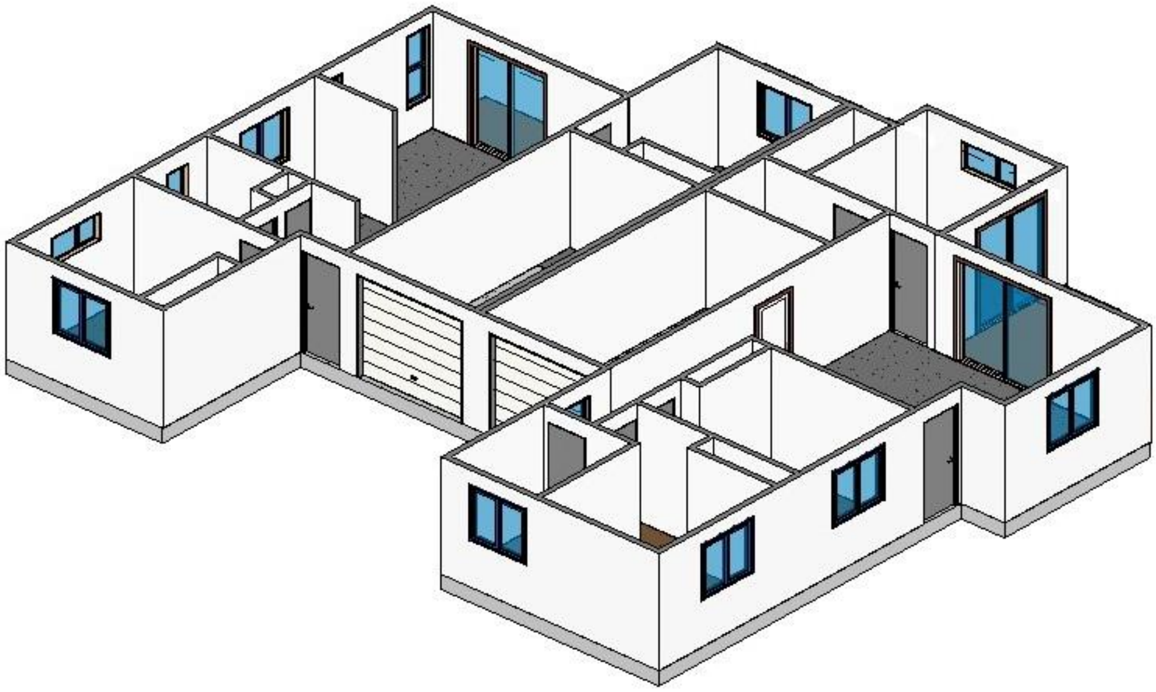

Figure 26-The wall-to-window ratio and the wall structure layout of the case study building

On this basis, it is justifiable to apply P21 test derived BUs in the assessment of bracing capacity for this FRP case study building. Furthermore, Clause 1.01 of B1/VM1 [45] specifies that, for any given building, compliance through the Verification Method is established by applying the AS/NZS 1170 suite of structural design actions.

6.3 BRANZ P21 Wall Bracing Test and Evaluation Procedure [51]

The BRANZ P21 test is an experimental wall bracing test and evaluation procedure used to determine the in-plane racking resistance of timber-framed wall bracing elements for use within the scope of NZS 3604. The test method shown in Figure 27 is based on subjecting three nominally identical, full-scale wall specimens to a controlled series of cyclic, in-plane lateral displacements applied at the top plate level. These displacements incrementally increase in magnitude, typically including target amplitudes of ±15 mm, ±22 mm, ±29 mm, ±36 mm, and ±43 mm, to simulate progressively increasing lateral demands consistent with both wind and earthquake loading scenarios. During testing, the applied force and corresponding top plate displacement are continuously recorded to establish a detailed load displacement relationship for each specimen. This approach enables the identification of key structural characteristics, including elastic stiffness, ultimate strength, energy dissipation capacity, residual deformation, and overall ductility of the bracing system.

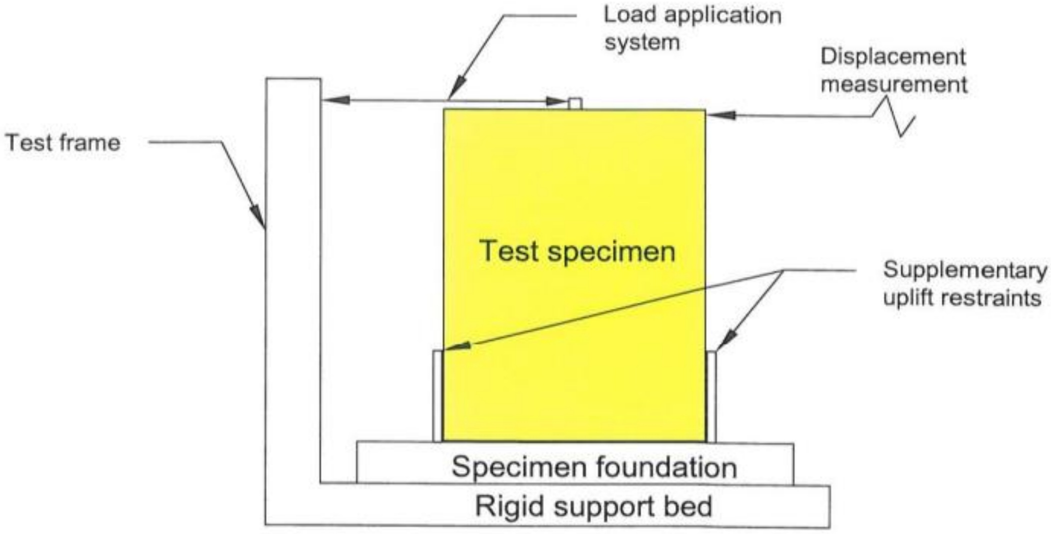

Figure 27-P21 Test Arrangement [51]

The P21 procedure evaluates two primary performance criteria. First, the serviceability limit state ("SLS") performance is derived from the force resisted by the wall at a nominated displacement level, ensuring that deformation and damage remain acceptable under frequent, low-intensity loading. Second, the ultimate limit state ("ULS") performance is determined based on the maximum force resisted during the fourth cycle of the selected displacement series, adjusted by an inelastic behaviour factor (K4) that accounts for the ductility of the system. These values are further modified by a systems factor (K2) to reflect the redundancy present in typical residential structural configurations. Bracing ratings are then calculated for both wind and earthquake and expressed in BU. When used in specifically engineered buildings or with materials outside conventional timber-framed construction, additional engineering judgement and justification are required, particularly in relation to ductility behaviour and load-resisting mechanisms. A critical feature of the P21 methodology is that the final bracing rating assigned to a system is the average of the three tested specimens.

Within the BRANZ P21 test methodology, result reliability and repeatability are controlled through the application of the displacement recovery factor (K_1) and the 20% consistency criterion. The K_1 factor is used to assess the degree of residual deformation that remains in a specimen following the initial 8 mm displacement cycles. It is defined in the equation below C where represents the average residual displacement recorded when the applied force returns to zero after the first 8 mm cycle.

$$K_1 = 1.4 - C/8 \leq 1.0 \qquad \text{(Eq.5)}$$

This parameter reflects the extent to which the wall exhibits predominantly elastic behaviour at serviceability-level deformation. If the calculated value of K1 is less than 0.8, the specimen is deemed to have experienced excessive permanent deformation, and its results are rejected and replaced with an additional test specimen. If more than one specimen fails this criterion, the entire bracing system is classified as unacceptable for rating purposes. In addition to the K1 check, the P21 procedure applies a 20% result variation limit to control the influence of anomalous test results. When averaging push and pull forces, if the force measured in one direction exceeds the force measured in the opposite direction by more than 20%, it is capped at 1.2 times the lower value prior to averaging. Similarly, during the final determination of the bracing rating for wind and earthquake, if the rating obtained from any specimen exceeds the rating of either of the other two specimens by more than 20%, that value is reduced to a maximum of 1.2 times the lower result before calculating the final average. This mechanism prevents a single unusually strong specimen from disproportionately increasing the overall BU rating and ensures that the published value represents consistent and repeatable construction performance rather than isolated peak behaviour.

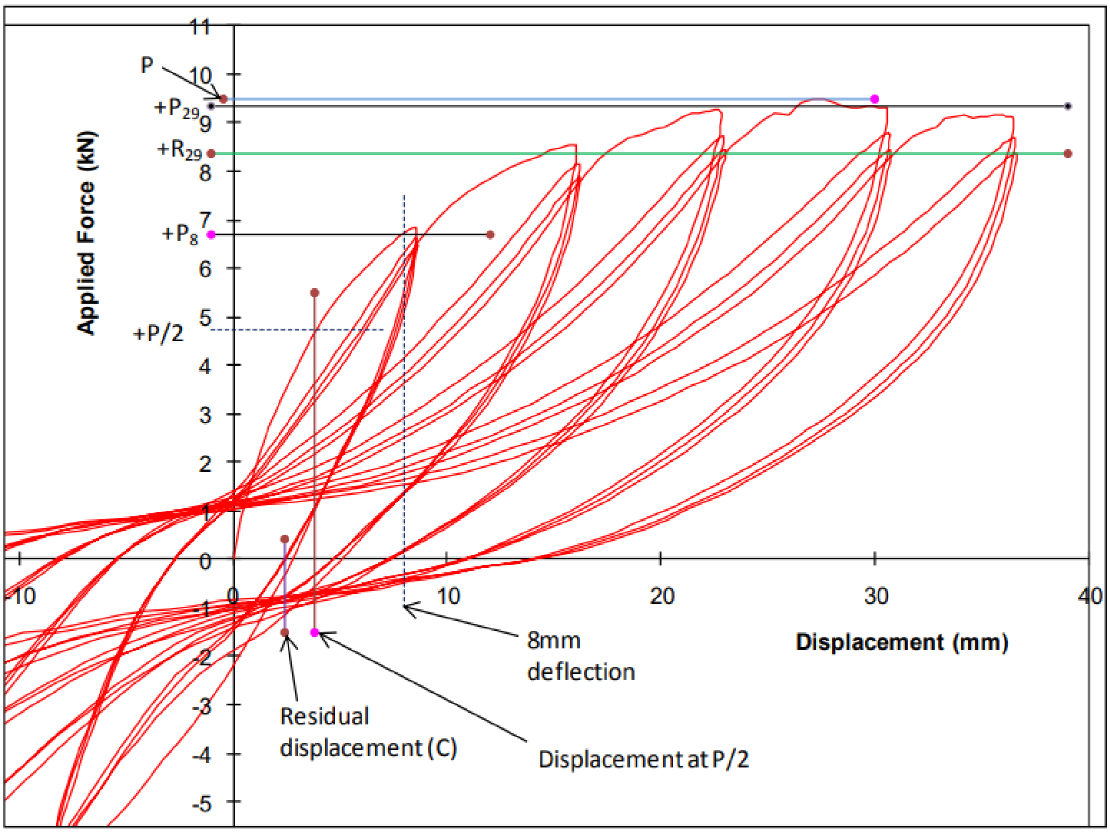

Figure 28-Force and displacement measurements (for y=29mm) [51]

Figure 28 illustrates a typical load displacement curve generated from the BRANZ P21 in-plane racking test, showing cyclic force displacement behaviour and key evaluation parameters including force at 8 mm displacement (P_8), peak load (P), force at half of the peak load (P/2), residual resistance (R_{29}), and residual displacement (C), which form the basis for calculating the nominal bracing capacity and corresponding BU for a tested wall bracing system.

The curve demonstrates a distinctly nonlinear behaviour, which is characteristic of wall bracing systems subjected to cyclic lateral deformation. At small displacements, the response is approximately linear, representing the initial elastic stiffness of the sample wall assembly and its connection system. As displacement increased, a gradual reduction in stiffness was observed, indicated by the flattening of the hysteresis loops. This behaviour exemplifies the gradual mobilisation of connections and localised deformation within the test specimen and its fixings.

The force recorded at a horizontal displacement of 8 mm, denoted as P8, is a key performance indicator in the P21 procedure and is used to derive the nominal serviceability bracing capacity of the system [51]. This value represents a deformation level associated with serviceability type events, such as moderate wind and low to moderate seismic actions, where significant structural damage is not expected.

The maximum force, P, attained during the test corresponds to the ultimate resistance of the wall specimen under monotonic envelope loading. Beyond this point, stiffness degradation and strength reduction are observed, which is consistent with the development of damage mechanisms such as localised shear deformation within the wall, fastener yielding, and minor separation at connection interfaces. The force corresponding to half of the peak load (P/2) and the associated displacement is used to evaluate the secant stiffness and displacement ductility of the tested system. Residual displacement, denoted as C, is measured upon complete unloading of the specimen at the end of selected loading cycles.

6.3.1 P21 Test Verification to the FRP Wall Panel System

The P21 test remains a widely recognised and robust framework for assessing wall bracing performance in residential construction. In this study, the principles and metrics established by the P21 test provide a relevant benchmark for evaluating the structural role and potential regulatory pathway of the FRP wall panel system, particularly in relation to its capacity to deliver equivalent or superior bracing performance when compared with standard NZS 3604 timber framed wall constructions.

6.3.2 First Test Run Standard FRP Wall Panel System with No Additional Reinforcements

(a) FRP wall sample (front view)

(b) Bottom U-channel to the floor screw fixing configuration

Figure 29-FRP wall panel system with no reinforcement

The first round of BRANZ P21 racking tests conducted on the FRP wall panel system was regarded as a preliminary, baseline investigation. Its primary objective was to establish the intrinsic structural behaviour of the FRP panel wall assembly and to identify governing failure mechanisms prior to any design optimisation or reinforcement enhancement. As shown in Figure

29 (a) and (b), the tested wall panel system had a nominal plan dimension of 1050 mm (length) × 2440 mm (height) and consisted of the following configuration:

- Two full-sized FRP panels with nominal dimensions of 450 mm × 100 mm;
- One FRP corner panel with nominal dimensions of 150 mm × 100 mm;
- Adjacent FRP panels were fixed together at the overlapped joints using 4.1 mm diameter (8 gague TEK screws, with five screws per joint on each face;
- Top and bottom steel U-channels with a cross-section of 101mm × 90mm × 1.2 mm;
- U-channels fixed to two welded 100mm × 50mm × 2.5 mm RHS steel bearers using 5.5 mm (12 gauge) TEK screws at 125 mm centres;
- FRP panels secured to the both top and bottom steel U-channels with seven 4.1 mm (8 gauge) TEK screws on each side of the panels;
- No supplementary bracing straps or mechanical reinforcement incorporated in the assembly.

6.3.2.1 Test Observation Load Deflection Behaviour

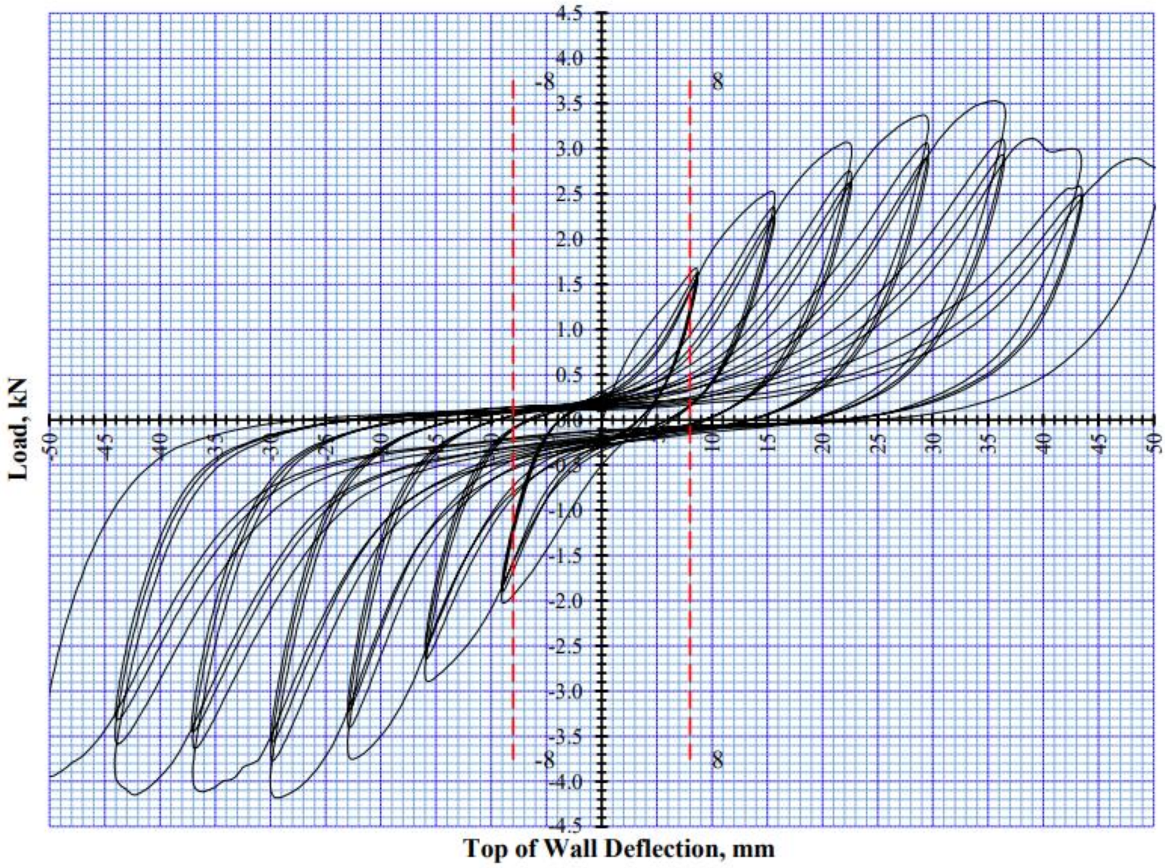

Figure 30-The load–deflection response of the 1050 mm wide FRP panel wall (No Straps)

As shown in Figure 30, the load deflection plot obtained from the first BRANZ P21 test provides critical insight into the in-plane lateral behaviour of the FRP wall panel system. The horizontal axis represents the top-of-wall deflection (in millimetres), while the vertical axis records the applied racking load (in kilonewtons). The graph illustrates a series of cyclic hysteresis loops, generated as the wall was subjected to repeated positive and negative racking displacements in accordance with the P21 loading protocol.

During the initial loading cycles, the hysteresis loops are relatively narrow, indicating a predominantly elastic response of the wall system with limited energy dissipation. As the displacement amplitude increases, the loops become progressively wider and more elongated, demonstrating the development of non-linear inelastic behaviour. This transition indicates an increased engagement of the connection system, micro-slip at fastener interfaces, and progressive deformation of the steel U-channel, rather than a brittle fracture of the FRP panel itself. No sudden loss of load was observed in any cycle, suggesting that the system exhibits ductile and progressive behaviour rather than catastrophic failure. The maximum racking resistance is reached at a top-of- wall deflection of approximately ±36 mm, where the applied load approaches ±3.8kN. Beyond this displacement, a reduction in lateral stiffness is evident.

However, the wall continues to carry a significant proportion of the peak load even at large deformations, as reflected by the persistent width of the hysteresis loops at higher deflections. This confirms the presence of residual strength and effective energy dissipation capacity. The comparatively symmetrical shape of the loops in both loading directions indicates a stable and consistent response of the wall system under cyclic loading. This symmetry is an important indicator of reliable structural behaviour under reversing lateral forces, such as those induced by earthquake ground motion. The vertical dashed lines marked at ±8 mm deflection correspond to the reference displacement for assessing nominal bracing strength. This displacement limit is intended to control damage to non-structural linings, such as plasterboard, within the wall bracing system when subjected to serviceability-level loading from wind or seismic actions [52]. The fact that the wall demonstrates substantial reserve capacity well beyond this displacement confirms that the FRP wall panel is capable of sustaining significant lateral deformation prior to reaching its capacity limit.

6.3.2.2 Failure Mode

Accompanying observations shown in Figure 31 (a) and (b) noted that bottom screws connecting the FRP panel to the U-channel had begun to pull out, and the bottom U-channel exhibited visible flexing, while the FRP panels themselves showed no cracking, crushing, or delamination. This confirms that the governing mechanism was connection-controlled rather than material-controlled, indicating that the intrinsic strength of the FRP panels exceeds that of the current connection detail. `

(a) Middle screws pulled out

(b) Screws on the edge pulled

Figure 31-Screw failure

The primary mode of degradation was the progressive withdrawal of the TEK screws connecting the lower edge of the panel to the steel U-channel, indicating that the screw to FRP interface and the associated local bearing stresses in the FRP web formed the weakest links in the lateral load path. Concurrently, the U-channel experienced plastic flexural deformation as the wall rocked under cyclic loading, which further reduced anchorage stiffness and promoted additional screw prying and pull-out. The absence of any panel cracking, delamination, or crushing confirms that neither global shear failure nor local face-sheet distress was approached, and that ultimate resistance was fully controlled by the steel connection hardware rather than by the FRP panels.

From an engineering perspective, this configuration behaves as a flexible and low-capacity bracing element: although it is capable of sustaining large global drifts ($\delta_y \approx 36$ mm), the attainable lateral resistance remains limited by base-connection withdrawal rather than by the intrinsic shear strength or stiffness of the FRP panels. Accordingly, if this unstrapped configuration were to be used as part of a structural bracing system, improvements would be required at the base connection, such as increasing screw diameter, edge distance, or fixing density, or utilising a stiffer or thicker U-channel to address the observed anchorage vulnerability and enhance overall structural performance.

6.3.2.3 Test Results and Bracing Capacity Evaluation

The initial P21 test on the FRP wall panel system, conducted without the use of reinforcements, comprised a series of cyclic loadings followed by a final monotonic push to failure. Throughout this process, lateral load and displacement responses were continuously monitored. The principal values measured from both the positive and negative loading directions are presented in Table 3.

Table 3-The key measured values from the first P21 test

Parameter	Value	Average	Meaning
P8 service load	1.63 kN -1.90 kN	1.77 kN	Load at Serviceability deflection limit (H/300)
Residual (C)	3.30 mm -3.80 mm	3.55 mm	Permanent deformation after unloading
Peak load (P)	3.52 kN -4.11 kN	3.82 kN	Maximum racking resistance achieved
y_{max}	36 mm	36mm	Maximum lateral displacement recorded
Ry	2.77 kN -3.15 kN	2.96 kN	Force recorded during the fourth displacement cycle
d @ P/2	9.5 mm	9.5 mm	Used for ductility calculation

To calculate the bracing capacity of the FRP wall panel system in accordance with the procedure set out in the BRANZ P21 test and evaluation method, it is first necessary to determine the modification factors K_1 and K_4 from the experimental results. These factors are used to adjust the measured racking resistance of the wall to account for serviceability limits and ductility considerations, respectively.

The peak racking loads measured in the positive and negative loading directions were 1.63 kN and 1.90 kN, respectively, resulting in an average ultimate racking resistance (P_8) of 1.77 kN. At the point of maximum resistance, the corresponding lateral displacement was measured as 36.0 mm, while the average residual deformation following unloading was recorded as 3.55 mm.

These measured values provided the basis for determining the deformation characteristics, ductility behaviour, and equivalent bracing capacity of the system. The structural displacement ductility factor (μ) is calculated as the ratio of maximum displacement at ultimate load to the effective yield (or first-cycle) displacement [51]:

$$\mu = \frac{y}{d} \qquad \text{(Eq. 6)}$$

The maximum displacement (y) is measured as 36 mm and the initial elastic displacement (d) is measured during the first loading cycle as 9.5 mm. Therefore, to apply equation 6, μ = 3.79.

The ductility modification factor K_4 is formally defined in BRANZ Technical Recommendation TR10 [53] as the ratio of ductility modified seismic coefficients. The ration is $K_4 = \frac{C_{b\,(0.4,4)}}{C_{b\,(0.4,\mu)}}$, where C_b (0.4,4) represents the coefficient corresponding to a reference ductility of 4.0 and C_b (0.4,μ) corresponds to the measured structural displacement ductility of the test specimen [53]. However, it is important to recognise that 2011 version NZS 3604 typically considers a structural ductility as μ=3.5 for lightweight timber-framed buildings rather than 4.0 [51] [55].

Consequently, direct substitution of μ=4.0 in analytical formulations may not accurately reflect the expected in-service behaviour of residential wall systems. For this reason, the BRANZ P21 adopts a more practical and representative implementation of the K_4 concept by providing a tabulated relationship between ductility and K4 as shown in Table 4 [51]. Intermediate values are then obtained by linear interpolation between adjacent tabulated points.

Table 4-Ductility and K4 Factors [51]

μ	1.0	2.0	2.5	3.0	3.5	4.0
K4	0.35	0.60	0.67	0.74	0.87	1.00

We interpolate between the two tabulated points:

- Lower point: $(\mu_1, K_{4,1}) = (3.5, 0.87)$
- Upper point: $(\mu_2, K_{4,2}) = (4.0, 1.00)$
- Target ductility: μ=3.79

Fraction along the interval in μ:

$$\text{Ratio} = \frac{\mu-\mu 1}{\mu 2-\mu 1} = \frac{3.79-3.5}{4.0-3.5} = \frac{0.29}{0.5} = 0.58$$

Difference in K_4 between the tabulated points:

$\Delta K_4 = K_{4,2} - K_{4,1} = 1.00 - 0.87 = 0.13$

Increment to add to the lower K_4 value:

Increment = Ratio × ΔK_4 = 0.58 × 0.13 = 0.0754

Interpolated K_4 at μ = 3.79:

$K_4 = K_{4,1}$ + increment = 0.87 + 0.0754 ≈ 0.94

In accordance with the BRANZ P21 test procedure, the displacement recovery factor K_1 is determined from the residual deformation recorded at the completion of the 8 mm displacement cycle, when the applied force returns to zero [51]. For both the push and pull directions, the residual displacements are measured, and their absolute values averaged. This average residual deformation is denoted as C. BRANZ P21 specifies that the displacement recovery factor shall be calculated using Equation 5:

For the tested FRP wall system specimen, the measured residual displacements in the push and pull directions resulted in an average value of 3.55 mm.

Substituting into equation 5 gives: $K_1 = 1.4 - \frac{3.55}{8}$ = 1.4-0.444 ≈ 0.96

6.3.2.4 Bracing Units of FRP wall panel system No mechanical reinforcement

Based on the displacement recovery factor of K_1=0.96, the ductility modification factor K_4, conservatively taken as 0.94 for the purposes of Bracing Unit (BU) calculations, and the measured test results presented in Table 3, the nominal bracing capacities of the FRP wall panel system for earthquake and wind resistance are derived using the formulae prescribed in the BRANZ P21 [51]. These values correspond to the first round P21 testing of the FRP wall panel system, undertaken without the inclusion of any supplementary mechanical reinforcement, such as straps or proprietary hold-down devices.

- Earthquake Ultimate (EQ,ULS)

$$BR_{EQ,ULS} = K_4 \times R_y \times 20 \qquad \text{(Eq. 7)}$$

Where force recorded during the fourth displacement cycle (Ry) is 2.96 kN, substituting the values gives:

$BR_{EQ,ULS} = 0.94 \times 2.96 \times 20 \approx 56$ BU

This calculation corresponds to $BR_{EQ,ULS} \approx 53$ BU/m when normalized to a 1.0 m wall length from a 1.05 m test specimen length.

- Earthquake Serviceability (EQ,SLS),

$$BR_{EQ,SLS} = (P_8 \times K1) \times \left(\frac{K2}{0.55}\right) \times 20 \tag{Eq. 8}$$

where the average of P_8 is 1.77 kN and $K_2 = 1.2$ given by BRANZ P21 [51], substituting the values gives:

$BR_{EQ,SLS} = (1.77 \times 0.96) \times (\frac{1.20}{0.55}) \times 20 \approx 74$ BU

This calculation corresponds to $BR_{EQ,SLS} \approx 70$ BU/m when normalized to a 1.0 m wall length from a 1.05 m test specimen length.

- Wind Ultimate (W,ULS)

$$BR_{W,ULS} = P \times 20 \tag{Eq. 9}$$

where the average of Peak Load is 3.82 kN, substituting the values gives:

$BR_{W,ULS} = 3.82 \times 20 \approx 77$ BU

This calculation corresponds to $BR_{W,ULS} \approx 73$ BU/m when normalized to a 1.0 m wall length from a 1.05 m test specimen length.

- Wind Serviceability (W,SLS)

$$BR_{W,SLS} = (P_8 \times K1) \times \left(\frac{K2}{0.71}\right) \times 20 \tag{Eq. 10}$$

where the average of P_8 is 1.77 kN and $K_2 = 1.2$ given by BRANZ P21 [51], substituting the values gives:

$BR_{W,SLS} = (1.77 \times 0.96) \times (\frac{1.20}{0.71}) \times 20 \approx 57$ BU

This calculation corresponds to $BR_{W,SLS} \approx 54$ BU/m when normalized to a 1.0 m wall length from a 1.05 m test specimen length.

In accordance with the design philosophy of NZS 3604, the governing design bracing capacity for a wall element is taken as the lower of the serviceability and ultimate values for each loading case[3]. On this basis, the controlling design capacities for the FRP wall panel system without any mechanical reinforcement are: Earthquake: 53 BU/m (ULS); Wind: 54 BU/m (SLS).

In summary, the first round of BRANZ P21 testing indicates that the proposed FRP wall panel system exhibits distinctly ductile cyclic behaviour under in-plane racking loads, characterised by a stable and repeatable hysteresis response, a high deformation capacity without brittle rupture, and a substantial potential for energy dissipation. The observed failure mechanism was governed primarily by connection behaviour rather than material degradation of the FRP panels, which is a favourable outcome for systems intended to resist lateral actions. These characteristics are highly desirable for lateral load resisting systems in low-risk buildings subjected to wind and seismic demands. Although these results represent only the initial phase of experimental investigation, they provide strong preliminary evidence that the FRP wall panel system possesses the fundamental mechanical attributes required to function effectively as a structural bracing element. Moreover, the findings clearly suggest that further optimisation of the connection design, such as the use of enhanced fasteners or the incorporation of additional reinforcing components (e.g. straps or proprietary hold-downs), is likely to yield even greater bracing capacities in subsequent rounds of P21 testing.

6.3.3 Second Test Run-Standard FRP Wall Panel System with 25mm Bracing Straps

Following the first round of BRANZ P21 testing, which demonstrated stable, ductile behaviour but highlighted connection-governed limitations, a second round of experimental investigation was undertaken to evaluate the structural enhancement provided by the introduction of mechanical reinforcement. In this phase, the FRP wall panel system was modified by incorporating three full-sized FRP panels without a corner panel (Figure 32 (a) and (b)) and attaching 25 mm steel straps (Figure 32 (c) and (d)). These modifications were implemented to enhance load transfer between the panel assembly and the boundary elements, as well as to mitigate localised connection deformation at the base and top restraints. The tested wall panel system had a nominal plan dimension of 1350 mm (length) × 2440 mm (height) and consisted of the following configuration:

- Three full size FRP panels: 450 mm × 100 mm;
- The three FRP panels fixed together using 4.1 mm diameter (8 gauge) TEK screws, 5 screws per joint on each face;
- Top and bottom U-channels: 101mm × 90mm × 1.2 mm, installed to the FRP panels;
- U-channels fixed to the steel bearers with 5.5 mm diameter (12 gauge) TEK screws 3 @ 25 mm spacing + 3 @ 125 mm spacing;
- Two steel bearers: 100 × 50 × 2.5 mm RHS, welded together;
- The FRP panels fixed to the U-channels using seven 4.1 mm diameter (8 gauge) TEK screws on each side;
- 25mm × 0.9 mm steel straps installed from the bearer to the FRP panel on one side;
- Each end of the strap fixed with 6 × 4.1 mm diameter (8 gauge) TEK screws.

(a) FRP wall sample (front view)

(b) FRP wall sample (back view)

	
(c) 25mm steel strap fixing (Left)	(d) 25mm steel strap fixing (right)

Figure 32-FRP Wall Panel System with 25mm Bracing Straps

6.3.3.1 Test Observation Load Deflection Behaviour

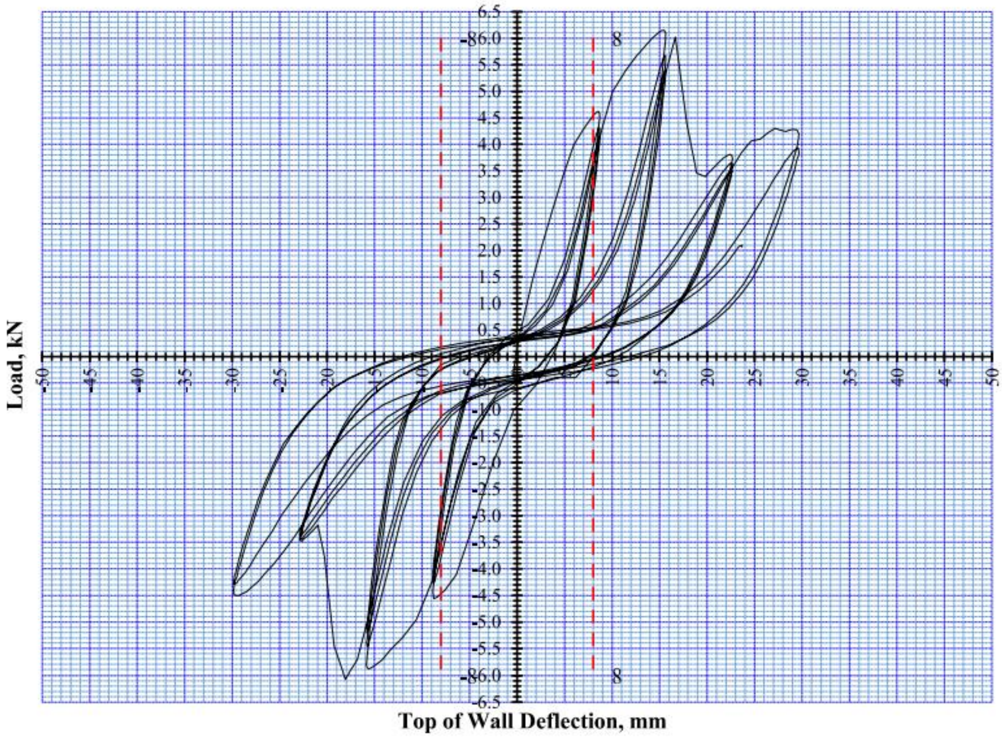

Figure 33-The load–deflection response of the 1350 mm wide FRP panel wall (25mm Straps)

Figure 33 presents the cyclic racking load–displacement response of the FRP wall panel system reinforced with 25 mm steel straps, tested in accordance with the BRANZ P21 procedure.

The specimen exhibited a maximum racking resistance of approximately +5.5 to +6.0 kN in the positive loading direction and –5.5 to –6.0 kN in the negative direction, indicating a generally symmetric strength response. This symmetry suggests balanced load transfer through the wall assembly and uniform performance of the connections in both loading directions. As the imposed displacement increased through successive cycles, the applied racking force also increased in a controlled manner, consistent with the incremental displacement protocol prescribed in BRANZ P21 [51].

The initial loading stiffness of the wall was relatively high, as indicated by the steep slope of the loops near the origin. However, with increasing displacement amplitudes, a gradual reduction in stiffness was observed, evidenced by the progressive flattening and widening of the hysteresis loops. This behaviour is indicative of progressive connection degradation, such as screw slip, local yielding, or minor deformation in the U-channel and strap interfaces, rather than a sudden loss of capacity or brittle fracture of the FRP panels.

In terms of energy dissipation, the loops enclosed a substantial area, particularly at larger displacement levels (approximately ±20–30 mm and beyond). This indicates that the system is capable of dissipating a significant amount of input energy under cyclic loading, a highly desirable property for structures subjected to seismic actions. The persistence of wide and stable hysteresis loops at increased deformations further confirms the ductile nature of the response. A degree of pinching behaviour is evident around the origin in several cycles, which is typically associated with local slip or seating effects at the connection interfaces. This behaviour is common in mechanically fastened systems and further supports the conclusion that the global response is governed by the performance of the connections, rather than by the FRP material itself.

6.3.3.2 Failure mode

Visual observations recorded during the test corroborate the graphical response. The bottom screws exhibited pull-out from the U-brackets, which aligns with the observed reduction in stiffness and changes in loop shape during larger displacement cycles. Additionally, the 25 mm straps were snapped (Figure 34) after the −15 mm cycles, corresponding to noticeable alterations in the hysteresis response at advanced stages of loading. Importantly, no visible damage or cracking was observed in the FRP panels, confirming that the primary failure mechanisms were connection-governed rather than material-driven.

Figure 34-The snapped 25mm steel reinforcement strap

The 1350 mm FRP wall strengthened with 25 mm diagonal steel straps exhibited a distinct tension-controlled failure mechanism, fundamentally different from that of the unstrapped configuration. Under increasing lateral displacement, the tension-side strap accumulated significant cyclic strain, eventually leading to tensile rupture of the thin-gauge steel. The straps “snapped,” a behaviour consistent with low-cycle fatigue or tensile fracture localised near screw holes or other regions of geometric irregularity where stress concentrations are highest. Once a strap fractured, the wall’s racking resistance dropped rapidly, with the remaining lateral load carried predominantly by the panel-to-channel screws and any residual stiffness in the damaged strap. Similar to the unstrapped wall, some distress was still evident in the base connection, particularly screw withdrawal and distortion of the U-channel. However, in this configuration the diagonal straps reliably governed the limit state, reaching their ultimate condition before connection failure became critical. No cracking, delamination, or crushing of the FRP panels was observed, confirming that damage was confined to the steel elements rather than the composite wall system.

From an engineering perspective, the addition of the 25mm bracing straps substantially increases both stiffness and strength. However, the ultimate capacity becomes constrained by the tensile capacity and fatigue resistance of the strap-screw–FRP panel connection assembly. Consequently, the system behaves as a tension-bracing mechanism with relatively limited ductility, as indicated by its lower ultimate displacement (approximately 15 mm) and the sudden post-fracture strength loss. Within a capacity-design framework, the straps effectively function as the structural “fuse,” meaning that their geometry, thickness, hole layout, steel grade, and detailing critically determine the system’s overall seismic performance.

6.3.3.3 Test Results and Bracing Capacity Evaluation- 25mm Strap Reinforced

The second-round P21 test on the FRP wall panel system, conducted with the incorporation of 25 mm steel strap reinforcements. Throughout the testing programme, the lateral load resistance and corresponding top-of-wall displacement responses were continuously monitored and recorded. The principal force–displacement values obtained from the repeated loading cycles in both directions are summarised in Table 5 and form the basis for the subsequent derivation of displacement recovery, ductility, and bracing capacity parameters.

Parameter	Value	Average
P8 service load	4.55 kN & -4.46 kN	4.5 kN
Residual (C)	3 mm & -2.70 mm	2.85 mm
Peak load (P)	6.12 kN & -5.33kN	5.73 kN

y_{max}	15 mm	15mm
Ry	4.9 kN & -4.5 kN	4.7 kN
d @ P/2	4.3 mm	4.3 mm

Table 5-The key measured values from the P21 test with 25mm steel strap reinforcement

From these values, the governing modification factors were derived:

- Displacement recovery factor (K_1) ≈ 1 (Applying Equation 5);
- Displacement ductility (μ) ≈ 3.49 (Applying Equation 6)

The value of K_1 = 1.0 signifies excellent post-cycle recovery and minimal permanent deformation upon unloading, which is a highly desirable structural characteristic in wall bracing systems. The ductility value is closely aligned with the μ=3.5 typical target range for light-frame bracing systems as specified by NZS 3604 [51][55]. Using interpolation guidance from Table 4, the corresponding ductility modification factor was conservatively taken as: K_4 = 0.88.

6.3.3.4 Bracing Units of FRP Wall Panel System with 25mm Strap Reinforcement

Following the same BRANZ P21 based analytical framework adopted for the unreinforced FRP wall specimen in the previous section, the present section determines the bracing capacities of the 25 mm strap-reinforced FRP wall for both serviceability and ultimate limit states, considering earthquake and wind actions.

- **Earthquake Ultimate (EQ,ULS)**

Using Equation 7, the ultimate earthquake bracing capacity of the 25 mm strap reinforced FRP wall panel system is determined at the ultimate limit state. With a measured force recorded during the fourth displacement cycle (Ry=4.70 kN) and a ductility modification factor of 0.88, the corresponding capacity was calculated as $BR_{EQ,ULS}$≈83 BU for the 1350 mm-long wall, equivalent to $BR_{EQ,ULS}$ ≈ 61 BU/m.

- **Earthquake Serviceability (EQ,SLS)**

For earthquake actions at the serviceability limit state, the nominal bracing capacity is calculated using Equation 8. Substituting the measured and derived parameters (P_8 = 4.5 kN, K_1 = 1.00, K_2 = 1.20), the resulting bracing capacity is $BR_{EQ,ULS}$ ≈ 197 BU for the 1350 mm wall length, which corresponds to $BR_{EQ,ULS}$ ≈ 146 BU/m when normalised by 1000mm wall length.

- **Wind Ultimate (W,ULS)**

For wind actions at the ultimate limit state, the bracing capacity is calculated using Equation 9 and applying the same peak load value (P = 5.73 kN), the wind ultimate capacity was determined to be $BR_{W,ULS} \approx 115$ BU per 1350 mm wall, or $BR_{W,ULS} \approx 85$ BU/m.

- **Wind Serviceability (W,SLS)**

In the context of wind actions at the serviceability limit state, the nominal bracing strength is directly derived from the 8 mm displacement load, as specified by Equation 11. With $P_8 = 4.50$ kN, $K_1 = 1.00$, and $K_2 = 1.20$, the calculated capacity is BRW,SLS $\approx$ 152 BU per 1350 mm wall, which is equivalent to BRW,SLS $\approx$ 113 BU/m.

Again based on the NZS 3604 design philosophy, the controlling design capacities for the 25 mm strap-reinforced FRP wall panel system are:
Earthquake (ULS): 61 BU/m; Wind (ULS): 85 BU/m.

6.3.4 Limitations of the Results of the Two Test Rounds

Although the outcomes of the two BRANZ P21 test rounds are encouraging, several limitations must be acknowledged when interpreting and applying the results. Most notably, the <20% variability requirement specified in BRANZ P21 was not satisfied [51], as only a single specimen was tested for each configuration. This limitation prevented the use of statistical averaging and the determination of a formal characteristic bracing capacity, which typically requires a minimum of three replicate specimens per configuration.

Despite these limitations, the testing programme has provided valuable qualitative and quantitative insights into the behaviour of the FRP wall panel system. The strap-reinforced specimen demonstrated stable, ductile, and repeatable cyclic behaviour, together with good deformation capacity and meaningful energy dissipation potential, which are key attributes of an effective bracing element in low-risk buildings subjected to seismic and wind actions. The findings underscore the potential for significant enhancement in bracing performance through further optimisation of the connection system. This may include the implementation of advanced fasteners, increased steel thickness, or refined strap detailing, which should be prioritized in subsequent testing phases.

6.3.5 Final Test Run-Standard FRP Wall Panel System with 100mm Customised Straps

The structural performance of the FRP wall panel system, both with and without additional mechanical bracing reinforcement, was systematically evaluated through the first two rounds of BRANZ P21 testing. The results demonstrated a clear improvement in bracing capacity during the second test phase, where the incorporation of 25 mm steel bracing straps significantly enhanced the lateral resistance of the system. This finding confirms that the structural capacity of the FRP wall panel system can be substantially increased through the integration of appropriate reinforcement mechanisms. However, although the 25 mm straps contributed additional strength and stiffness in the early stages of testing, they were unable to sustain repeated high-amplitude cyclic displacements and ultimately fractured after the −15 mm loading cycles. This failure introduced local instability and reduced the consistency of the FRP wall panel system's structural response in the latter stages of the test.

Based on the observations and analysis of the first two test rounds, a specifically designed bracing strap was therefore developed and implemented in the final round of P21 testing. The application of this newly designed strap, featuring a diamond-pattern screw arrangement, was intended to provide a more controlled and robust load transfer mechanism between the FRP panels and the steel base joist, thereby improving the stability of the connections.

6.3.5.1 Customised Steel Bracing Plate

The bracing plate illustrated in Figure 35 is a purpose-designed steel connector developed to enhance the load transfer capacity and cyclic stability of the FRP wall panel system during BRANZ P21 racking tests. The plate replaces the simple straight strap used in the second test round with a geometry-optimised anchorage device that promotes controlled deformation, improved load distribution, and reduced risk of brittle connection failure.

Figure 35-Overview of the 100mm × 400mm × 1.2 mm strap connected onto the steel joist

The bracing plate exhibits a rectangular geometry, characterised by an overall height of 400 mm, a width of 100 mm, and a thickness of 1.2 mm, which affords it a slender profile conducive to installation between the FRP wall panel and the steel base joist. The primary function of the plate is to operate in tension and shear under lateral racking loads.

Figure 36 shows a symmetrical diamond-shaped screw pattern with 4.8 mm diameter (8 gauge) TEK screws is configured about the central vertical axis of the plate. This pattern consists of two mirrored triangular arrangements, one in the upper half and one in the lower half of the plate, converging toward the central region. The diagonal alignment of the outer fasteners reflects the principal tensile load paths under in-plane racking forces, allowing stresses to be distributed across a wider area of the connection instead of concentrating at a single point. Along the plate's vertical centreline, multiple fastener holes are arranged at 30 mm vertical spacing, forming a dense anchorage zone at the region of highest force transfer. This configuration aims to improve strain compatibility and ensures that the applied forces are shared among multiple fasteners, thereby reducing the likelihood of localised failure such as screw pull-out or bearing tearing in the steel plate or FRP substrate.

(a) The plate is fixed on the corner side	(b) The bracing plate is fixed on the wall side

Figure 36-The customised bracing plate is fixed between the FRP panel and the steel joist

Figure 36 also shows at the upper and lower ends of the plate, additional fastener holes are positioned symmetrically near the corners, maintaining consistent edge distances (approximately

20 mm) from the plate boundaries. These end fixings act as primary anchorage points, providing resistance to uplift, sliding, and rotational movement of the panel relative to the base. The intermediate fasteners along the diagonal edges serve a secondary role in stabilising the connection and confining deformation within the intended bracing zone. This diamond-shaped load path is intended to enhance the ductility of the connection by promoting progressive yielding and distributed energy dissipation across multiple fasteners under cyclic loading, rather than triggering a sudden, localised fracture of a single reinforcing element. Under in-plane racking action, the conceptual load-transfer mechanism redirects tensile forces diagonally through the plate toward its central axis, thereby mobilising a broader portion of the bracing system and improving the stability of the overall response.

6.3.5.2 Final Phase Test Specimen Configuration Incorporating Customised Bracing Plate

The final phase of experimental P21 testing incorporated the customised steel bracing plate, specifically developed to enhance the connection performance the FRP wall panel system. This reinforcement was integrated into the wall assembly forming a modified load-transfer path intended to distribute racking forces more evenly through the fasteners and surrounding structural elements. By adopting a consistent specimen geometry, fixing arrangement, and loading protocol, the test series was designed to verify that the observed structural behaviour could be attributed to the customised reinforcement mechanism. The tested wall panel system had a nominal plan dimension of 1050 mm (length) × 2440 mm (height) and consisted of the following configuration:

- Two full-sized FRP panels with nominal dimensions of 450 mm × 100 mm;
- One FRP corner panel with nominal dimensions of 150 mm × 100 mm;
- Adjacent FRP panels were fixed together at the overlapped joints using 4.1 mm diameter (8 gague TEK screws, with five screws per joint on each face;
- Top and bottom steel U-channels with a cross-section of 101mm × 90mm × 1.2 mm;
- U-channels fixed to two welded 100mm × 50mm × 2.5 mm RHS steel bearers using 5.5 mm (12 gauge) TEK screws at 125 mm centres;
- FRP panels secured to the both top and bottom steel U-channels with seven 4.1 mm (8 gauge) TEK screws on each side of the panels;
- 100 mm × 1.2 mm steel straps were installed between the FRP wall and the steel joists at both ends of the wall;
- Each strap was fixed using: Nine 4.8 mm diameter (10 g) TEK screws into the bottom U FRP, Nine 4.8 mm diameter (10 g) TEK screws into the steel joist.

Three identical test specimens were constructed using this configuration and tested in accordance with the BRANZ P21 wall bracing test and evaluation procedure [51] to ensure repeatability, reliability, and statistical validity of the results.

6.3.5.3 Test Observation Load Deflection Behaviour

Figures 37,38,39 present the cyclic load–deflection hysteresis responses of the three FRP wall panel specimens (Walls 282524, 282525, and 282526) reinforced using a customised steel bracing plate and dual strap configuration.

Wall 282524

Wall 282524 demonstrated a stable and repeatable hysteresis response across the full range of applied displacements. The load–deflection curves show gradual stiffness degradation with increasing cycle amplitude, which is indicative of progressive internal damage and connection slip. The hysteresis loops are well-developed and rounded, confirming a high energy dissipation capacity and favourable ductile response. Unlike the results observed in the earlier strap-only configurations, Wall 282524 maintained mechanical integrity without strap snapping, screw pull-out, or sudden drop in resistance.

Minor pinching near the origin was observed, which is typical of connection-governed systems and can be attributed to slight joint slip and screw deformation. Although residual deformation accumulated progressively throughout the test, there was no sudden strength loss, brittle fracture, or instability was detected. This confirms that the system maintained its load resistance even after entering the post-elastic deformation range.

Wall 282525

Wall 282525 exhibited the most consistent and symmetric hysteresis loops among the three specimens. The load–displacement relationship in both positive and negative directions was highly uniform, suggesting effective and balanced force transfer within the brace plate reinforced walls. The hysteresis loops became wider and more stable as the displacement cycles increased, reflecting enhanced energy dissipation capacity and sustained post-yield strength.

Like the results observed in the test to Wall 282524, Wall 282525 also maintained mechanical integrity without strap snapping, screw pull-out, or sudden drop in resistance. The improved performance of this specimen suggests optimal interaction between the FRP panels, the customised bracing plate, and all other structural fixing, such as the U-channels, allowing gradual stress redistribution and deformation accommodation.

Wall 282526

Wall 282526 displayed the largest deformation amplitudes and exhibited slightly increased loop asymmetry compared with the other two specimens. While the hysteresis loops remained stable, an increase in pinching and a reduction in reloading stiffness were evident at larger displacements, indicating a higher degree of accumulated damage in the mechanical connections.

The increased deformability suggests more pronounced vertical sliding between adjacent FRP panels, which in turn contributed to additional screw shear and gradual degradation of joint stiffness. Despite these effects, no abrupt strength degradation occurred, and the wall continued to sustain cyclic loading without catastrophic failure.

This behaviour indicates that Wall 282526 experienced a greater degree of progressive joint degradation, yet still maintained its structural integrity due to the ductile action provided by the customised bracing plate and strap system.

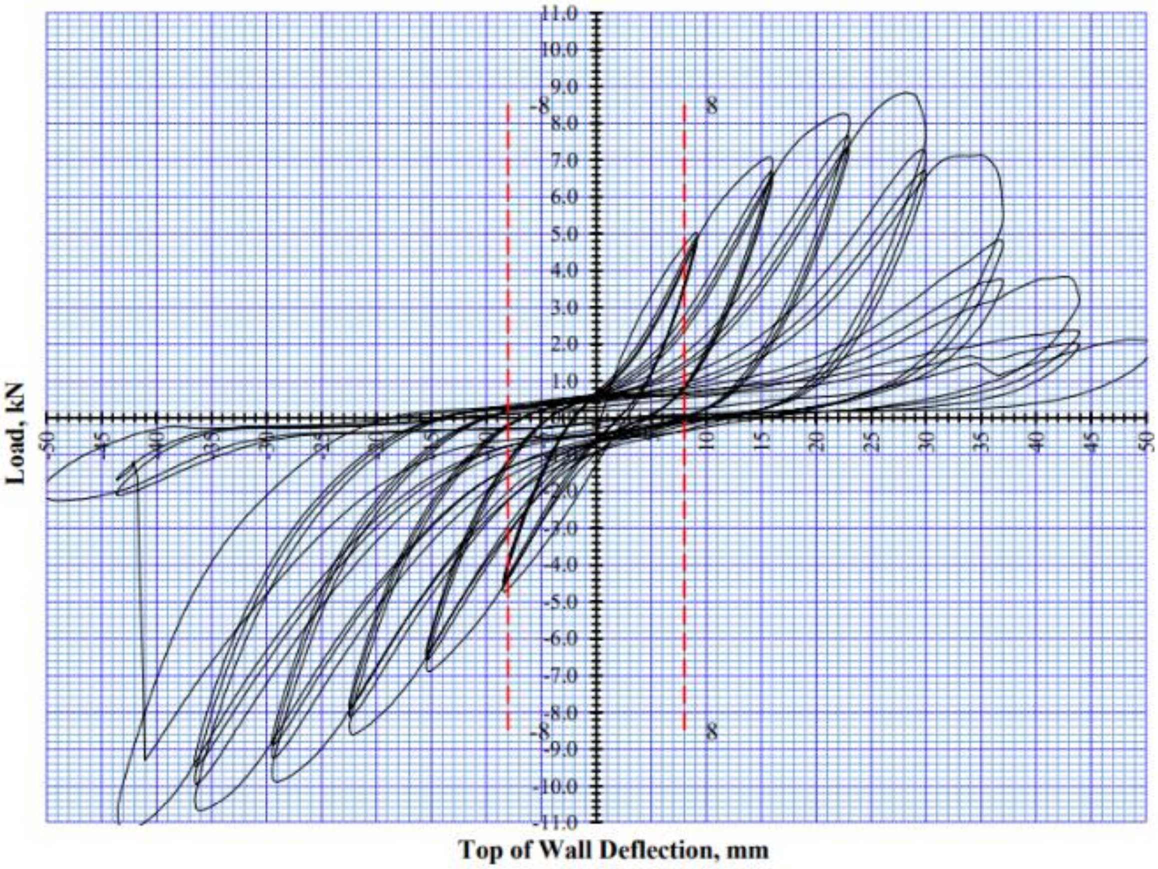

Figure 37-The load–deflection response of wall specimen 282524

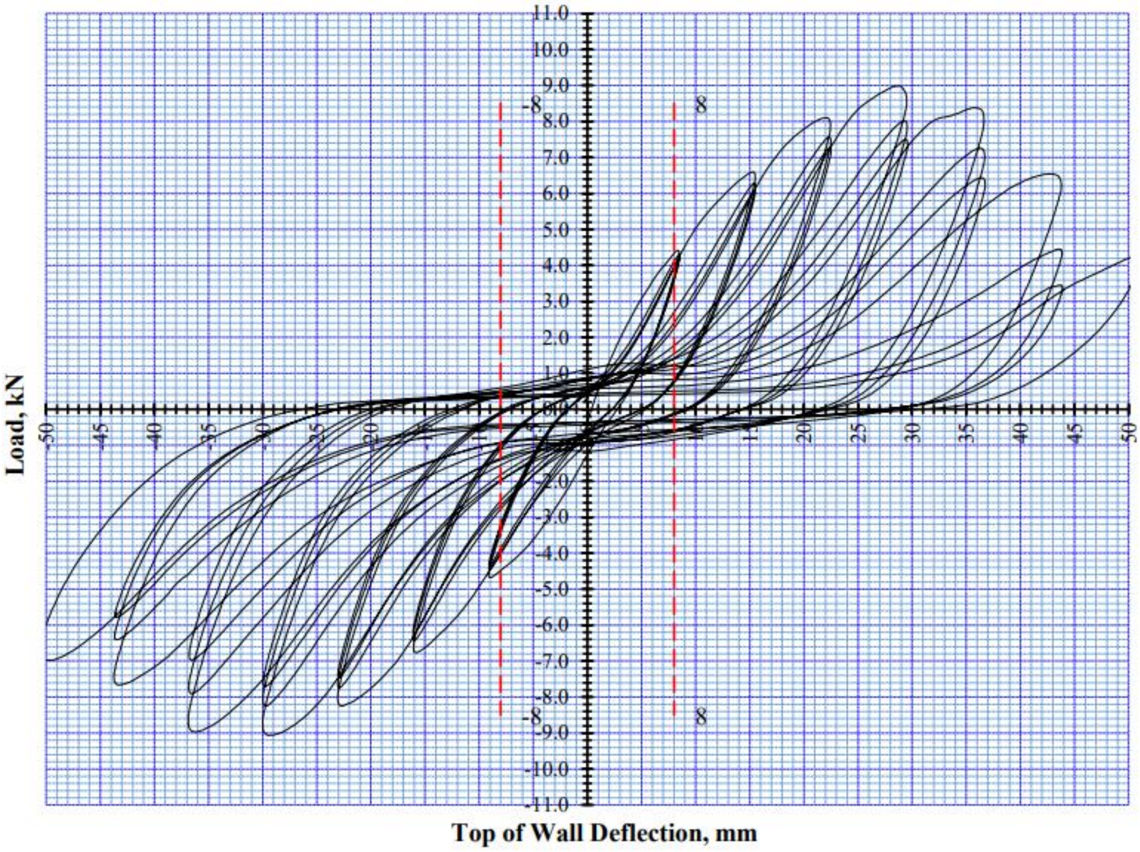

Figure 38-The load–deflection response of wall specimen 282525

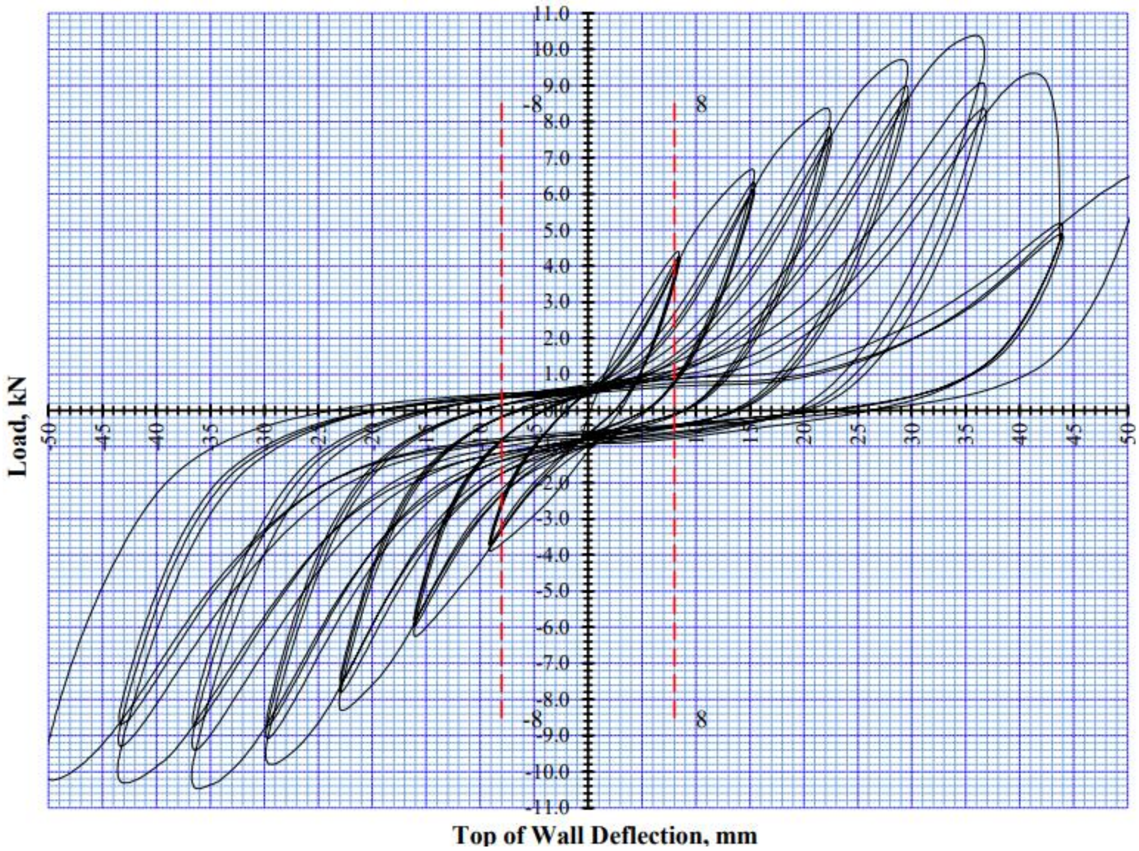

Figure 39-The load–deflection response of wall specimen 282526

6.3.5.4 The Behaviour of the Customised Bracing Plate During the Testing

Figures 40 (a) and (b) illustrate the deformation of the bracing plates on each side of the sample walls under increased load pressure. The figures demonstrate that the customized bracing plates functioned as a flexible suspension mechanism. As load was transferred through the FRP wall panel system, the bracing plate fixed at the far end of the wall was observed to bend under tension, while the plate at the near end deformed in turn during load reversal. This alternating bending behaviour indicates that both bracing plates were engaged sequentially and collectively, rather than concentrating demand at a single connection. Such interaction allowed forces to be redirected and progressively dissipated through controlled deformation of the plates and straps, rather than being resisted purely by rigid fixation. Consequently, the system was able to maintain wall stability while permitting a greater degree of movement in a more regulated and controlled response.

(a) Corner Strap Flexing (b) Wall Side Strap Flexing

Figure 40-Behaviour of the customised bracing plate during the testing

6.3.5.5 Other Observations:

Across all three tests, apart from the specially designed bracing plates operated as flexible suspension elements, the following consistent behavioural mechanisms were also observed:

- The FRP panels experienced controlled vertical sliding relative to one another, which reduced stress concentration and acted as a form of mechanical energy dissipation.
- Several connection screws at the joints between the FRP panels exhibited shear cutting and progressive loss of capacity due to repeated sliding cycles. This mechanism governed the gradual stiffness reduction observed in the hysteresis loops.
- No significant screw pull-out was observed from either the U-channel fixings or the customised bracing plate fixings.

Overall, from the engineering perspective, the observed sliding movement, strap flexing, and controlled degradation demonstrate that the customised bracing plate configuration enables the FRP wall system to absorb and dissipate shear forces imposed by earthquake and wind actions more effectively than the previous reinforcement strategies.

6.4 Bracing Units of FRP Wall Panel System with Customised Bracing Reinforcement

The subsequent section delineates the testing results of the three FRP wall specimens and provides a comprehensive derivation of the corresponding bracing capacities in accordance with BRANZ P21 provisions. This analysis ultimately establishes the optimized design Bracing Units for the FRP wall panel system.

The principal values measured from both the positive and negative loading directions of Wall 28254 are presented in Table 6.

Table 6-The key measured values from Wall 28254

Parameter	Value	Average
P8 service load	4.88 kN & -4.50 kN	4.69 kN
Residual (C)	1.50 mm & -2.40 mm	1.95 mm
Peak load (P)	8.40 kN & -9.83 kN	9.12 kN
y_{max}	29 mm	29 mm
Ry	6.38 kN & -8.30 kN	7.34 kN
d @ P/2	6.4 mm	6.4 mm

The principal values measured from both the positive and negative loading directions of Wall 28255 are presented in Table 7.

Table 7-The key measured values from Wall 28255

Parameter	Value	Average
P8 service load	4.32 kN & -4.48 kN	4.40 kN
Residual (C)	2.30 mm & -1.80 mm	2.05 mm
Peak load (P)	9.00 kN & -9.05 kN	9.03 kN
y_{max}	29 mm	29 mm
Ry	7.05 kN & -7.12 kN	7.09 kN
d @ P/2	9.0 mm	9.0 mm

The principal values measured from both the positive and negative loading directions of Wall 28256 are presented in Table 8.

Table 8-The key measured values from Wall 28256

Parameter	Value	Average
P8 service load	4.30 kN & - 3.67 kN	3.99 kN
Residual (C)	2.40 mm & -2.00 mm	2.20 mm
Peak load (P)	9.71 kN & -9.79 kN	9.75 kN
y_{max}	29 mm	29 mm
Ry	8.30 kN & -8.32 kN	8.31 kN
d @ P/2	9.7 mm	9.7 mm

Table 9 presents the average measured response parameters obtained from the three FRP wall specimens tested in the final round of BRANZ P21 tests, which are subsequently used as the basis for calculating the bracing capacity of the wall system in accordance with the BRANZ P21.

Table 9-The key measured values in average from the three wall specimens

Parameter	Average
P8 service load	4.36 kN
Residual (C)	2.07 mm
Peak load (P)	9.30 kN

y_{max}	29 mm
Ry	7.58 kN
d @ P/2	8.37 mm

From these values, the governing modification factors were derived:

- Displacement recovery factor (K_1) ≈ 1 (Applying Equation 5);
- Displacement ductility (μ) ≈ 3.47 (Applying Equation 6)

The value of K_1 = 1.0 signifies excellent post-cycle recovery and minimal permanent deformation upon unloading, which is a highly desirable structural characteristic in wall bracing systems. The ductility value of 3.47 is closely aligned with the μ=3.5 typical target range for light-frame bracing systems as specified by NZS 3604 [51][55]. Using interpolation guidance from Table 4, the corresponding ductility modification factor was conservatively taken as: K_4 = 0.87.

- **Earthquake Ultimate (EQ,ULS)**

Using Equation 7, the ultimate earthquake bracing capacity of the 100mm bracing plate reinforced FRP wall panel system is determined at the ultimate limit state. With a measured force recorded during the fourth displacement cycle (Ry = 7.58kN) and a ductility modification factor of 0.87, the corresponding capacity was calculated as $BR_{EQ,ULS}$ ≈ 132 BU for the 1050 mm-long wall, equivalent to $BR_{EQ,ULS}$ ≈ 126 BU/m.

- **Earthquake Serviceability (EQ,SLS)**

For earthquake actions at the serviceability limit state, the nominal bracing capacity is calculated using Equation 8. Substituting the measured and derived parameters (P_8 = 4.36 kN, K_1 = 1.00, K_2 = 1.20), the resulting bracing capacity is $BR_{EQ,ULS}$ ≈ 190 BU for the 1050 mm wall length, which corresponds to $BR_{EQ,ULS}$ ≈ 181 BU/m when normalised by 1000mm wall length.

- **Wind Ultimate (W,ULS)**

For wind actions at the ultimate limit state, the bracing capacity is calculated using Equation 9 and applying the same peak load value (P = 9.30 kN), the wind ultimate capacity was determined to be $BR_{W,ULS}$ ≈ 186 BU per 1050 mm wall, or $BR_{W,ULS}$ ≈ 177 BU/m.

- **Wind Serviceability (W,SLS)**

In the context of wind actions at the serviceability limit state, the nominal bracing strength is directly derived from the 8 mm displacement load, as specified by Equation 11. With P_8 = 4.36 kN, K_1 = 1.00, and K_2 = 1.20, the calculated capacity is BRW,SLS ≈ 147 BU per 1050 mm wall, which is equivalent to BRW,SLS ≈ 140 BU/m.

According to the design philosophy outlined in NZS 3604, the governing design bracing capacity for a wall element is determined by the lesser of the serviceability and ultimate values for each loading scenario [3]. Therefore, the controlling design capacities for the 100 mm bracing plate reinforced FRP wall panel system are as follows:

Earthquake (ULS): 126 BU/m; Wind (SLS): 140 BU/m.

6.4.1 Comparative Analysis of P21 Load–Deflection Response

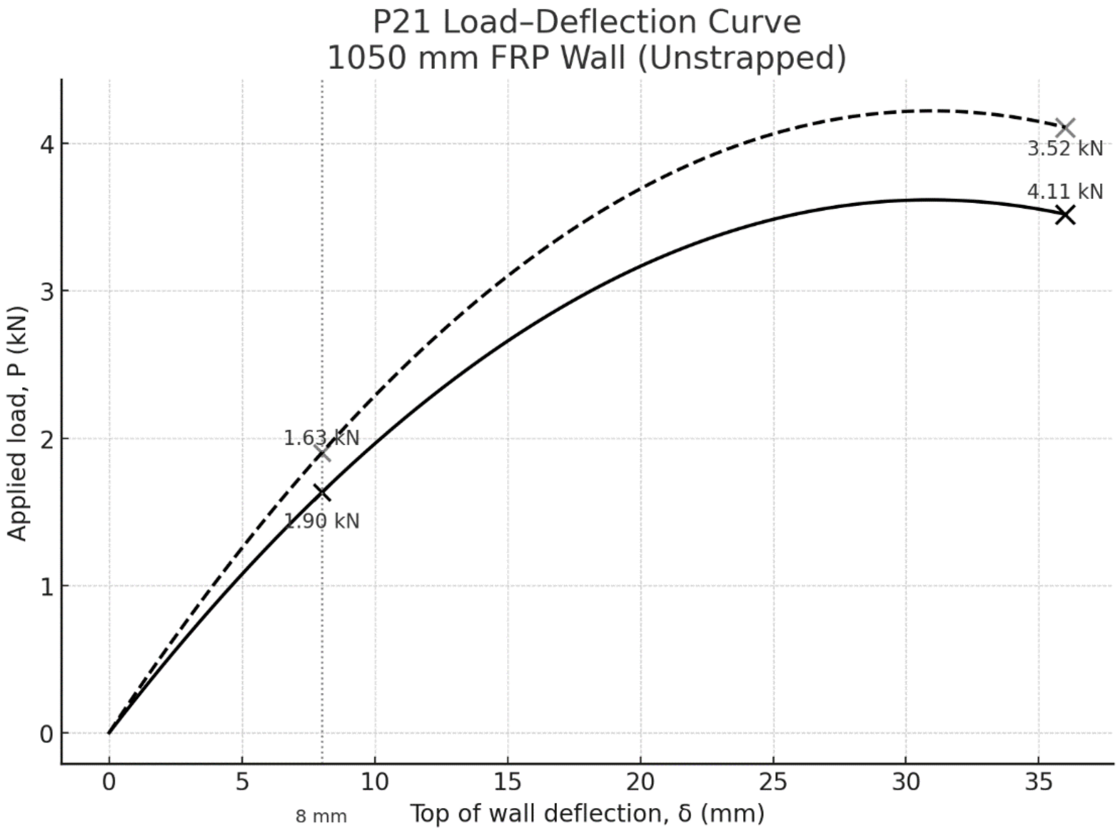

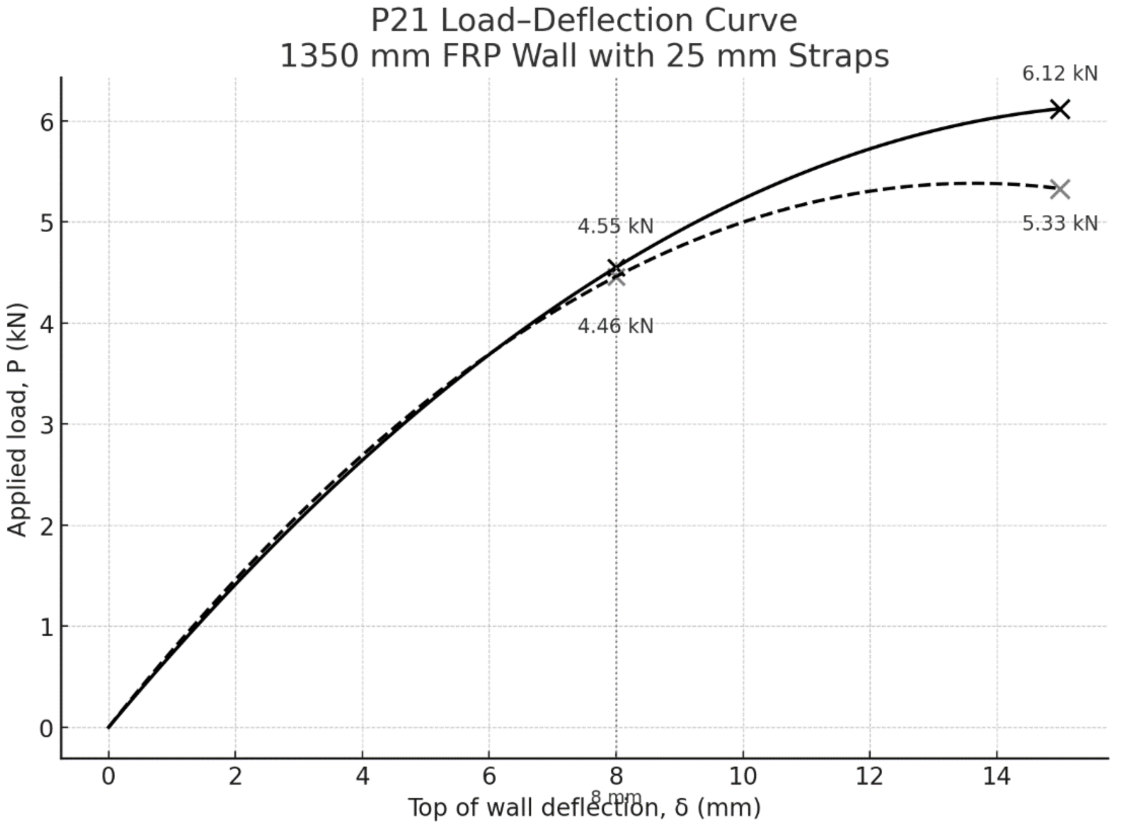
P21 Load–Deflection Curve
1350 mm FRP Wall with 25 mm Straps
6.12 kN
4.55 kN
5.33 kN
4.46 kN
Applied load, P (kN)
Top of wall deflection, δ (mm)
8 mm

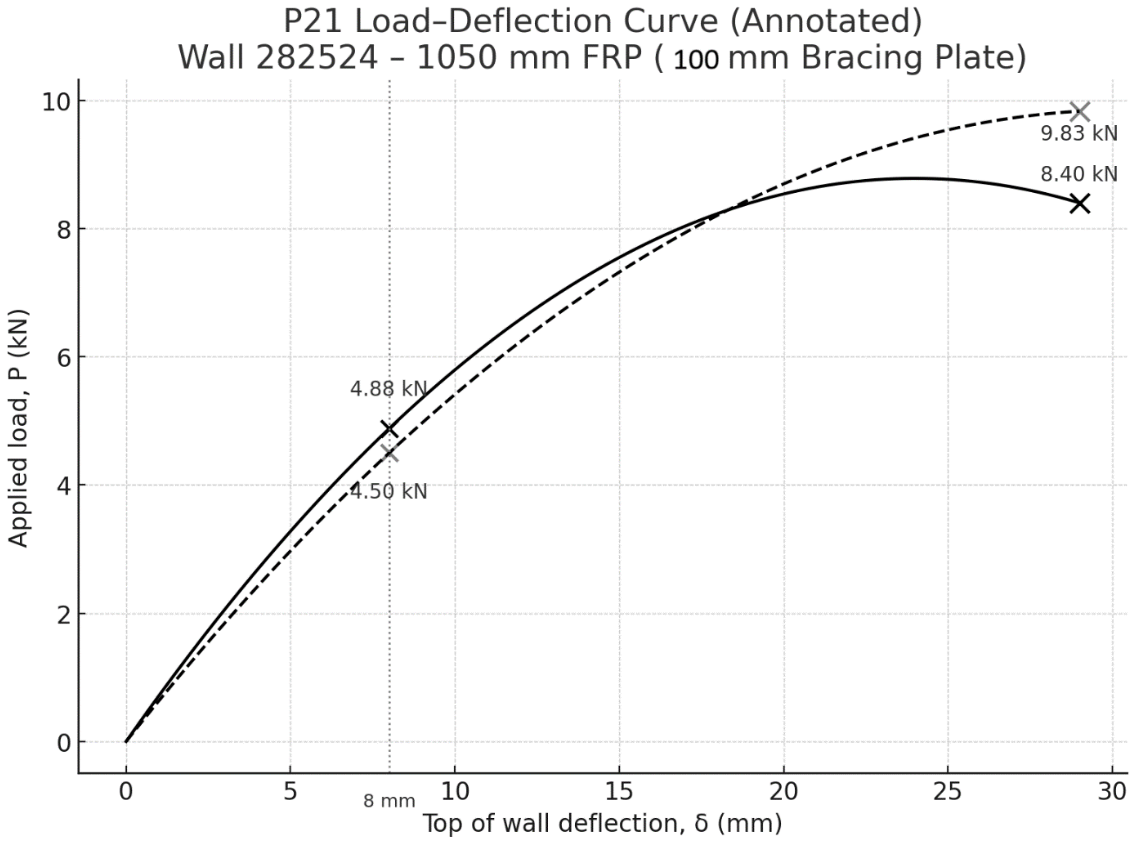
P21 Load–Deflection Curve (Annotated)
Wall 282524 – 1050 mm FRP (100 mm Bracing Plate)
9.83 kN
8.40 kN
4.88 kN
4.50 kN
Applied load, P (kN)
Top of wall deflection, δ (mm)
8 mm

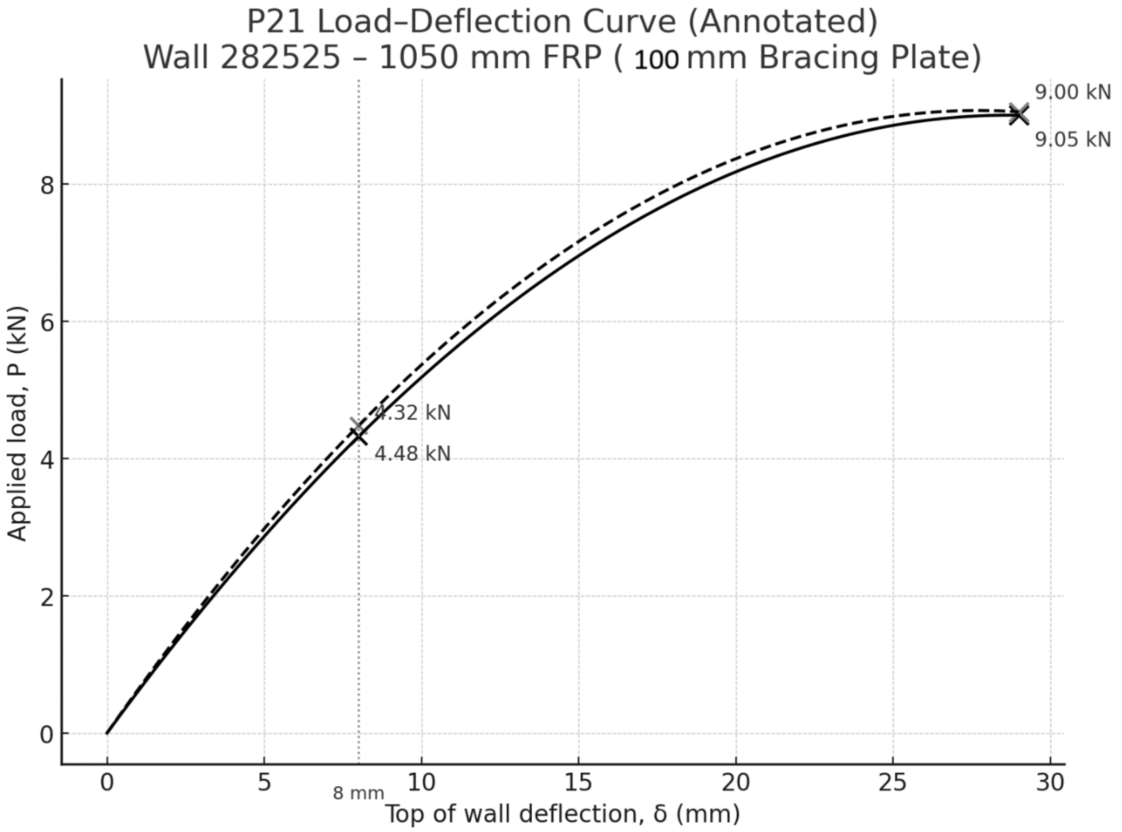
P21 Load–Deflection Curve (Annotated)
Wall 282525 – 1050 mm FRP (100 mm Bracing Plate)
9.00 kN
9.05 kN
4.32 kN
4.48 kN
Applied load, P (kN)
8 mm
Top of wall deflection, δ (mm)

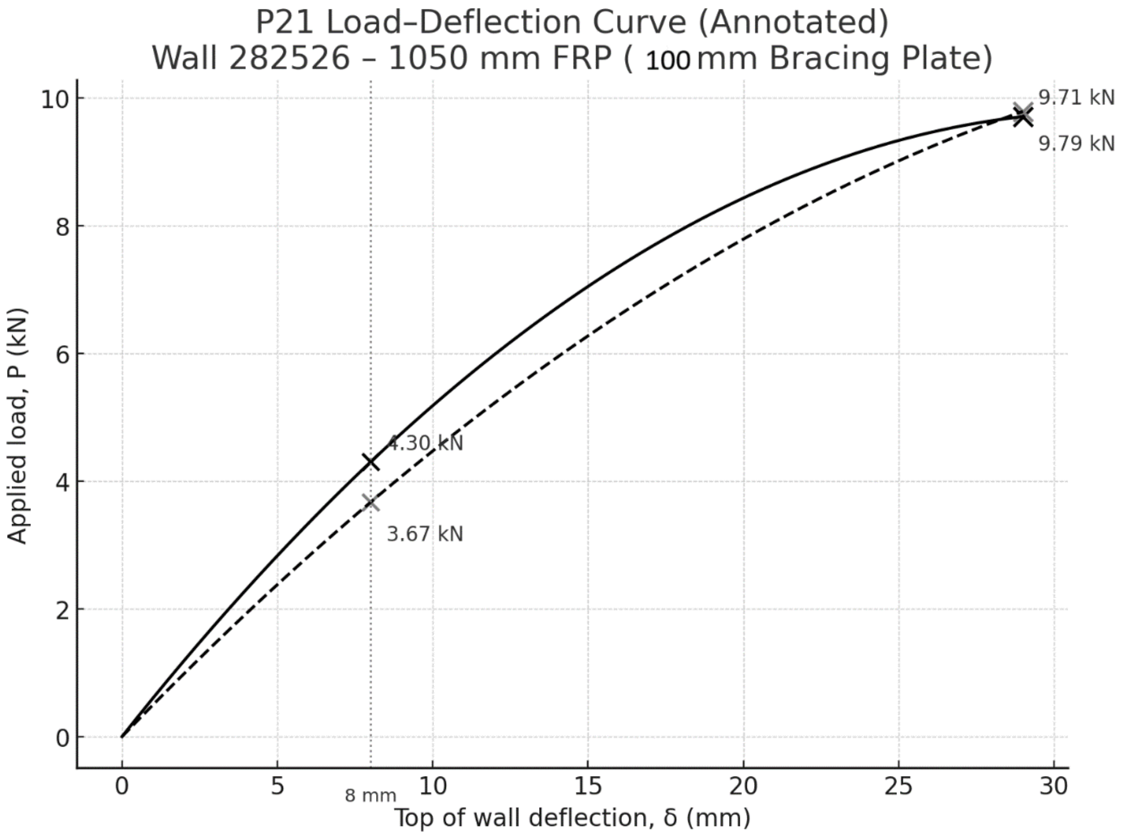
P21 Load–Deflection Curve (Annotated)
Wall 282526 – 1050 mm FRP (100 mm Bracing Plate)
9.71 kN
9.79 kN
4.30 kN
3.67 kN
Applied load, P (kN)
8 mm
Top of wall deflection, δ (mm)

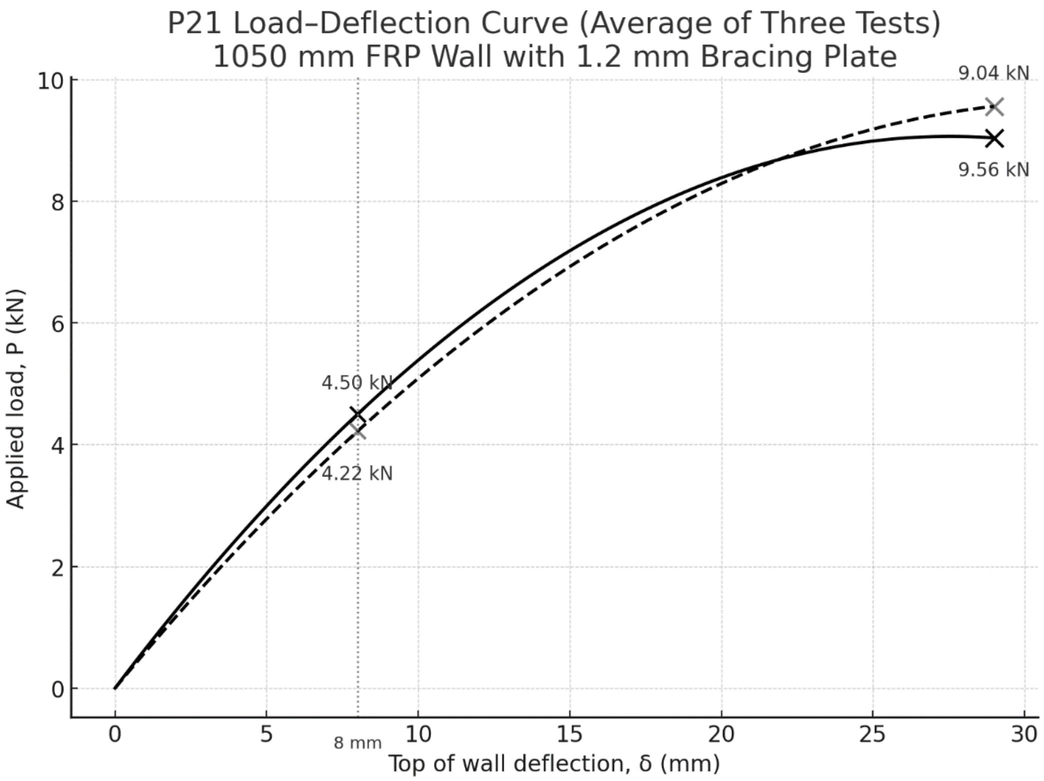

From an engineering perspective the reconstructed P21 load–deflection curves tell a very clear story about how the different FRP wall configurations change stiffness, strength and ductility.

6.5 Serviceability Stiffness and Strength (δ = 8 mm)

Using the P21-defined serviceability displacement of 8 mm, the 1050 mm unstrapped wall resists on average about 1.77 kN (midpoint of 1.63 and 1.90 kN), giving an effective serviceability stiffness of roughly 0.22 kN/mm. In contrast, the 1350 mm wall with 25 mm straps carries about 4.50 kN at 8 mm, and the 1050 mm bracing-plate wall (average of three tests) about 4.36 kN. For the 1050 mm specimens this means the bracing-plate wall has around 150% higher serviceability resistance and stiffness than the unstrapped wall at the same drift. Even when normalised per metre of wall length, the progression is clear:

- Unstrapped 1050 mm: ~1.68 kN/m at 8 mm
- 25 mm strap 1350 mm: ~3.34 kN/m at 8 mm
- 100 mm × 1.2mm bracing plate 1050 mm (avg): ~4.15 kN/m at 8 mm

So in terms of serviceability, the 100 mm×1.2 mm bracing-plate configuration provides roughly 2.5× the lateral stiffness and resistance per metre compared with the unstrapped wall, and is also significantly stiffer than the 25 mm strap configuration.

6.5.1 Ultimate Lateral Capacity

At the ultimate displacement δ_γ, the unstrapped 1050 mm wall reaches only about 3.8 kN on average (3.52–4.11 kN). The 25 mm strap wall achieves roughly 5.7 kN, while the 100mm bracing-plate wall average reaches about 9.3 kN.

Relative to the unstrapped case, this corresponds to an increase in ultimate load of about 50% for the 25 mm straps and about 140% for the bracing-plate configuration. Normalised per metre, the bracing-plate wall again stands out, with an ultimate resistance of 8.85 kN/m, compared with 3.63 kN/m for the unstrapped wall and 4.24 kN/m for the strapped 1350 mm wall. In simple terms, the 100mm bracing plate roughly 2-3 times of the ultimate racking capacity per metre compared with the baseline unstrapped FRP wall.

6.5.2 Ductility and Deformation Capacity

The ultimate displacement also reveals important behavioural differences. The unstrapped wall reaches its peak at about 36 mm, but at relatively low load. The system is quite flexible but weak. The 25 mm strapped wall peaks at only 15 mm, indicating a much stiffer but less deformable response and strength-focused but with limited drift capacity. The wall sample reinforced with 100mm straps sits between these in terms of displacement ($\delta_\gamma \approx 29$ mm) but at a much higher load level. This implies a desirable combination of high strength and significant deformation capacity, i.e. a more ductile response compared with the 25 mm strap case, and much higher strength than the unstrapped wall at similar or smaller drifts.

6.5.3 Directional Symmetry and Robustness

Across all configurations the positive and negative directions are reasonably close, with differences typically within about 5–10% of each other at both P_8 and P. This is consistent with a geometrically symmetric wall layout and symmetric fixing details: there is no indication of pronounced eccentricity or one-sided weakness. For the bracing-plate walls, the three individual specimens (282524, 282525, 282526) cluster tightly around the averaged curve, with ultimate loads between about 8.4–9.8 kN and similar δ_γ values. That spread is acceptable for full-scale cyclic testing and suggests that the bracing-plate detail provides repeatable structural performance rather than being overly sensitive to local variability.

6.5.4 Overall Engineering Interpretation

Taken together, the envelope curves indicate that:

- The baseline unstrapped FRP wall behaves as a relatively flexible, low-capacity system.
- Adding 25 mm straps significantly improves stiffness and strength, but with a relatively low ultimate displacement, implying a stiffer, more limited-ductility response.
- The 1.2 mm bracing-plate system delivers the most favourable combination: very high stiffness and strength at serviceability, substantially increased ultimate capacity per metre, and good deformation capacity compared with the strapped wall.

6.6 P21 < 20% Consistency Check

In accordance with the ±20% consistency requirement specified in BRANZ P21 [51], the three FRP wall specimens (Lab No. 282526, 282524 and 282525) were evaluated by comparing their individual bracing capacities against the mean values derived from the test set. The percentage variation for specimen 282524 was −5%, +11%, −3% and +11%, for specimen 282525 −10%, +1%, −5% and +1%, and for specimen 282526 +13%, +14%, +7% and −14%, across the four calculated bracing parameters (Earthquake and Wind, at both ultimate and serviceability limit states). None of the individual results exceeded the ±20% threshold relative to the other two specimens. Consequently, the adjustment rule specified in BRANZ P21, requiring a reduction to 1.2 times the lower value when a difference exceeds 20%, was not triggered in this test series.

This confirms a high level of repeatability and consistency in the structural performance of the brace reinforced FRP wall panel system and validates the use of the simple average values of all three specimens as representative Bracing Unit capacities for subsequent design calculations.

6.7 Verification of the 1% Damage-Control Storey Drift

The adoption of a 1% storey drift limit as the damage-control threshold in this study is directly based on the design guidance established in Section 3.7 of BRANZ Study Report SR337 [56]. In the guidance, the damage-control limit state for light timber-framed residential buildings is defined as a storey drift of 1%, on the basis that the rated bracing capacity of plasterboard-sheathed timber framed walls of reasonable lengths is typically reached at a lateral deflection of approximately 22 mm [56]. The storey drift of 1% (22mm lateral deflection) represents the deformation level at which conventional timber framed bracing walls begin to experience significant strength degradation and softening. The guidance further specifies that this drift limit is to be evaluated at the ULS, associated with a 500-year return period seismic event, because P21-derived bracing ratings are used directly in ULS seismic design under the NZS 3604 framework. In accordance with the structural design requirements, timber-framed buildings should adhere to a 1% storey-drift limit to ensure damage-controlled seismic performance.

The BRANZ P21 test results for the FRP wall panel system provide a direct basis for assessing its compatibility with this defined damage control criterion. In the first-round test on the unreinforced FRP wall specimen, a stable and repeatable hysteretic response was observed, governed by connection behaviour rather than brittle rupture of the FRP panels. The specimen sustained lateral deformation up to an ultimate displacement of approximately 36 mm, with a measured average structural displacement ductility of 3.79. For the test wall height of approximately 2.44 m, a 1% inter-storey drift corresponds to a lateral displacement in the range of 22–24 mm. This displacement is significantly lower than the ultimate deformation capacity observed in the unreinforced FRP wall during the P21 test. It falls within a range where the wall demonstrated a ductile response, stable energy dissipation, and an absence of brittle failure.

The use of the first-round, unreinforced configuration as the primary reference for this verification is a conservative approach. This configuration represents the baseline and least-reinforced form of the FRP wall panel system. Demonstrating that even this minimum configuration can sustain lateral deformation exceeding the 1% drift threshold without loss of stability provides robust, conservative evidence of deformation compatibility with NZS3604 construction. There is no indication that the FRP wall panel system would experience strength loss or unacceptable structural damage at the 1% drift level adopted for damage control in timber framed residential construction. Therefore, when P21 derived bracing ratings for the FRP wall panel system are used in ULS seismic design of residential buildings within the scope of NZS 3604, it is reasonable to conclude that the building system satisfies the 1% storey drift damage control limit state.

6.8 Summary and Implications of the P21 Testing on the FRP Wall Panel System

In this section, the elaborated and discussed three rounds of BRANZ P21 racking tests conducted on the FRP wall panel system have progressively established a comprehensive understanding of its in-plane lateral load-resisting behaviour and bracing potential of the wall system. The first round of testing confirmed that the unreinforced FRP wall system exhibits stable, repeatable, and ductile structural response under cyclic loading, with failure mechanisms governed predominantly by connection behaviour rather than material rupture of the FRP panels. The second round, incorporating 25 mm steel bracing straps, demonstrated a notable increase in initial bracing capacity; however, the premature fracture of the straps during higher displacement cycles highlighted the limitations of generic reinforcement solutions and the need for a more robust and purpose-designed fixing strategy. The final round of P21 testing, which implemented a specially designed bracing plate and optimised mechanical fastening configuration, achieved a stable and consistent structural response without brittle failure.

In addition to the observed structural performance, the ductility of the FRP wall panel system can be formally assessed against the definition provided in NZS 1170.5 [54], which states that "a ductile structure is one where the structural ductility factor is greater than 1.25 but does not exceed 6.0." Based on the final round of BRANZ P21 testing, the average displacement ductility of the FRP wall system was calculated to be approximately $\mu \approx 3.5$. This value lies comfortably within the ductile range specified by NZS 1170 and is also closely aligned with the typical ductility assumption for timber-framed structures designed in accordance with NZS 3604.

Collectively, these test results demonstrate that the FRP wall panel system is a flexible and structurally advantageous bracing solution whose performance can be further optimised through the selection of appropriate mechanical fixing and fastening strategies to suit varying structural design needs and construction contexts. The P21 tests have therefore established a robust experimental foundation for understanding the bracing behaviour of the FRP wall panel systems, supporting their use in the structural design of NZS 3604 type low-rise residential buildings.

6.9 Case Study Building Brace Wall Design

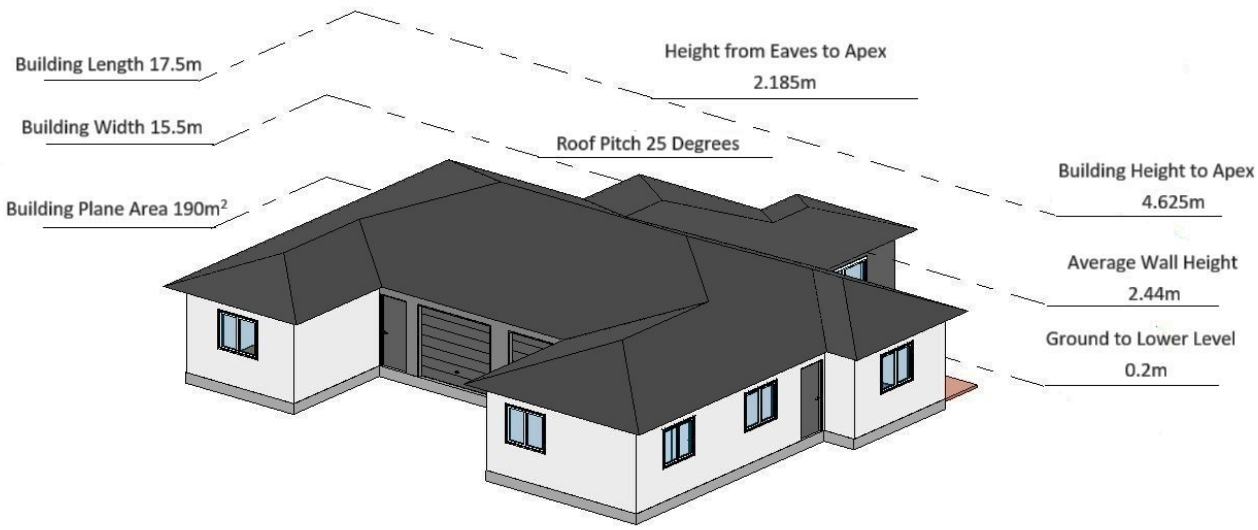

Figure 41-3D view and the dimension of the case study building

Figure 41 presents a 3D architectural representation of the case study building, with key dimensional and height parameters clearly annotated. The diagram establishes the principal geometric inputs required for subsequent structural analysis and calculations. The measurements addressed in the picture form the basis for deriving envelope areas, load paths, and load capacity assessments used throughout the later sections of this research study.

6.9.1 Demand Load Capacity for the Brace Walls

The design of wall bracing in low-rise buildings must ensure that the available lateral resistance exceeds the applied lateral demand. This principle is explicitly stated in Section 5.1.1 of NZS 3604, which requires that "wall bracing shall be designed and built to provide bracing capacity that exceeds the bracing demand." [3] This requirement establishes a fundamental safety criterion, ensuring that the structure possesses sufficient lateral load–resisting capacity to withstand both earthquake and wind actions without experiencing instability or excessive deformation. Consequently, evaluating the demand for bracing constitutes a crucial phase in the structural design and compliance process for light timber-framed buildings, as well as for any alternative building systems, such as the newly developed FRP wall panel system examined in this thesis.

Horizontal forces generated by earthquake and wind events are expressed in terms of BUs, which provide a standardised method for quantifying lateral load demand within the NZS 3604 framework. Section 5.1.2 specifies that both wind and earthquake forces must be determined in BUs, and that the respective procedures for calculation are set out in Sections 5.2 (wind) and 5.3 (earthquake) [3]. The use of BUs allows engineers to compare demand directly against the rated capacity of bracing elements, providing a rational and consistent basis for designing lateral load resisting systems.

Together, these provisions establish a comprehensive and conservative framework for the determination of lateral bracing demand in residential buildings within the New Zealand context. They ensure that both seismic events and corresponding responses are explicitly considered that site- and structure-specific parameters are robustly integrated, and that unique geometric conditions, such as hip roof configurations, are appropriately addressed. This framework provides the regulatory and methodological basis for assessing and designing the bracing capacity of the FRP wall panel system investigated in this research, and for verifying that the proposed building system can meet or exceed the minimum performance requirements set out in NZS 3604.

6.9.2 The Specified Bracing Design Parameters of the Case Study Building

The values shown in Table 10 are based on typical New Zealand residential construction as referenced in NZS3604 [3] for bracing demand and are used to characterise the permanent (self-weight) actions applied to the structural system. The dead loads presented in this table form the basis for subsequent gravity, lateral and seismic load calculations in the study, ensuring consistency between assumed material weights, structural demand assessment and compliance with the relevant requirements of NZS1170 and NZS3604.

Dead loads

Application		Dead load (kPa)
Roof	Light	0.2
	Heavy	0.6
Ceiling		0.24
Walls	Light	0.3
	Medium	0.8
	Heavy	2.2
Partitions (based on floor area)		0.2
Floor		0.6

Table 10-Assumed loads in NZS 3604 [55]

For the case study building as shown in Figure 41, the relevant parameters are:

- Building Type: Single-storey Duplex
- Roof: Light Roof (light gauge steel trusses: 0.4Kpa)
- Walls: Medium Walls (FRP Panels: 0.41Kpa + Internal Board: 0.07Kpa + External Cladding: 0.3Kpa = Total 0.78 Kpa)
- Roof Pitch: 25°
- Soil Class: D (Geotech Report)
- Seismic Zone: Hamilton (Zone 1, Figure 5.4 of NZS 3604) [3]
- Total floor area: 190 m²

According to the specified parameters, the case study building can be classified as an NZS 3604 structure, characterised by a light roof, medium walls, and a concrete slab-on-ground foundation.

6.9.3 Earthquake Bracing Demand of the Case Study Building

The earthquake bracing demand is established according to the procedure described in Section 5.3.1 of NZS3604 [3]. The demand on the building is evaluated as a function of various site and building specific parameters, including the building's location (earthquake zone), subsoil type, building height and level under consideration, overall building size, and the dead-load resulting from roofing, cladding, and floor usage. The overall earthquake demand is obtained from standardised tables (Tables 5.8, 5.9 and 5.10), with the tabulated values adjusted by appropriate factors that reflect the building’s seismic zone and site subsoil classification [3]. The resulting bracing unit value is then multiplied by the gross floor area of the building at the level being considered, providing the total earthquake bracing demand in BUs [3].

Table 5.10 - Bracing demand for various combinations of cladding for single and two-storey buildings on concrete slab-on-ground (2 kPa floor load, soil type D/E, earthquake zone 3) (see 5.3.1)

Roof cladding	Single or upper storey cladding	Lower storey cladding	Roof pitch degrees	Single storey walls (BU/m²)	Lower storey walls (BU/m²)	Upper storey walls (BU/m²)
Light roof	Light	Light	0-25	6	15	9
			25-45	6	16	9
			45-60	7	17	10
		Medium	0-25	N/A	17	9
			25-45	N/A	18	10
			45-60	N/A	19	11
		Heavy	0-25	N/A	23	10
			25-45	N/A	23	11
			45-60	N/A	24	12
	Medium	Medium	0-25	6	20	10
			25-45	7	20	11
			45-60	8	21	12
		Heavy	0-25	N/A	25	11
			25-45	N/A	26	12
			45-60	N/A	27	13

Table 11-Earthquake demand bracing calculation reference chart [3]

Based on the case study building’s parameters, it is relevant to refer to Table 5.10 of NZS3604 cited in Table 11 to calculate the earthquake bracing demand for the case study building.

Earthquake bracing is calculated for both Along and Across directions to ensure that a building can withstand seismic forces from any orientation [3]. The base earthquake bracing demand given in Table 11 for light roof and medium wall construction with roof pitch to 25° is 7 BU/m². The roof pitch of the case study building is 25°, which precisely marks the threshold between the 0-25° range for 6 BU/m² and the 25°-45° range for 7 BU/m². A conservative approach is adopted by selecting 7 BU/m² as the design baseline. Table 5.10 of NZS 3604, as reproduced in Table 12, is based on design actions corresponding to Seismic Zone 3. To reflect the site-specific seismic conditions of the case study building, located in Seismic Zone 1 on Soil Class D, the base bracing demand is modified by applying the prescribed seismic zone multiplier of 0.5 shown in Table 12.

Multiplication factors		EQ zone			
Soil class		1	2	3	4
A & B	Rock	0.3	0.5	0.6	0.9
C	Shallow	0.4	0.6	0.7	1.1
D & E	Deep to Very soft	0.5	0.8	1.0	1.5
NOTE – See 5.3.4 for additional bracing demand.					

Table 12-Multiplication Factors affiliated to Table 5.10 of NZS604 [3]

The Earthquake Demand Bracing based on NZS 3604 calculation:

- Adjusted earthquake demand = 7×0.5 = 3.5 BU/m^2.
- Total earthquake bracing demand = 3.5 BU/m^2 ×190m^2 = 665 BU

Nevertheless, the calculation of bracing demand remains incomplete, as the standard engineering design practice involves factoring both the design actions and the characteristic strengths of materials when employing verification methods, thereby ensuring appropriate safety margins[50]. NZS 3604 states that BUs derived from P21 testing do not represent characteristic strength values, and that the application of reduction factors may therefore be necessary when these BUs are used in the relevant structural design [3]. As indicated in Section 6.5.2 [3], the FRP wall panel system falls outside the scope of NZS604. Therefore, the adoption of a scale-up calculation for the P21 tested BUs in accordance with the seismic action coefficients and modification factors prescribed in the AS/NZS 1170 suite of standards, provides a logical and defensible framework for applying appropriate reduction factors to verify the bracing capacity of the FRP wall system in the case study building. Based on this rationale, while BRANZ P21 testing suggests that the FRP wall panel system achieves an overall displacement ductility approaching $\mu \approx 3.5$, a reduced and conservative value of $\mu = 2.0$ is selected in this study for the purpose of assessing the bracing capacity required to be provided by the system to the case study building.

In accordance with NZS 1170.5 [54], the horizontal design action coefficient is obtained by modifying the elastic site hazard spectrum to account for the inelastic response capacity and expected energy dissipation behaviour of the structural system. It reflects the reduced level of seismic force that the structure is required to resist, while maintaining acceptable levels of strength, ductility, and deformation control under both the ULS and SLS conditions. This study exclusively considers the ULS condition for the purpose of scale-up verification.

For the ULS, the horizontal design action coefficient, C_d (T_1), shall be as determined by the following equation [54],

$$C_d(T_1) = \frac{C(T_1)S_p}{k_\mu} \quad \text{(Eq. 11)}$$

Where,

- $C(T_1)$ = the ordinate of the elastic site hazard spectrum determined from Clause 3.1.1
- S_p = the structural performance factor determined by Clause 4.4.2: the structural performance factor, S_p, for the ULS shall be taken as 0.7, except where 1.0<μ<2.0.

For soil classes A, B, C and D:

$K\mu = \mu$ for $T_1 \geq 0.7$

$$= (\mu - 1)\,\frac{T_1}{0.7} + 1 \text{ for } T_1 < 0.7 \quad \text{(Eq. 12)}$$

Provided that for the purposes of calculating $K\mu$, T_1 shall not be taken less than 0.4s [54].

In accordance with Clause 3.1.1, the elastic site hazard spectrum for horizontal loading $C(T)$ for a given return period shall be as given by the following equation:

$$C(T) = Ch(T)\, Z\, R\, N(T, D) \quad \text{(Eq. 13)}$$

where:

- $C_h(T)$ = the spectral shape factor determined from Clause 3.1.2
- Z = the hazard factor determined from Clause 3.1.4
- R = the return period factor Rs or Ru for the appropriate limit state determined from Clause 3.1.5 but limited such that ZR_u does not exceed 0.7
- $N(T,D)$ = the near-fault factor determined from Clause 3.1.6

Equation 13 expresses the elastic spectral ordinate as the product of four independent contributing factors:

1) **Spectral shape factor, $C_h(T)$** – obtained from Table 3.1, this accounts for the amplification of ground motion at different vibration periods due to local soil conditions. In Soil Class D, $C_h(T)$ is highest in the short-period band typically associated with low-rise buildings.
2) **Hazard factor, Z** – represents the regional seismicity of the site, with higher values in more seismically active areas of New Zealand (e.g. Wellington) and lower values in less active regions (e.g. Hamilton).
3) **Return period factor, R** – adjusts the level of shaking based on the limit state being considered. For ultimate limit state (ULS) R_u corresponding to a rare, high-intensity earthquake (typically 1 in 500 years). ZR_u is limited to a maximum of 0.7 to avoid unrealistically large design accelerations in high seismicity zones.
4) **Near-fault factor, $N(T,D)$** – modifies the spectrum if the structure is located close to an active fault with potential for velocity pulses or directivity effects.

By combining these four components, Equation 13 cited from NZS 1170.5 [54] produces the elastic site hazard spectrum, $C(T)$, which represents the upper-bound seismic demand at the site. In subsequent design steps, this value is reduced through the application of ductility and performance factors to obtain the design horizontal action coefficient, $C_d(T)$, that is used in structural design. Therefore, Equation 13 forms the foundation of the seismic design process in NZS 1170.5 and provides the reference point for all further adjustments related to the structural design of the case study building.

The site of the case study building is identified as Soil Class D. Based on Table 3.1, the corresponding spectral shape factor $C_h(T)$ is taken as 3.0, which lies within the short-period plateau of the design spectrum for soft soil conditions [54]. The hazard factor for the Hamilton region is Z=0.16, as specified in Table 3.3 of NZS 1170.5 [54]. In accordance with the relevant return periods for the two limit states considered, the return-period factor for the ULS is taken as R_u=1.0, for an Importance Level 2 building [54]. As the site is not located within a near-fault zone, the near-fault factor is taken as $N(T,D)$=1.0. To implement Equation 13, $C(T)$ is determined in the present scenario as follows,

$C(T)_{\text{ULS}} = 3.0 \times 0.16 \times 1.0 \times 1.0 = 0.48$

The fundamental period of the case study building is taken as $T1$=0.40, representing a conservative estimate for a low-rise, wall-braced residential structure incorporating the proposed

FRP wall panel system. In this study, a reduced structural ductility factor of μ=2.0 is adopted for the seismic resistance calculation to reflect a prudent and conservative design assumption. This factor directly influences the magnitude of the horizontal design action coefficient and, consequently, the seismic bracing demand required for the case study building.

Accordingly, the inelastic spectrum scaling factor $k\mu$ is determined by applying Equation 12 for short-period structures $T1$<0.7 s, which governs the reduction of the elastic site hazard spectrum to design-level seismic actions.

$k\mu = (2.0\text{-}1) \times \frac{0.4}{0.7} + 1 \approx 1.57$

The standard structural ductility factor, denoted as μ=3.5, serves as a benchmark for comparison with the reduced factor of μ=2.0, which is applied to derive the conversion factor for the horizontal design action coefficient.

$k\mu = (3.5\text{-}1) \times \frac{0.4}{0.7} + 1 \approx 2.43$

By employing the two inelastic spectrum scaling factors derived from ductility assumptions of μ=3.5 and μ=2.0, Equation 11 is applied to determine the corresponding values of the ULS horizontal design action coefficient, $C_d\ (T_1)_{ULS}$. This verification approach seeks to quantify the differences in seismic demand between the structural design principles for conventional timber framed residential buildings and the design practice for the proposed FRP wall panel system.

i) Design scenario: μ=2.0

$$C_d(T_1) = \frac{0.48 \times 0.7}{1.57} \approx 0.214$$

ii) Design scenario: μ=3.5

$$C_d(T_1) = \frac{0.48 \times 0.7}{2.43} \approx 0.138$$

The conversion factor for the horizontal design action coefficient is calculated as follows,

Conversion Factor $= \frac{C_d(T_{1,}\mu=2.0)}{C_d(T_{1,}\mu=3.5)} = \frac{0.214}{0.138} = 1.55$

To apply this conversion factor to the previously calculated earthquake bracing demand for the case study building 665 BU, the total scaled-up earthquake bracing demand for the case study building constructed with the FRP wall panel system is

Earthquake Bracing Demand: 665 BU × 1.55 = 1031 BU.

Liu et al. [56] argues there is a fundamental inconsistency between the seismic bracing provisions prescribed in NZS 3604 and the seismic demand levels derived in accordance with NZS 1170.5. In particular, the minimum earthquake bracing capacity required by NZS 3604 may be insufficient to meet the stiffness and performance requirements implied by NZS 1170.5 for low-rise residential buildings [56]. Moreover, performance level for earthquake resistance achieved by timber framings designed for solely to the minimum provisions of NZS 3604 should not be considered appropriate when establishing the required performance of specifically engineered bracing systems [56]. Therefore, Liu et al. [56] suggests an increase of approximately 50% in the seismic bracing demand specified by NZS 3604 would be necessary.

The factor of 1.55 applied to the seismic bracing demand represents an approximate 55% increase over the base demand derived using a conventional structural ductility assumption of $\mu = 3.5$. It is derived directly from the ratio of the design seismic action coefficients, which are calculated in accordance with NZS 1170.5 for two distinct ductility levels: $\mu=2.0$ and $\mu=3.5$. By reducing the assumed ductility to $\mu=2.0$ for the proposed FRP wall panel system, a more pronounced inelastic spectrum scaling effect is introduced. This adjustment results in an increased horizontal design action coefficient, which leads to a greater seismic force demand. The resulting 1.55 amplification factor therefore reflects the theoretical and code-consistent increase in seismic demand associated with a lower-ductility structural system at the same site and period conditions. This adjusted seismic bracing demand establishes a deliberately conservative benchmark for the FRP case study building and should not be interpreted as being derived from, or limited to, the minimum prescriptive provisions of NZS 3604. Instead, it represents a more stringent, performance-informed demand level, anchored in the principles of NZS 1170.5, and is intended to ensure a robust and cautious evaluation of the FRP wall panel system in the absence of explicit codification for this innovative structural technology.

6.9.4 Wind Bracing Demand of the Case Study Building

Unlike earthquake bracing demand, wind bracing demand in NZS 3604 is governed primarily by the geometry, the roof form and height of the building. Section 5.2.8 of NZS 3604 specifies that for buildings with hip roofs, the wind values provided in Tables 5.5 to 5.7 must be used to determine the bracing demand in both the along and across directions [3]. This reflects the aerodynamic behaviour of hip roofs, where wind loads are distributed more uniformly around the building envelope and can therefore produce significant lateral forces in both principal directions [3]. Table 5.6 of NZS3604 shown in Table 13 below is applicable and defines demand as a function of two parameters: Floor-to-apex roof height (H) Apex-to-eaves roof height (h)

Table 5.6 – Wind bracing demand for single or upper storey walls (BU/m)

Single or upper floor level to apex (H)	Roof height above eaves (h)	High Wind Zone	
(m)	(m)	Across	Along
3	0	35	35
	1	30	35
4	0	45	45
	1	40	45
	2	40	45
5	0	55	55
	1	50	55
	2	50	55
	3	60	55

Table 13-Wind demand bracing calculation reference chart [3]

For the case study building constructed with the proposed FRP wall panel system, the parameters as shown in Figure 41 are:

- Overall height to apex (H): 4.625 m
- Stud height: 2.440 m
- Roof height above eaves (h): 4.625m – 2.440m=2.185m

For the relevant part of Table 13 above, the four surrounding grid points are:

- At H=4m, h=2m
- At H=5m, h=2m
- At H=4m, h=3m
- At H=5m, h =3m

The parameters can be simplified to:

- H≈4.5 m (mid-point between 4 m and 5 m)
- h≈ 2.0 m

Accordingly, simple linear interpolation is carried out between the two bracketing values corresponding to H=4 m and H=5 m, at h=2.0 m. Table 13 shows the relevant tabulated values at h=2.0m are:

- Across: 40 BU/m at H= 4 m & 50 BU/m at H=5 m
- Along: 45 BU/m at H=4 m & 55 BU/m at H=5 m

As H=4.5m represents the midpoint between 4 m and 5 m, the bracing demand per metre was calculated using simple averaging, producing the following interpolated values:

- **Across:** Q_{across} (H=4.5m, h=2.0m) = $\frac{40+50}{2}$ = 45 BU/m
- **Along:** Q_{along} (H=4.5m, h=2.0m) = $\frac{45+50}{2}$ = 50 BU/m

These values represent the simplified wind bracing demand per linear metre of bracing line for the case study building. The total wind bracing demand in each principal direction was then obtained by multiplying these values by the effective bracing-line length in the corresponding direction, as determined from the building layout.

Figure 44 illustrates that the dimensions of the case study building are 17.5 meters in length and 15.5 meters in width. Therefore, the wind bracing demand for the case study building are:

- **Across:** Q_{across} = 17.5 m × 45 BU/m = 788 BU
- **Along:** Q_{along} = 15.5 m × 50 BU/m = 775 BU

The total wind bracing demands for the case study building were calculated as Across the Ridge: 788 BU and Along the Ridge: 775 BU, respectively. These values, which reflect the governing lateral load requirements under High Wind Zone conditions, establish the performance benchmark against which the structural adequacy of the proposed FRP wall panel system must be evaluated. The subsequent section offers a direct comparison between the calculated demands for wind and earthquake bracing and the experimentally determined bracing capacity of the FRP wall panel system. This analysis aims to evaluate the system's suitability as a viable alternative to timber framing for constructing the case study building.

6.9.5 FRP Wall Panel System Design Capacity VS Demand Bracing Capacity

This section presents an evaluation of the design bracing capacity and required bracing demand for the case study building under both earthquake and wind loading conditions. The governing bracing demands have been determined based on the building's geometry, location, construction typology and hazard classification, while the available bracing capacity is derived from the experimentally validated performance of the proposed FRP wall panel system, including results obtained from BRANZ P21 racking tests. This assessment establishes the verification for why the FRP wall panel system is capable of satisfying or exceeding the minimum structural bracing requirements for compliance and safety in the case study building. The following subsections therefore integrate the previously determined wind and earthquake demands with the experimentally derived bracing capacity to verify the structural adequacy and robustness of the FRP solution as a primary lateral load-resisting system.

In designing the braced-wall layout for the case study building, the FRP wall panel system is treated as an alternative lateral load-resisting system to conventional timber-framed bracing walls. Figures 42 and 43 (a) depict the design methodology for both the external and internal wall configurations, which is directly influenced by the P21 test specimen configurations. In these configurations, overlapping vertical FRP panels are connected using tongue-and-groove joints secured with mechanical fasteners and anchored to steel U-channels, thereby ensuring a continuous load path from the roof to the foundation.

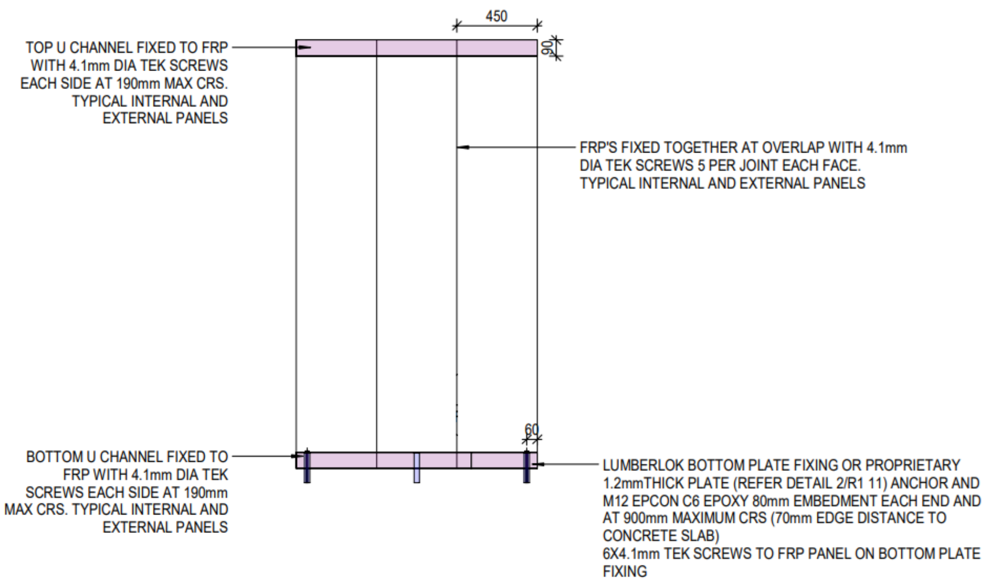

Figure 42-The external wall configurations designed with the FRP wall panel system

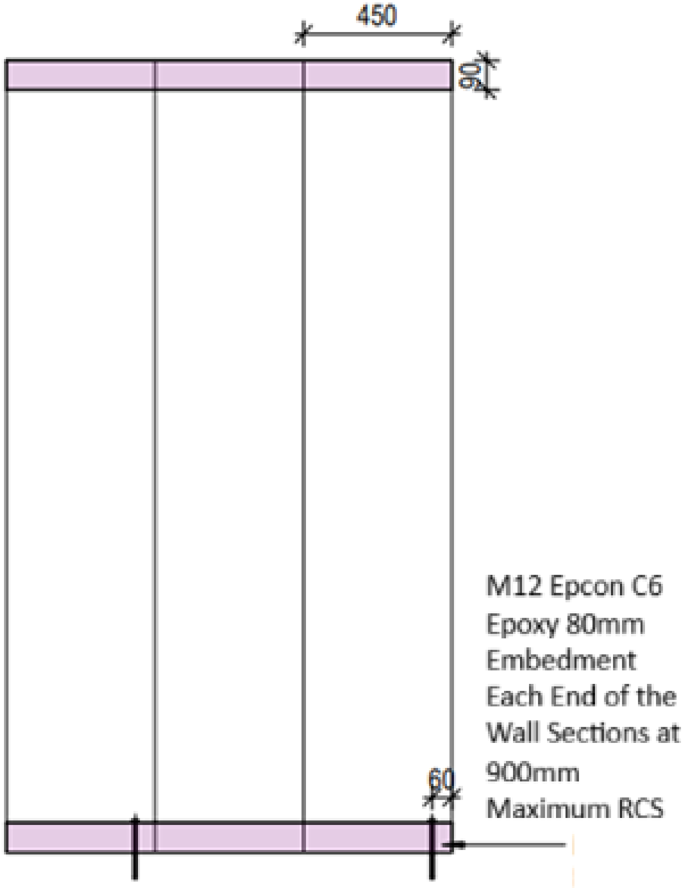

(a) The internal wall configurations

(b) Lumberlok bottom plate

Figure 43-FRP wall panel bracing configuration

The bracing layout for the case study building shown in Figure 44 adopts a simple and balanced strategy, with the primary FRP wall panel bracing line located near the longitudinal centre of the plan. This centralised configuration reduces torsional effects and allows wind and seismic forces to be transferred efficiently to the foundations in both the across and along directions. Additional internal and perimeter walls provide supporting load paths, demonstrating that the FRP wall panel system can be integrated within a typical residential layout while satisfying the intent of NZS 3604 bracing design principles.

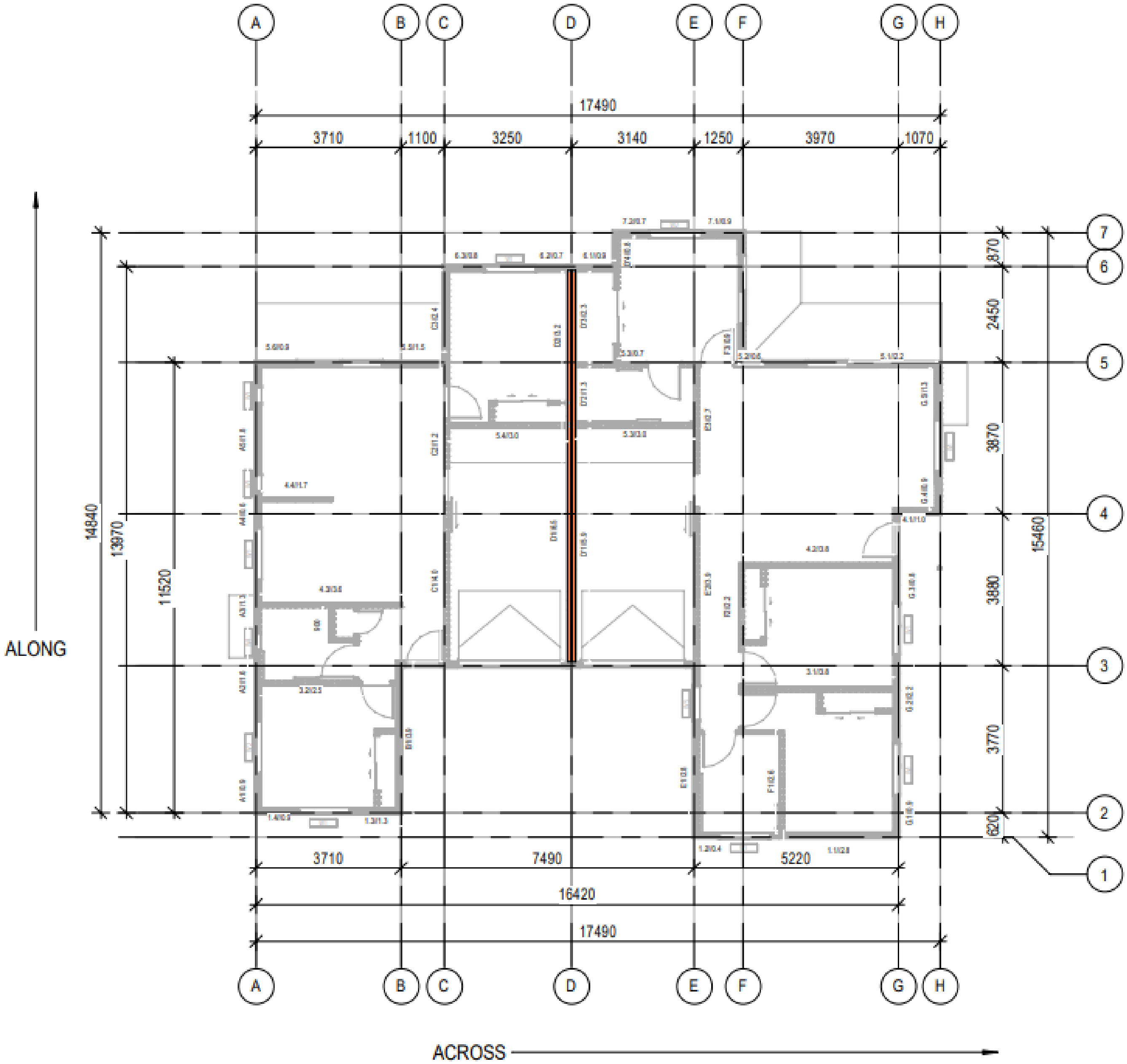

Figure 44-The braceline of the case study building

Table 14-Across FRP wall brace capacity check

- P21 Test FPR Wall Panel System (No Bracing Strap)
- EQ: 53 BU/m; Wind: 54 BU/m
- Considering 50 BU/m for both EQ and Wind

					Demand	
					Wind (BU)	EQ (BU)
					788 BU	1032 BU
					Achieved	
					Wind (BU)	EQ (BU)
Line	Element	Length (m)	Wind (BU)	EQ(BU)	2689 (341%)	2813 (273%)
A	1	0.9	45	45		
	2	1.6	80	80		
	3	1.3	65	65		
	4	0.6	30	30		
	5	1.8	90	90		
	External FRP Wall Length 11.5m				310	310
=B	1	3.9	195	195		
	External FRP Wall Length 11.5m				195	195
C	1	4	200	200		
	2	1.2	60	60		
	3	2.4	120	120		
	External FRP Wall Length 10.2m				380	380
D	1	6.5	390	455	390	455
	Intertenancy Wall (Steel Frame with GB GS1)					
D’	1	5.9	354	413		
	Intertenancy Wall (Steel Frame with GB GS1)				354	413
E	1	2.8	140	140		
	2	3.9	195	195		
	3	2.7	135	135		
	External FRP Wall Length 12.2m				470	470
F	1	2.6	130	130		
	2	2.2	110	110		
	3	0.9	45	45		
	External FRP Wall Length 15.4m				285	285
G	1	0.9	45	45		
	2	2.2	110	110		
	3	0.8	40	40		
	4	0.9	45	45		
	5	1.3	65	65		
	External FRP Wall Length 12.2m				305	305

Table 14 demonstrates that the total across-direction bracing capacity provided by the FRP wall panel system significantly exceeds the design demand for both wind and earthquake actions in the case study building. The governing demands are 788 BU for wind and 1,032 BU for earthquake, whereas the calculated capacities achieved are 2,689 BU (341%) under wind loading and 2,813 BU (273%) under earthquake loading. This capacity is primarily contributed by the external FRP wall lengths on Lines A to G of the bracing plan in Figure 44, which collectively provide several times the required bracing units, based on an assumed conservative value of 50 BU/m for both loading cases.

The two intertenancy walls (Lines D and D′), which are light gauge steel framed internal walls lined with GIB plasterboard to one side, have been assessed in accordance with the GIB plasterboard bracing product specifications, providing approximately 70 BU/m for earthquake and 60 BU/m for wind [57]. While these walls do contribute to the overall bracing capacity, they are not relied upon as primary structural bracing elements in this assessment. Even if the bracing contribution from both intertenancy walls is completely disregarded, the remaining FRP walls alone still provide approximately 1,945 BU for both wind and earthquake loading, which is already well more than the design demand in the across direction.

It is also important to note that the bracing unit values adopted in this calculation are derived from the first round of BRANZ P21 testing on the FRP wall panel system, conducted without any additional mechanical reinforcement such as straps or enhanced bottom-plate fixings. In the construction of the case study building, as depicted in Figures 45 (a) and (b), all external FRP walls have been designed and installed with additional bracing plates, as illustrated in Figure 43(b). This design is anticipated to enhance the system's resistance to lateral loads. This reinforcement strategy is comparable in performance to the second round of P21 testing that incorporated 25 mm bracing straps, where the system achieved approximately 61 BU/m for earthquake and 85 BU/m for wind. Even adopting a simplified and conservative design assumption of 61 BU/m for earthquake and 80 BU/m for wind, the resulting bracing capacity in the as-built condition would be substantially higher than that presented bracing capacity values in Table 14. Accordingly, the present calculations intentionally adopt a highly conservative engineering approach using unreinforced P21 test values and demonstrate that the FRP wall panel system can comfortably and reliably satisfy the required across-direction bracing demand for both wind and earthquake actions.

Table 15-Along FRP wall brace capacity check

- P21 Test FPR Wall Panel System (No Bracing Strap)
- EQ: 53 BU/m; Wind: 54 BU/m
- Considering 50 BU/m for both EQ and Wind

					Demand	
					Wind (BU)	EQ (BU)
					775 BU	1032 BU
					Achieved	
					Wind (BU)	EQ (BU)
Line	Element	Length (m)	Wind (BU)	EQ(BU)	1850 (239%)	1850 (179%)
1	1	2.8	140	140		
	2	0.4	20	20		
	External FRP Wall Length 5.2m				160	160
2	1	1.3	65	65		
	2	0.9	45	45		
	External FRP Wall Length 3.7m				110	110
3	1	3.8	190	190		
	2	2.5	125	125		
	External FRP Wall Length 16.5m				315	315
4	1	1.0	50	50		
	2	3.8	190	190		
	3	3.6	180	180		
	4	1.7	85	85		
	External FRP Wall Length 17.49m				505	505
5’	1	2.2	110	110		
	2	0.6	30	30		
	3	3.0	150	150		
	4	3.0	150	150		
	5	1.5	75	75		
	6	0.9	45	45		
	External FRP Wall Length 17.49m				560	560
6	1	0.9	45	45		
	2	0.8	30	30		
	3	0.7	40	40		
	External FRP Wall Length 12.2m				120	120
7	1	0.9	45	45		
	2	0.7	35	35		
	External FRP Wall Length 15.4m				80	80

Table 15 provides an evaluation of the along-direction bracing capacity of the FRP wall panel system, based on the initial phase of BRANZ P21 racking testing, without the inclusion of additional mechanical bracing straps. The bracing capacity calculations presented in this table adopt the same conservative methodology and assumptions as those previously applied in the across-direction verification, ensuring consistency in the analytical approach. This assessment employs conservative design bracing values of 50 BU/m for both wind and earthquake actions. The calculated total bracing capacity provided by the distributed FRP wall segments is 1850 BU for both wind and earthquake, compared with corresponding design demands of 775 BU (wind) and 1032 BU (earthquake). The resulting utilisation ratios of approximately 239% for wind and 179% for earthquake indicate that the proposed configuration possesses a pronounced excess of lateral resistance capacity relative to the design demands in the along direction.

Furthermore, the same scenario applies in the along direction as in the across direction with respect to the additional mechanical bracing reinforcement provided to all external walls. As a result, consistent with the across direction configuration, the external FRP walls will, in practice, deliver a greater bracing capacity than that calculated and reported in Table 15. Accordingly, the values presented in Table 15 should be regarded as conservative baseline estimates, with the as-built FRP wall panel system expected to achieve an even higher level of lateral resistance.

(a) Bracing plate fixed into the foundation

(b) Bracing plate in the panel walls

Figure 45-Bracing plate fixed

To further test the robustness of the design, a hypothetical global reduction of 10% in bracing capacity is assumed to all contributing walls, representing a deliberately conservative engineering allowance for uncertainties such as construction tolerances, connection variability, material degradation, and modelling simplifications. Even after this reduction, the effective capacities remain approximately 1665 BU, which still exceed the required demands by a comfortable margin around 215% of wind demand and 161% of earthquake demand.

Table 16-Structural compliance matrix – FRP wall bracing (case study building)

ID	Direction	Load Case	Bracing Demand (BU)	Bracing Capacity (BU)	Capacity > Demand	Compliance
1	Across the ridge	Wind	788	2,689	3.41	Met
2	Across the ridge	Earthquake	1,032	2,813	2.73	Met
3	Along the ridge	Wind	775	1,850	2.39	Met
4	Along the ridge	Earthquake	1,032	1,850	1.79	Met

6.10 Summary of Structural Verification of the FRP Panel Wall System

The structural verification conducted through experimental testing, real-world building design applications, and mathematical validation in this section demonstrates that the FRP wall panel system exhibits performance characteristics that are directly comparable to those of conventional light timber framed construction. The results of the BRANZ P21 racking tests confirm that the system behaves in a predominantly ductile manner, with stable hysteretic response, significant deformation capacity, and energy dissipation controlled primarily by connection behaviour rather than brittle material failure. In this respect, the FRP wall panel system can be regarded as a ductile structural system within the context of low-rise residential construction in New Zealand.

The structural verification presented in this section has also demonstrated that the FRP walls possess a distinct capability to maintain overall structural integrity while concurrently offering enhanced thermal performance in comparison to traditional timber framed walls. Overall, the bracing capacity verification confirms that the proposed FRP wall panel configuration provides a robust and reliable lateral load-resisting system, supporting its structural adequacy and suitability for application in the case study building.

6.11 FRP Lintel System Evaluation

As discussed in the preceding section, the FRP wall panel system has demonstrated a reliable and ductile lateral load–resisting behaviour, with bracing capacities that are comparable to, and in several respects exceed, those typically achieved by conventional light timber-framed construction. However, it is well established that lintels remain one of the most significant contributors to thermal bridging in external wall assemblies, largely due to the structural capacity required to span openings and support imposed gravity loads. Accordingly, the following section shifts the focus to an evaluation of the proposed FRP lintel system, with the objective of verifying whether it can deliver structural performance comparable to that of the full size FRP wall panels, while simultaneously mitigating the thermal performance deficiencies commonly associated with traditional timber or steel lintel solutions.

6.11.1 Thermal Bridging Issue in Timber Lintels

Timber lintels commonly employ solid timber beams, as shown in Figure 46 to span the window and door openings. Ryan et al. [2] stated that the framing around openings (including lintel sizing) is determined by the weight of the roof, the distance of the lintel below the top plate and the width of the window or door opening and any point loads in the structure above the window opening. Lintels in timber-framed buildings are typically regarded as thermal bridges because of their common lack of insulation and structural continuity along the building perimeter [20]. This results in localised short-circuiting of the wall insulation and contributes to an increased thermal bridging fraction of the overall building envelope. Ryan et al.[20] further states that NZS 4218 considers only studs, nogs, top plates, and bottom plates in the calculation of construction R-value, and therefore excludes lintels, supporting studs, as well as corner and junction studs from the assessment.

NZS 4218 has historically provided the thermal insulation requirements for housing and smaller buildings [9] and has been cited as the reference for insulation in H1/AS1(Fourth edition, Amendment 3) [58] and H1/VM1(Fourth edition, Amendment 3) [59] for housing and small buildings up to 300 m². The idealised wall layout defined in NZS 4218, which effectively allows the omission of thermal bridging effects from lintels [58,59]. Although the issue extends beyond wall openings, lintels exemplify how design decisions regarding window and door openings can significantly increase the overall percentage of framing required. The most recent updated versions are H1/AS1 [6] and H1/VM1 [7]. These amendments introduced more stringent thermal performance requirements and placed greater emphasis on whole-building heat-loss calculations, including the explicit treatment of the thermal bridging effects caused by structural components such as lintels. This elevates the overall framing percentage and amplifies conductive heat transfer through the building envelope in conventional timber framed houses.

Under the updated H1 provisions, these thermal losses must now be explicitly quantified rather than assumed [11]. Addressing thermal bridging associated with lintels in conventional timber-framed buildings presents significant challenges, as the integration of additional insulation into solid timber lintels is not practically achievable. This inherited difficulty highlights the growing need for thermally efficient lintel solutions and alternative construction methodologies that can provide both structural capacity and improved thermal performance.

Figure 46-Conventional solid timber lintel in time framing structure

6.11.2 Insulated FRP Lintel System

In contrast, the proposed FRP Wall Panel system forms the lintel system from 300mm FRP panel segments that are capped by light-gauge galvanised steel U-channels (same configurations with the wall system) to the required span and bearing geometry **(**Figure 47**)**. Figures 48 and 49 illustrate that the U-channels of the lintels in the case study building are positioned across the top of each opening and are mechanically fastened directly to the top edges of the adjacent FRP wall panels. This configuration establishes a continuous load path above the door openings and window penetrations. At each side of the opening, the steel U-channel is screwed into the vertical FRP segments' faces, anchoring the lintel to the supporting wall segments. Where two FRP panels meet at the opening corners, the channel is seated over the joint and fixed into both panels, bridging the gap and restoring continuity. It means the lintel is not a separate beam inserted into a framed wall, but a capping component integrated directly with the entire FRP wall panel system.

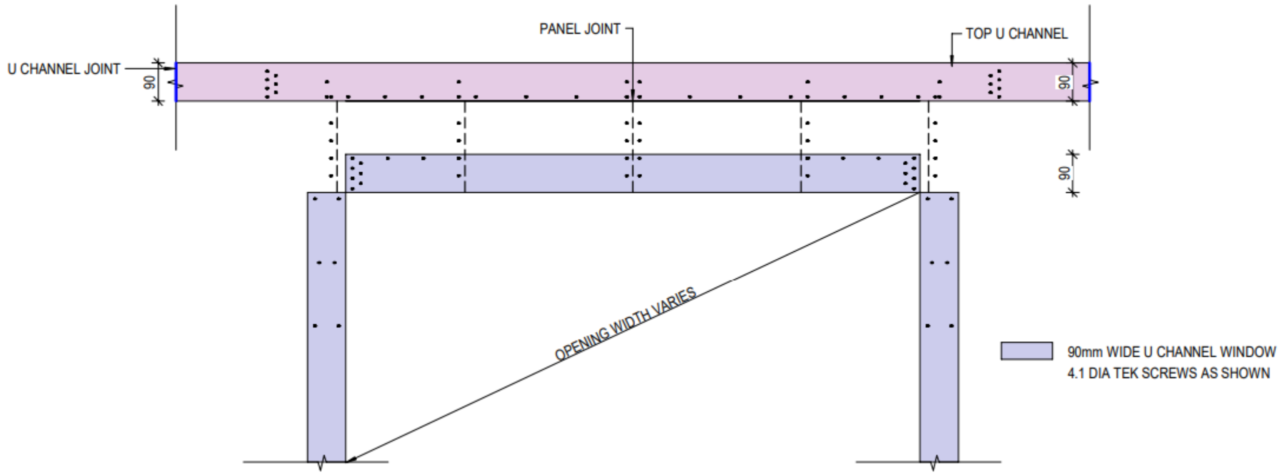

Figure 47-FRP lintel system design details

(a) Lintel and wall panel connection (b) Lintel fixing details

Figure 48-FRP lintel system design and construction details

Figure 49-Installation of lintels in the case study building with an FRP wall panel system

Figure 50-FRP wall panel system lintel insulation detail

Each FRP segment within the lintel system is filled with 60 mm phenolic foam insulation, consistent with the insulation method employed for the adjacent wall panels. These detailing strategies maintain the same level of insulation across window and door heads as in the adjoining wall panels, therefore substantially reducing the linear thermal transmittance at the openings compared with conventional timber lintels. By integrating insulation directly within the FRP lintel segments, the design aims to minimise thermal bridging at these critical junctions and enhance the overall thermal integrity of the wall assembly (Figure 50). Crucially, this approach enables the building envelope to achieve high thermal performance targeted at the design stage without the need for additional external thermal breaks, which are often costly and complex to implement at the building stage.

6.11.3 Structural Verification for the Load Capacity of the FRP Lintel System

The verification framework based on New Zealand load combinations, governed by the AS/NZS 1170 suite of structural design actions, and formally required by NZBC B1/VM1 [45], has already been addressed in the preceding sections in relation to the FRP wall panel system. Building on this established basis, the present section shifts its focus specifically to the structural verification of the FRP lintel system, applying the same code recognised methodology to assess the lintel system's capacity and suitability at openings within the case study building.

6.11.3.1 Principles of Lintel Load Design

The concept of a "loaded dimension" was introduced in NZ364 [3] to simplify the lintel design and quantify the portion of the construction weight carried by a lintel. This concept is analogous to the well-established notion of the tributary area, which has long been employed by structural engineers in design practice [55]. Lintels are not subjected directly to area pressures (kPa) but rather to line loads (kN/m) acting along their spans [55]. Clause 3.4 of AS/NZS 1170.0 [60] stipulates that area loads must be transformed into line loads by multiplying the surface action in the tributary width, which is defined as the portion of the roof area that contributes load to supporting walls.

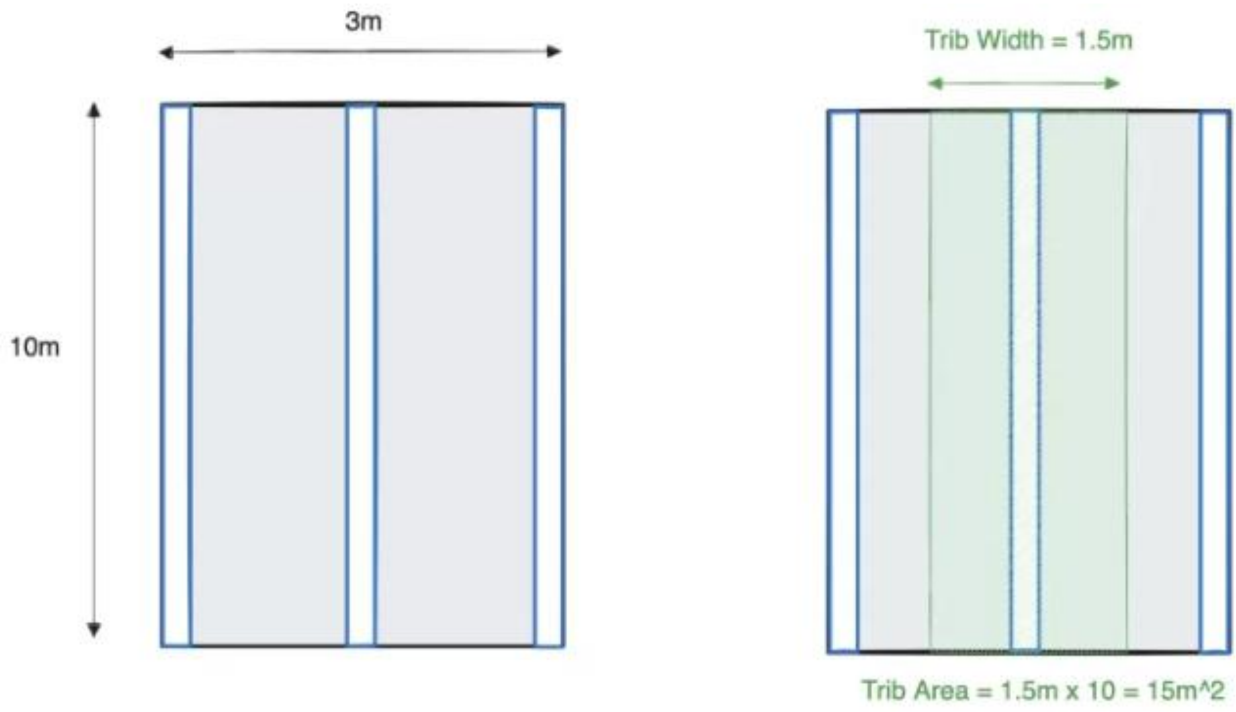

Figure 51-How tributary width is defined [61]

"Tributary Width" is a simplified representation of this concept, and it is often more practical to express it through the width of the tributary area, as illustrated in Figure 51.

When calculating the magnitude of the distributed load, this becomes an easier calculation using the following formula:

$$w = q \times TW \qquad \text{(Eq. 14)}$$

Where,

w = Line load (kN/m); q = Roof Action (kPa); TW = Tributary Width (m)

6.11.3.2 Roof Design of the Case Study Building

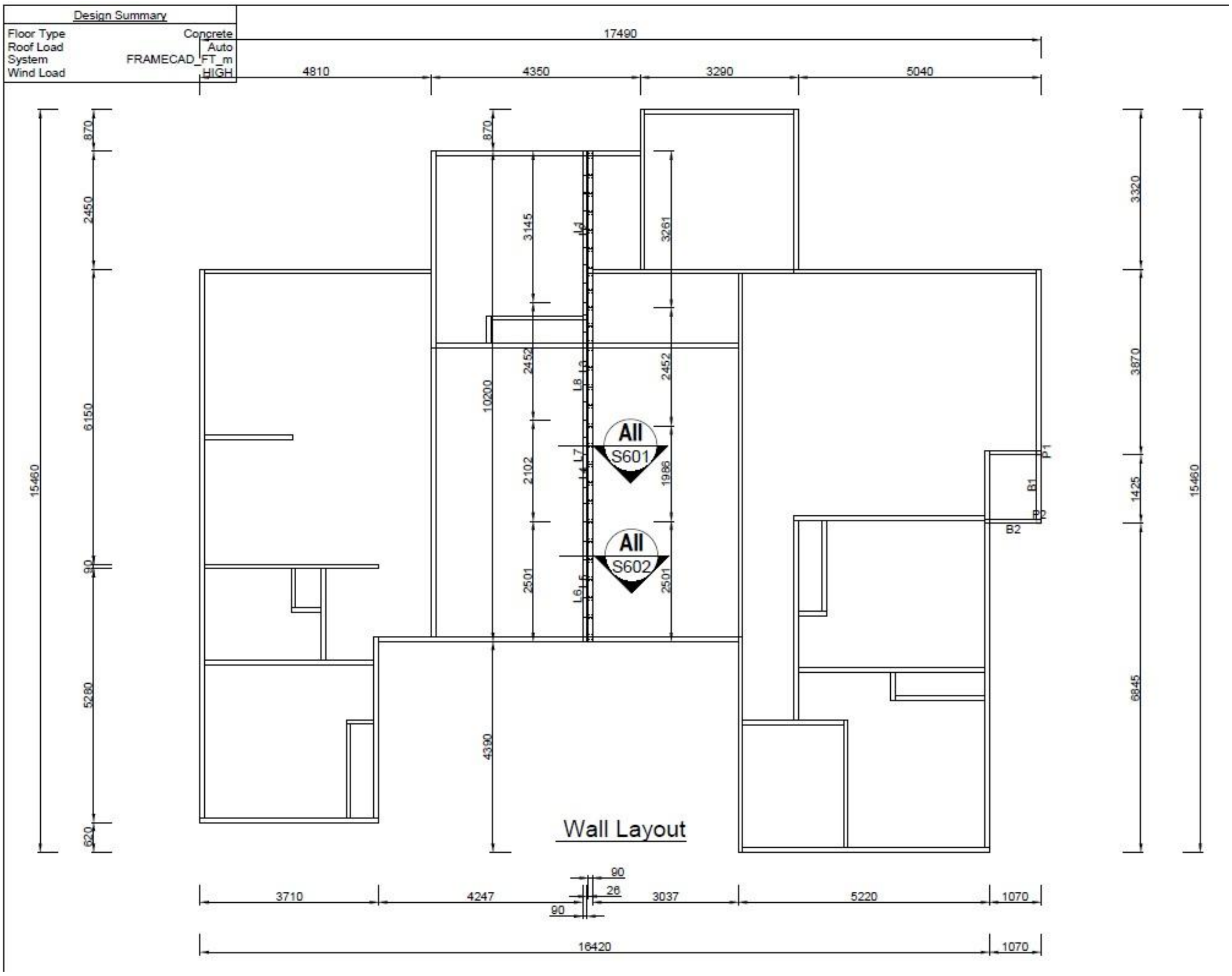

Figure 52-The wall layout plan for the roof design of the building

To establish the design demand on the lintels of the proposed case study building, it is necessary to initially determine the tributary width of the building's roof area contributing to the load of each supporting wall. Figure 52 presents the wall layout of the case study building corresponding to the roof truss plan, which provides the dimensional basis for this assessment.

The wall layout plan shown in Figure 52 illustrates that the roof is supported primarily by the inter-tenancy spine wall, identified as the double-line wall elements between the two units on the wall layout, together with long external walls that form the main bearing lines of the structure.

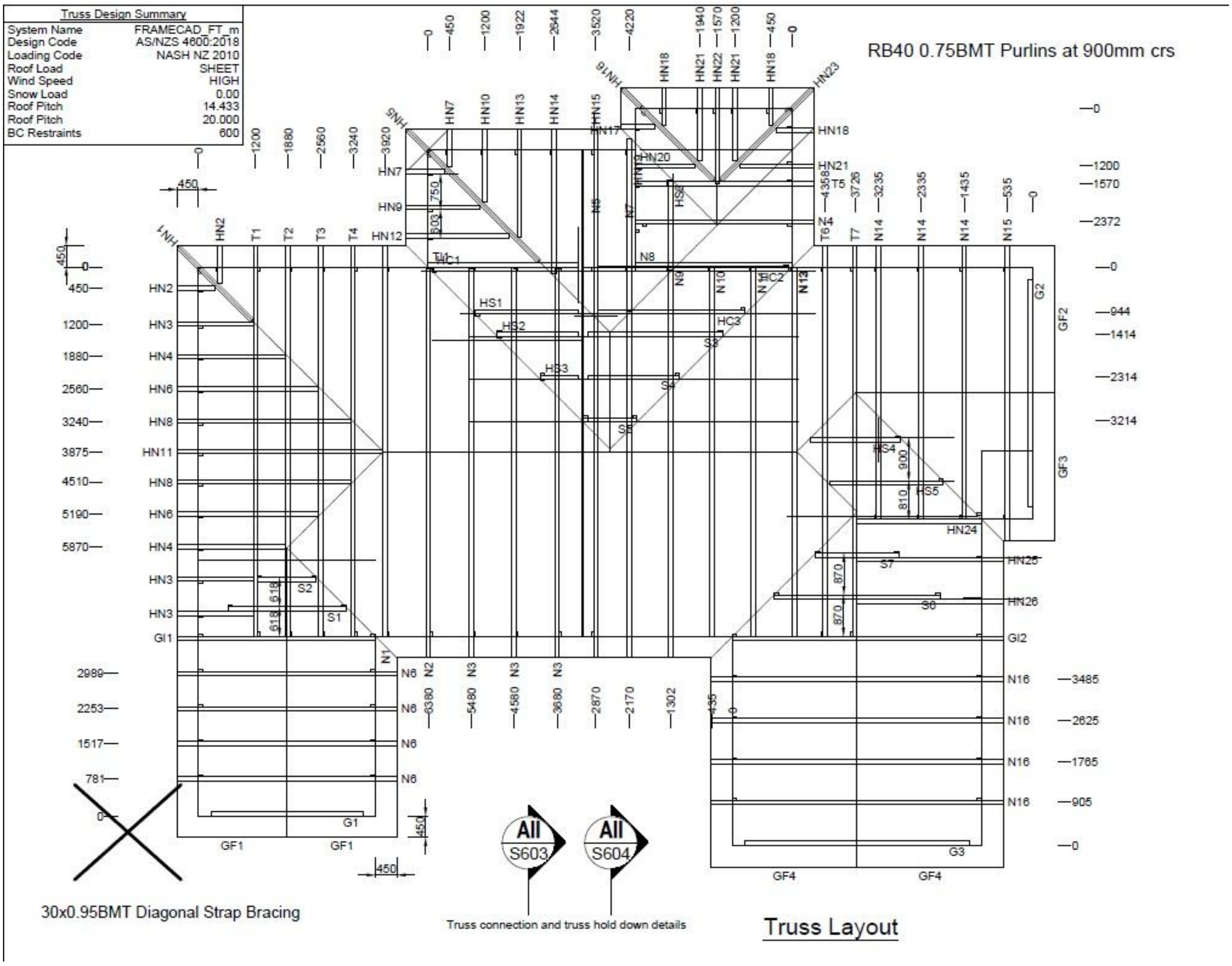

Figure 53-The truss layout plan for the roof design of the building

The truss layout shown in Figure 53 confirms that the HN-series roof trusses span transversely between the supports. Measurement of the wall layout dimension strings shows that the clear span between an exterior wall and the central spine is approximately 9.2 m on the left-hand side (4.81 m + 4.35 m = 9.16m), and approximately 8.3 m on the right-hand side (3.29 m + 5.04 m = 8.33 m). This indicates that the tributary width to each bearing line ranged between approximately 4.2 m and 4.6 m. For design purposes and to maintain a conservative and uniform basis for lintel verification across the building, a tributary width of 4.6 m is adopted in the demand load calculation for verification. This value governs the load assessment of lintels located in load-bearing exterior walls under the main roof of the building. The openings in these walls impose roof loads based on a tributary width of 4.6 m. These lintels include those above the garage door in the central block and the exterior wall lintels serving the living, dining, and kitchen areas.

6.11.3.3 Demand Load Calculations and Assumptions

The demand load on lintels is evaluated according to the combination rules of AS/NZS 1170.0[60], as referenced in B1/VM1 [45]. The load combinations are prescribed separately for the ULS and SLS designs.

For the ULS, Clause 4.2.2(b) of AS/NZS 1170.0 [60] specifies the governing equation for calculating the combination of permanent and imposed actions as:

$$Ed = 1.2G + 1.5Q \qquad \text{(Eq. 15)}$$

For the SLS, Clause 4.3 of AS/NZS 1170.0 [60] specifies the governing equation for calculating the combination of permanent and imposed actions as:

$$Ed = G + \Psi Q \qquad \text{(Eq. 16)}$$

E_d denotes the design action effect, which represents the structural demand arising from the combined effects of permanent and variable actions. The parameter G corresponds to permanent actions, typically referred to as self-weight or 'dead' loads, while Q represents imposed actions, more commonly described as 'live' loads. It is appropriate to adopt the standard load parameters for G and Q, as specified in the engineering guidance derived from AS/NZS 1170 suite as shown in Table 17, for the design of lintels in NZS 3604 timber framed buildings [55]. Accordingly, the roof dead load is taken as G=0.35 kPa (rounded to 4kPa for a conversative design approach) while the imposed roof live load is taken as Q = 0.25 kPa. These values are presented in the table below and are used as the basis for calculating the lintel demand in this study.

Table 17-Combined load on roof [55]

Component (light, medium, heavy cladding defined in clause 1.3)		Dead load (G) (kPa)	Live load (Q) (kPa)	Snow load (s_g) (kPa)
Roof (including framing and ceiling)	Light	0.35 (0.2 for wind uplift)	0.25	1.0 (section 8) 1.5 and 2.0 (section 15)
	Heavy	0.75 (0.4 under wind uplift)		

6.11.4 Demand Load for Load Bearing Lintels of the Case Study Building

The demand actions are determined through converting the applied area loads (kPa) into line loads, which is achieved by multiplying the relevant tributary widths. This approach allows for a direct assessment of the experimental testing supported calculations against the structural load requirements specified for the building's intended use.

6.11.4.1 Demand ULS and SLS

With a tributary width of 4.6 m, the design action on the load-bearing lintels can be determined by applying Equation 14 in conjunction with Equations 15 and 16. Based on these expressions, the corresponding line-load demand acting on the lintels of the proposed building is calculated as follows:

For the ULS, the combination of permanent and imposed actions is:

$E_{d,ULS} = (1.2G + 1.5Q) \times 4.6 = (1.2 \times 0.4 + 1.5 \times 0.25) \times 4.6 \approx 3.93$ kN/m

This represents the factored extreme demand on the lintel under the ultimate conditions.

For the SLS, the load combinations are determined in accordance with the ψ-factors specified in Table 4.1 of AS/NZS 1170.0 [60]. It is appropriate to consider the roof design in this study to be classified as “all other roofs.” Therefore, the applicable factors are ψ_s=0.7 for short-term imposed actions and ψ_l=0 for long-term imposed actions.

- **Short-term SLS** (relevant to deflection checks):

  $E_{d\ SLS,short} = (G + \Psi_s Q) \times 4.6 = (0.4 + 0.7 \times 0.25) \times 4.6 \approx 2.65$ kN/m

- **Long-term SLS** (relevant to sustained effects, such as creep):

  $E_{d,SLS,long} = (G + \Psi_l Q) \times 4.6 = (0.40 + 0 \times 0.25) \times 4.6 \approx 1.84$ kN/mw

The calculated line-load demands for the load-bearing lintels of the case study building establish the critical design actions required for the structural verification of the proposed FRP lintel system. Based on the tributary width of 4.6 m and the load combinations prescribed by AS/NZS 1170.0 [60], the governing ULS demand was determined to be approximately 3.93 kN/m, representing the factored extreme loading condition. The corresponding SLS is determined to be 2.65 kN/m for short-term conditions pertinent to deflection performance, and 1.84 kN/m for long-term conditions associated with sustained loading effects, such as creep.

6.11.4.2 Demand Serviceability Load with Wind Action

In accordance with Clause 4.3 and Table 4.1 of AS/NZS 1170.0 [60], the relevant serviceability load case considering the wind load for lintels is expressed as,

$$Ed = G + \Psi sQ + Ws \quad \text{(Eq. 17)}$$

This combination requires the lintel to be checked under gravity actions (G+ΨsQ) and serviceability wind action (W_s). Section 6.4.3 of the Engineering Basis of NZS 3604 [55] further specifies how wind action is converted into an equivalent line load on lintels. The significance of this combination is that the lintel deflection at serviceability is not governed by gravity alone but by the interaction of gravity and wind actions.

For roof slopes of 15° to 45°, wind action factors were applied to determine the equivalent lintel line loads [55]. This produced a maximum uplift load expressed as, as shown in the following equation. Based on the standards [60, 55], for downward wind pressure, the effective line load is taken as,

$$Ws, down = 0.3 \times p \times LD \quad \text{(Eq. 18)}$$

while for uplift suction, the line load is as follows,

$$Ws, up = 0.946 \times p \times LD \quad \text{(Eq. 19)}$$

Where,

p = the serviceability wind pressure (kPa); LD = the loaded dimension to the next support (m)

Table 18-Wind (Face Loads on Studs) [55]

Zone	Wind speed (V_{des})	Design wind pressure (p) (kPa)
Low (also internal walls)	26	0.40
Medium	30	0.53
High	37	0.82
Very high	42	1.06
Extra high	45	1.22

The *LD* is used to quantify the portion of the structural weight carried by the lintel. Functionally, it is analogous to T*ributary Area* employed in structural engineering practice to determine load distribution. (Clause 6.4.1) [55] The proposed case study building is designed for a High wind zone, and the relevant loading parameters are summarised in Table 18. Therefore, the applied wind pressure is p = 0.82 kPa [55]; the loaded dimension (LD) is 4.6 m; the roof dead load is G = 0.35 kPa; the imposed roof live load is Q = 0.25 kPa; and the serviceability load reduction factor is Ψs = 0.7 for all other roofs [60]. The significance of this loading combination is that serviceability deflection is not governed by gravity loading alone, but by the combined influence of gravity and wind actions. By applying Equation 14 and Equation 17, the gravity component is calculated as follows: $(G + \Psi_s Q) \times TW = (0.35 + 0.7 \times 0.25)\times 4.6 \approx 2.42$ kN/m

Applying Equation 18, the downward wind contribution is: $W_{s,down} = 0.3\times 0.82\times 4.6 \approx 1.13$ kN/m

Thus, the total downward serviceability wind action line load on the proposed building's lintels is: $W_{SLS,down} = 2.42+1.13=3.55$ kN/m.

For the uplift case, the effective gravity contribution is reduced in accordance with the Engineering Basis of NZS 3604 [55] to account for the reduced stabilising dead load for wind uplifts shown in Table 18: G=0.20 kPa. The line load from gravity and live actions is:

$$(G + \Psi_s Q) \times TW = (0.20 + 0.7 \times 0.25)\times 4.6 \approx 1.73 \text{ kN/m}$$

Applying Equation 19, the uplift wind contribution is: $W_{s,up} = 0.946 \times 0.82 \times 4.6 \approx 3.57$ kN/m.

Accordingly, the total uplift serviceability demand is: $W_{SLS,up} = 1.73 + 3.57 = 5.30$ kN/m

The calculations confirm that the lintels for the proposed case study building should be checked for both downward serviceability with a wind action of 3.55 kN/m and an uplift serviceability demand with a wind action of 5.30 kN/m. These calculated demands provide an essential benchmark for assessing the structural performance of the FRP lintel system. They define the threshold conditions that the lintel must satisfy under both strength and serviceability criteria to ensure compliance with the NZBC requirements. The established ULS and SLS values serve as reference parameters for evaluating the experimental results presented in the following section, enabling a direct comparison between the analytical design expectations and the empirically verified load-bearing capacity of the proposed insulated FRP lintel.

6.11.5 Experimental Testing to FRP Lintel Samples

The following section details the experimental evaluation conducted to assess the performance of the FRP lintel system under representative load conditions. This verification process validates that the incorporation of internal phenolic foam insulation within the FRP lintel cavities does not compromise the member's strength or stiffness, thereby confirming its suitability as both a load-bearing and thermally efficient component within the overall FRP wall panel system. This verification process establishes that the FRP lintel system successfully integrates structural strength and thermal performance within a single design. The composite configuration allows the lintel to function as both a robust load-bearing member and a thermally consistent component of the FRP wall assembly.

6.11.5.1 Three-point Bending Testing Rig Setup

Three-point bending tests were conducted on the FRP lintel specimens using a midspan point-load configuration. This method was selected to directly measure the bending response and stiffness (EI) of the member under controlled laboratory conditions. The experimental setup for the three-point bending tests on the FRP panel lintels is shown in Figure 54.

Figure 54-The three-point bending test setup to test the lintel specimen

The tests were conducted using a servocontrolled hydraulic testing machine configured for midspan loading. The rig consisted of two fixed steel roller supports and a single loading head located at the midspan of the specimens to induce symmetric bending moments. The total span was adjusted according to the specimen length. The loading frame could apply a static vertical load under displacement control to capture both the elastic and failure responses of the FRP lintel specimens. All bending tests were conducted in accordance with AS/NZS 4063.1:2010 (“AS/NZS 4063.1”) [62], which specifies the required methods for the structural characterisation of timber and engineered components. The statistical requirements outlined in AS/NZS 4063.2:2010 (“AS/NZS 4063.2”) [63] are applicable to this test program, as this section delineates the methodology for processing experimental bending data to derive the characteristic values of strength and stiffness necessary for the structural design. Structural design codes do not permit the direct use of a single maximum test result for the design. Instead, the characteristic resistance must be defined as a lower-bound value that accounts for natural material variability.

A load cell integrated with the actuator recorded the loads applied. The midspan deflection was measured using a Linear Variable Differential Transformer (LVDT) mounted independently from the test frame to eliminate machine compliance. Strain gauges were affixed to the tension and compression faces at midspan for the selected specimens to monitor the surface strain development during loading. The load was then applied monotonically at a constant displacement rate until failure. The load, deflection, and strain data were continuously logged using a digital data acquisition system.

6.11.5.2 The Testing Specimens Specifications and Testing Preparation

The experimental testing program involved several specimens for each specified span length, including three specimens for the 1.8 m span and two specimens each for the 3.0 m, 3.15 m, and 4.8 m spans. This methodology is designed to effectively capture the inherent variability due to fastener placement, the material properties of the FRP panels, and galvanised steel fixings. This approach ensures that the calculated lintel capacity reflects a reliable and conservative design value, as opposed to an overestimated average or an isolated high result.

The lintel specimens were fabricated from the proposed FRP wall panel system, comprising 300 mm deep FRP panel segments capped on both top and bottom edges with light gauge galvanised U-channels (approximately 101 mm × 90 mm × 1.2 mm). At each end of the lintel segments, 600 mm × 250 mm FRP wall sections were connected, replicating the boundary restraint provided by the adjoining wall panels in an actual wall assembly. At each joint between the FRP panel segments, 8 gauge (4.1 mm diameter) × 25 mm self-tapping screws were applied on both sides of the panel at an approximate spacing of 30 mm. Moreover, the same screws were employed to secure the FRP segments to the upper and lower galvanized U-channels, which were positioned approximately 150 mm apart along both sides. This fastening configuration ensured sufficient shear transfer between the FRP panels and the steel capping members, while also facilitating a realistic simulation of onsite construction practices.

The specimen preparation complied with Clause 4 AS/NZS 4063.2 [63], with full scale lintel assemblies constructed using the FRP wall panel system. The support and loading arrangement followed the simply supported three-point bending configuration prescribed in Clause 4.3 of to ensure that pure flexure was generated at midspan. The load and deflection were measured using a calibrated load cell and independently supported LVDTs, satisfying the accuracy and recording provisions of Clause 5.2. Multiple specimens were tested for each span length (three 1.8 m units and two of each longer span), allowing a statistical assessment of the variability in strength and stiffness, as required by AS/NZS 4063.2 [63]. Collectively, these measures confirm that the experimental program adheres to the procedural and measurement standards outlined in the standards and that the resultant load displacement data offer a dependable foundation for structural design evaluation.

The specimens were positioned horizontally on cylindrical steel roller supports that were fixed to a rigid steel base beam. Small steel tubes and steel plate assemblies provided uniform contact and load distributions along the support lines. A single loading actuator located above the specimen applied a vertical force through a polished steel loading nose with a hemispherical seating to ensure uniform contact at midspan and prevent local crushing. The span length was set as the clear distance between the two support centrelines, and the actuator was aligned vertically at the span midpoint. This configuration ensures a pure bending region under the central load and shear-dominant regions near the supports, conforming to the standard three-point bending test principle. The 1.8, 3.0, and 3.15m specimens were loaded at a constant rate of 8 mm/min, whereas the 4.8 m specimens were loaded at 14 mm/min to accommodate their larger deformation range and maintain test stability.

6.11.5.3 Experimental Test Procedure and Result Evaluation

The FRP lintel specimens exhibited a distinct sequence of deformation and failure mechanisms governed by the interaction between the FRP panel segments and galvanised steel U-channels. The specimens exhibited local buckling of the upper steel flange under compressive action and pronounced outward deformations of the lower flange under tension. These deformation patterns indicate that the flexural failure mechanism was predominantly governed by the local yielding and instability of the steel components rather than by the material failure of the FRP segments.

While performing the three tests on the 1.8m specimens, the corners on each end of the bottom U-channels were not fixed. The specimens exhibited linear elastic behaviour with minimal visible deformation. As the load increased, localised deformations began to develop around the screw connections. As illustrated in Figure 55, there was evidence of slight bearing deformation and minor pull-through around the screw heads, suggesting a progressive shear slip between the FRP panels and steel U-channels. This behaviour suggests that the load transfer mechanism at the connection was primarily governed by the bearing action of the fasteners and local flexibility of the thin-gauge steel.

Figure 55-The screws fixing the bottom channel were pulled out

Following the initial tests on the 1.8 m specimens, the screw configuration was modified for the remaining specimens with spans of 3.0, 3.15, and 4.8 m. In these specimens, seven additional screws were installed at the corners of each end of the bottom U-channels on both sides to enhance the structural fixing capacity and prevent pull-through failures around the screw heads.

This modification significantly improved the overall connection restraint, resulting in a more stable load transfer between the FRP panels and U-channels. With further loading, the overall flexural response of the specimens became more significant. Notable local buckling developed on the top galvanised steel channel beneath the central loading point, accompanied by outward bulging of the bottom channel under tension. (Figure 56) These deformations indicate that the steel capping components experienced local yielding and instability before the FRP core reached its ultimate limit. Despite the evident distortion of the steel channels, the FRP segments remained largely intact with no visible cracks or delamination. This observation highlights that the failure mode was dominated by local buckling and bearing failure of the steel capping and screw connections rather than by the material rupture of the FRP segments.

Figure 56-Local buckling of top steel channel during the three-point bending tests

6.11.6 Experimental Testing Checks v Demand Capacity for Lintels

6.11.6.1 Centre Point Load to UDLs

Figure 57 illustrates that, although the test configuration employed a central point load, the structural design in practice typically involves uniformly distributed loads (UDLs**)** arising from roof or floor actions. The FRP lintel system developed in this study was evaluated through a series of experimental tests to establish its flexural stiffness and load-deflection behaviour. Therefore, to enable direct comparison between the experimental results and design load requirements defined in AS/NZS 1170.0 [60], the test results have been converted into an equivalent uniformly UDL, facilitating a comparison with the NZBC based line-load demands (kN/m). This conversion ensures that the sample lintel capacities can be directly compared with the design line load demands in the proposed case study building. The equations and tables prescribed for the engineering design of solid timber lintels are referenced to establish the demand loads arising from the roof actions in the proposed case study building. The FRP lintels at the wall openings are conceptualised as simply supported prismatic beams. This approach allows the structural performance of FRP lintels to be evaluated under the assumption that they behave in a manner analogous to solid timber beams, thereby providing a consistent and building code aligned benchmark for assessment.

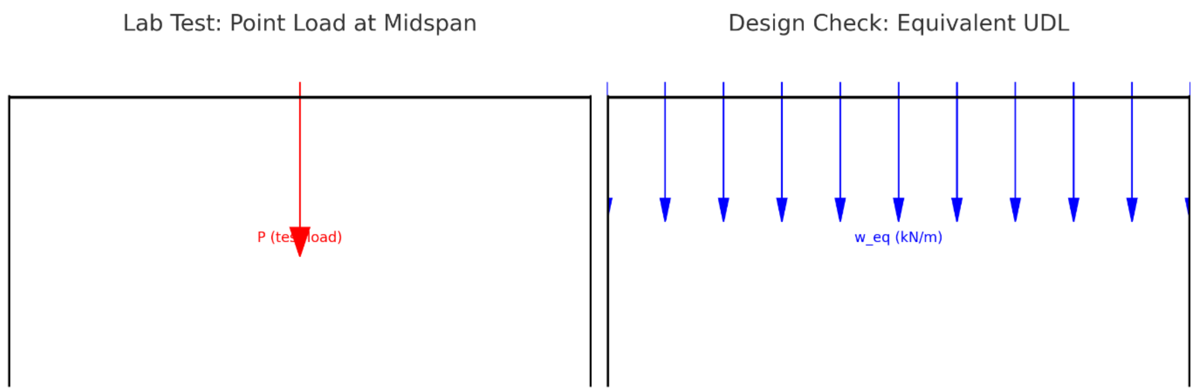

Figure 57-Comparison of Laboratory Point Load Test and Equivalent Design UDL

6.11.6.2 Experimental Test Results

Figure 58 presents the load displacement behaviour of the FRP lintel specimens tested. The curves correspond to the lintels of four different span lengths (1.8, 3.0, 3.15, and 4.8 m), with two or three repeated specimens tested for each span. In all cases, the lintels display an initial linear response, indicating elastic behaviour with proportional increases in load and displacement.

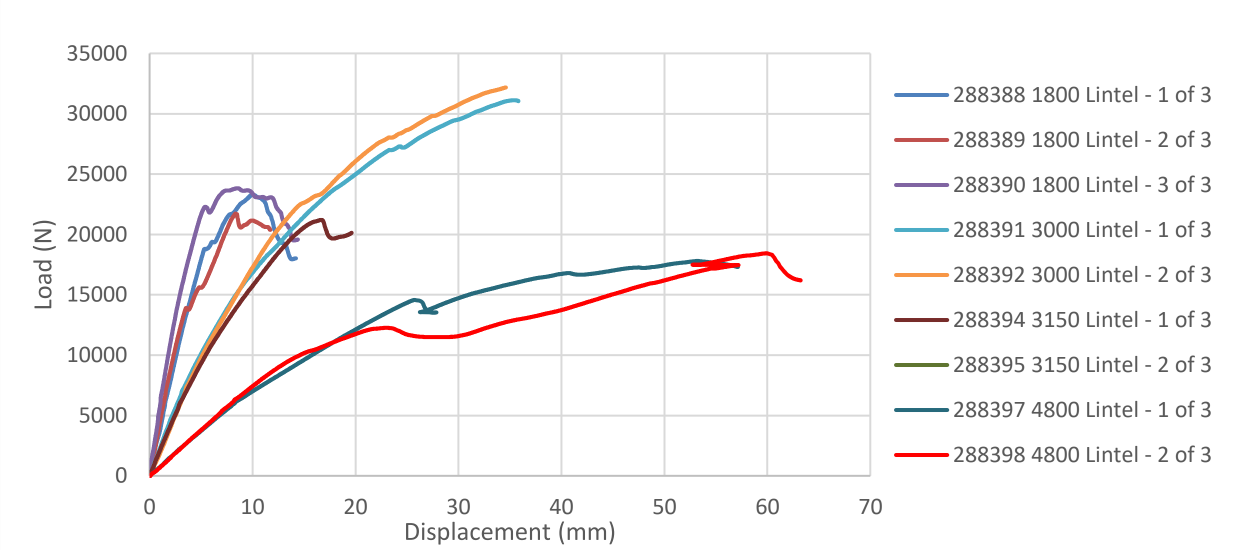

Figure 58-Load and displacement behaviour of FRP lintel specimens of different lengths

The 1.8 m specimens exhibited the highest initial stiffness and reached peak loads of approximately 22–25 kN before a rapid post-peak capacity reduction. The 3.0 m and 3.15 m lintels achieved higher ultimate load capacities of approximately 30–33 kN but showed a more gradual reduction in load after the peak, along with extended displacement, indicating increased ductility and energy absorption. The longest span (4.8 m) demonstrated the lowest stiffness and peak capacity, reaching approximately 15 kN with a large midspan displacement exceeding 60 mm before failure.

6.11.7 The Garage Lintel Structural Verification

The 2.6m garage lintel is selected as the baseline case for structural verification. Serving as the primary support over the garage door, the 2.6m lintel bears a wider tributary area and consequently experiences the highest line load due to the roof and wall actions. Verifying the performance of the FRP lintel system for this span establishes the governing design condition. Upon verification that the garage lintel satisfies the prescribed structural requirements, it follows by analogy that all shorter lintel spans within the building, such as those over window and sliding door openings, also comply. This inference is justified by the fact that shorter spans are subjected to lower bending moments and reduced deflection demands under equivalent loading conditions. This approach is consistent with standard engineering practices, where the largest span or most heavily loaded member is used as the critical verification case for validating the structural adequacy across a uniform design system.

Among the various lintel specimens with different spans, the results from the 3m specimens were selected as the primary reference. This selection is justified by the fact that the 3m span closely approximates the 2.6m garage lintel under verification. Furthermore, since the 3m span is slightly larger than the two garage lintels with a designed length of 2.6 m, its performance results are considered conservative, thereby providing sufficient justification for the structural adequacy of the 2.6m lintels in the case study. The three-point bending test on a 3 m FRP lintel specimen produced the following midspan load deflection readings near the 10 mm serviceability threshold, as shown in Table 19:

Specimen	Span (m)	Load (N)	Deflection (mm)
288391	3.0	17670.83	10.802
288392	3.0	18359.12	10.794

Table 19-Load capacities of the two 3m lintel specimens

The 10.8 mm deflection level was chosen based on the serviceability limit prescribed in Table C1 of AS/NZS 1170.0 [60], which specifies that the deflection for lintels supporting door and window jams shall not exceed 12 mm at a span ratio of L/240. This ratio defines the maximum permissible deflection under serviceability loading as a fraction of the total span, thereby providing a consistent criterion for members with varying lengths. For the garage lintel with a span of L=2600mm, this corresponds to a serviceability deflection limit of approximately 10.8mm.

The results indicate consistent behaviour between the two 3m specimens, with the lowest load of over 17kN at 10.8 mm deflection. Therefore, the measured 17kN midspan point load represents the serviceability limited capacity of the 3m FRP lintel under laboratory conditions. To enable a direct comparison with the design loads expressed as line loads (kN/m), the test result is converted into an equivalent UDL using the relationship derived from the elastic beam theory [64, 65], as shown in the equation chart below:

For a simply supported beam under a central point load P, the maximum mid-span deflection is given by:

$$\delta P = \frac{PL^3}{48EI} \qquad \text{(Eq.20)}$$

For a uniformly distributed load w, the corresponding mid-span deflection is

$$\delta w \ = \frac{5wL^4}{384EI} \qquad \text{(Eq.21)}$$

Equating the two deflections ($\delta_P = \delta_w$) provides the relationship between the point load and the equivalent UDL that produces the same mid-span displacement:

$$\frac{PL^3}{48EI} = \frac{5wL^4}{384EI}$$

Simplifying and rearranging yields: 8P = 5wL, therefore, $w \ = \frac{8}{5} \times \ \frac{P}{L} \ = \ 1.6 \ \times \frac{P}{L}$ (Eq.22)

This relationship was used to interpret the results of the experimental three-point bending tests. During laboratory testing, the 3.0 m FRP lintels reached a mid-span deflection of approximately 10.8 mm under a central point load of slightly above 17 kN. A value of 17kN was adopted as the serviceability reference load, representing the lowest and the most conservative performance result among the two 3.0 m span specimens.

To determine the equivalent uniformly distributed load for the 2.6 m garage door lintel in the case study building, Equation (22) was applied, and the calculation is as follows:

$$w_{eq} = 1.6 \times \frac{17\text{kN}}{3\text{m}} \approx 9.06\text{kN/m}$$

Accordingly, a UDL of approximately 9.06 kN/m would generate a midspan deflection comparable to that produced by a 17kN point load on the 3.0 m FRP lintel specimen. This provides a conservative serviceability benchmark for the 2.6 m garage lintel based on the validated experimental behaviour.

6.11.8 Capacity Verification Under Gravity and Wind Serviceability Load Cases

The conversion from a central point load to an equivalent uniformly distributed load (UDL) enables a direct comparison between the experimentally derived flexural capacity and the design load demands calculated in accordance with AS/NZS 1170.0 [60], as outlined in Section 6.11.6.1 above. The equivalent UDL capacity of 9.06 kN/m substantially exceeds the ULS demand of 3.93 kN/m, confirming a satisfactory structural safety margin under factored loading. It also surpasses all relevant SLS demands: the gravity-controlled SLS range of 1.84–2.65 kN/m (depending on the selected ψ-factor), the windwards serviceability demand of 3.55 kN/m, and the more critical uplift serviceability demand of 5.295 kN/m. These results demonstrate that the FRP lintel system possesses adequate stiffness and strength to resist both gravity and wind induced actions without exceeding permissible deflection limits or compromising serviceability performance.

6.11.9 Dual-Function FRP Lintels for Structural and Thermal Performance

The FRP lintel system investigated in this study addresses the thermal bridging issue of conventional timber lintels by combining high structural performance with high thermal compatibility. Unlike conventional lintels, in which insulation is interrupted, the FRP lintel system integrates insulation within the structural form. This internal insulation integration does not affect the lintel load-carrying function. Consequently, the insulated FRP lintel system achieves a dual objective of maintaining structural significance while mitigating thermal bridging.

Structural verification through three-point bending experimental testing demonstrates that the FRP lintel system can achieve a much higher UDL than the required ULS and SLS of the case study building. This structural efficiency permits the formation of internal cavities within the lintel, accommodating insulation without compromising the bending performance. Consequently, the FRP lintel system supports both load-bearing and thermal continuity functions simultaneously, which is an integration that cannot be achieved with conventional building materials without supplementary insulation detailing or thermal breaks.

The integrated FRP lintel system demonstrates synergistic structural and thermal performances. This duel-function FRP lintel design approach not only prevents localised heat loss but also simplifies the thermal modelling and compliance assessment. Because the lintel region is thermally equivalent to the wall panel system, the overall wall performance can be evaluated using uniform R-values without the need for separate linear transmittance corrections. This ensures that the lintel maintains the same thermal bridging characteristics as the adjoining FRP wall panels, preserving a consistent and continuous thermal profile across the entire building envelope. Furthermore, because the FRP lintel system provides both high stiffness and low thermal conductivity, it enables a single-material design solution that aligns with advanced wall system concepts, prioritising both structural reliability and envelope performance.

7 Weathertightness Fixing Verification

Beyond carrying the structural loads and providing sufficient bracing capacity, the wall framing must also supply the structural support required for cladding systems referenced in E2/AS1 [42]. NZS 3604 specifies that dwangs provide lateral restraint [3]. As discussed in the preceding sections, particularly Section 5.9, while these E2 driven measures have improved weathertightness and fixing robustness in timber framing construction, they have also substantially increased framing ratios and intensified thermal bridging across the building envelope [2,20]. In this context, the shear fixing capacity of the FRP wall panel system is examined in the following section by demonstrating that the FRP panel walls can achieve the required structural fixing for cladding without supplementary structural support, this analysis directly addresses one of the key drivers of thermal inefficiency identified in conventional construction practice.

7.1 Weathertightness under E2 for Cladding

Weathertightness is a fundamental performance requirement of the building envelope, ensuring that external moisture is effectively excluded from the interior structure and habitable spaces of a building. In New Zealand, this requirement is governed primarily by Clause E2 of the NZBC, which establishes the need to prevent the penetration and accumulation of water that could compromise structural integrity, thermal performance, durability, and occupant health [8]. The primary line of defence against moisture ingress is the external cladding system, which is designed to deflect, drain, and dry water away from the underlying structure [42]. In addition to its moisture management role, the cladding assembly must also satisfy structural functions, including resistance to wind pressures, accommodation of thermal and moisture-related movements, and provision of protection to insulation and framing components[42]. Consequently, the performance of a cladding system is not dependent solely on the cladding material itself, but also on the integrity and capacity of its fixings, sub-framing, junction details, and interfaces with other building elements [66]. In timber framed residential buildings, these components collectively constitute an integrated envelope system designed to meet the objectives of weathertightness, structural safety, and energy efficiency under both standard service conditions and extreme environmental events.

7.2 Fixing Requirements for Cladding to Resist Wind Pressure

In the context of wind design in New Zealand shown in Figure 59, a design differential ULS pressure of 2.5 kPa represents the maximum net wind pressure that external cladding systems are required to resist during an extreme wind event, typically associated with a 1 in 500-year return period in accordance with AS/NZS 1170.2 [66]. This value, which is used in many BRANZ Appraisals and referenced in the NZBC E2/VM1, defines the governing pressure differential acting across the building envelope and therefore controls the strength design of cladding elements, sub-framing, and mechanical fixings [67]. In practical terms, a differential pressure of 2.5 kPa corresponds to a load of 2.5 kN acting on every square metre of wall area, which must be safely resisted and transferred through the cladding and its connections to the supporting structure without compromising structural integrity, weathertightness performance, public safety. This pressure generally represents the differential between external and internal air pressures acting on the building envelope. However, for individual cladding components, the governing action is often the external pressure alone, as internal pressure is commonly resisted or balanced by the interior lining [67].

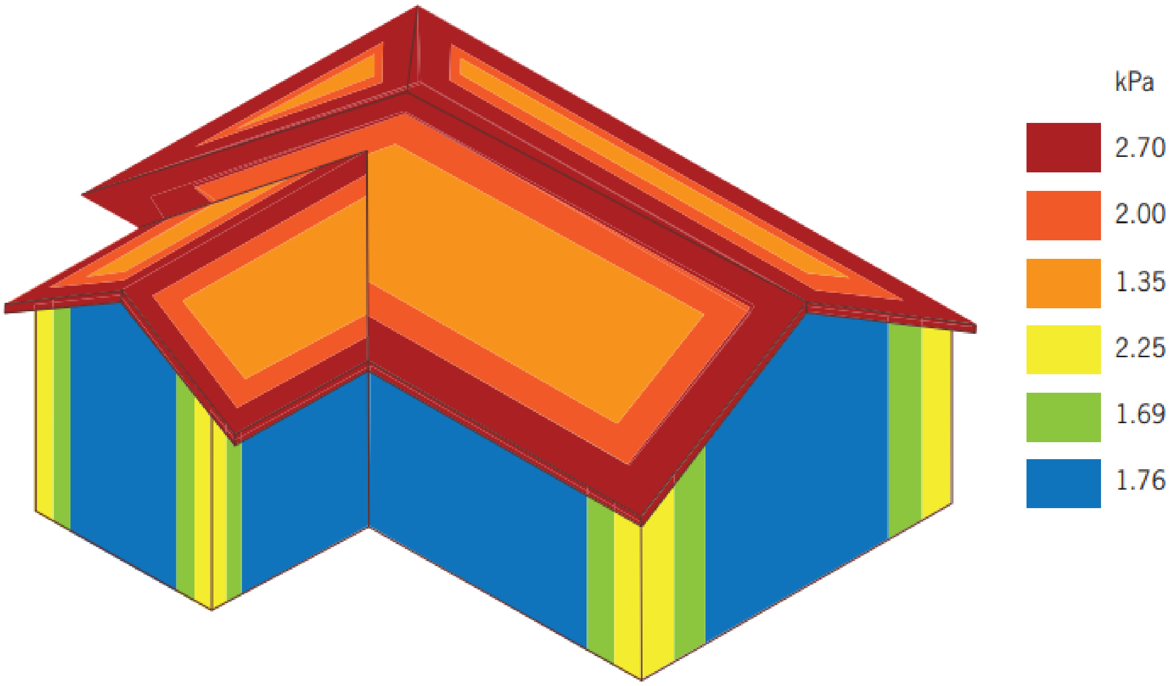

Figure 59-Wind pressure on different surfaces of a single storey building [67]

7.3 Cladding Fixing to FRP Wall System vs fixing to Timber Framing

Due to the profile the FRP wall panel, which incorporates a continuous composite FRP skin and rigid internal core, the panel itself resists internal pressurisation and prevents air movement through the wall assembly. As a result, the internal pressure component that typically contributes to a differential load on lightweight framed walls is effectively eliminated or reduced in the FRP wall panel system. In the context of cladding and fixing design, the primary consideration is the external wind pressure exerted perpendicularly to the cladding surface. This pressure must be effectively resisted and transmitted through the cladding system and its fixings into the FRP substrate, without depending on internal linings for additional resistance. This behaviour represents a fundamental departure from conventional timber framing structure.

As illustrated in Figure 60, in traditional timber framed construction, cladding systems and cavity battens are generally affixed directly to structural framing studs [68]. This often requires an increased density of studs and additional blocking to ensure sufficient structural support for the fixings [20]. This requirement potentially contributes to higher framing percentages and greater thermal bridging [20].

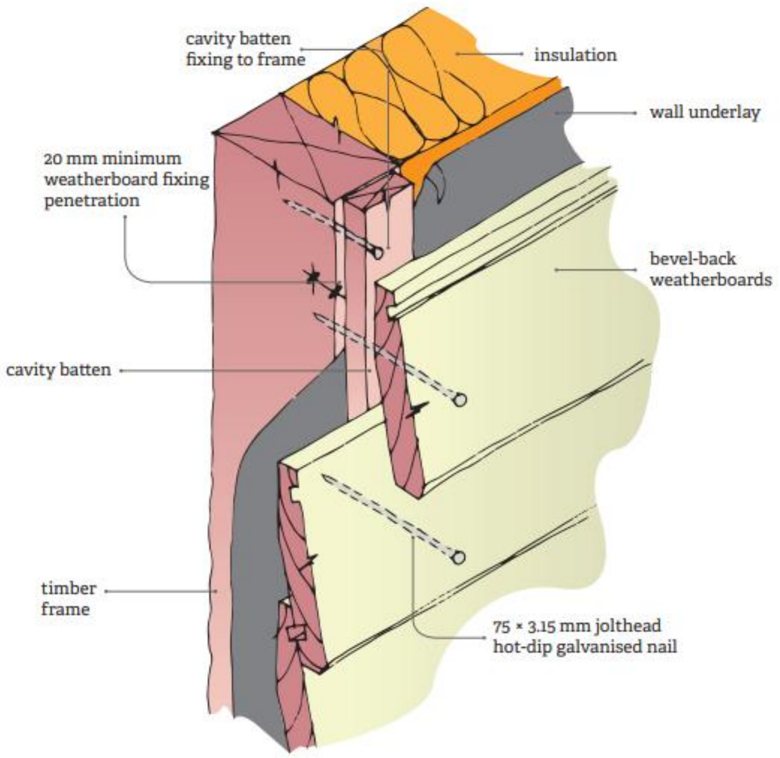

Figure 60-Example of weatherboard cladding fixing to the timber framing structure [68]

By contrast, the FRP wall panel system enables cladding or cavity battens to be fixed directly to a continuous FRP substrate, eliminating the need for additional stud framing, and reducing reliance on internal linings to resist pressure differentials and limit deformation under wind loading.

As illustrated in Figures 61 and 62, the installation of cavity battens and external cladding onto the FRP wall surface in the case study building is notably more straightforward and efficient compared to traditional timber framed construction methods. Fasteners can be installed at regular intervals of 600 mm directly into the continuous external surface of the FRP panels, without the necessity of aligning with underlying studs, nogs, or additional framing components. No supplementary structural support is required at corners, junctions, or other complex locations that would typically demand local reinforcement in a conventional framing system.

Figure 61-600m spacing cavity batten vertical fixing for the horizontal cladding

Figure 62-600m spacing cavity batten horizontal fixing for the vertical cladding

7.4 Screw Fixing to the FRP Panel Walls-Lateral Resistance Testing

The screw lateral resistance tests were conducted to evaluate the in-plane shear performance of mechanical fasteners used to fix cladding components to the FRP wall panels and to characterise the governing failure modes of the connection under progressively increasing load. The test result is critical for assessing the adequacy of the FRP panel as a fixing substrate for external claddings subjected to wind actions.

The tests were conducted using a calibrated universal testing machine, with the test procedure carried out in general accordance with the provisions of AS1649:2001 [69], which establishes standard methods for determining the basic working loads and characteristic strengths of mechanical fasteners. Each test specimen comprised a 1.0 mm thick galvanized steel U-section, which was mechanically affixed to a 250 mm deep FRP panel substrate using four screws, with two screws positioned on each side. Two types of screws were evaluated: a 10×10-gauge, 32 mm long galvanized screw (Figure 63 (a)) and a 6×12-gauge, 25 mm long galvanized screw (Figure 63 (b)). A lateral force was applied at 1.25mm/minute to the top U-section in the plane of the FRP panel, therefore placing the screws in shear. Displacement was measured and the load–displacement response was recorded until specimens reached and exceeded their peak resistance. The load measured at a displacement of 2.5 mm was of particular significance, as it is widely regarded as indicative of a functional connection state in fastener testing.

(a) Sample for 10 Gauge Screw Fixing (b) Sample for 12 Gauge Screw Fixing

Figure 63-Screw fixing

Figure 63 (a) presents the test results for all 10-gauge screws, while Figure 63 (b) displays the test results for all 12-gauge screws. The test results indicate that both screw types provide substantial resistance to lateral loading when fixed into the FRP panel substrate. At a displacement of 2.5 mm, the average lateral resistance per screw for the 10 gauge screws was approximately 3.26 kN, with the lowest measured value being approximately 2.01kN (Figure 65). The 12 gauge screws exhibited an average lateral resistance of approximately 2.44 kN at the same displacement, with a minimum value of approximately 1.53 kN (Figure 64).

The failure modes observed during testing were primarily caused by deformation of the thin steel U-section and bending or minor rotation of the screws, rather than fracture or pull-out of the screws from the FRP panel. Figure 66 shows that localised buckling of the steel section was frequently observed at elevated load levels, accompanied by progressive deformation of the screw shank under increasing shear demand. However, there was no indication of brittle failure or splitting within the FRP substrate itself.

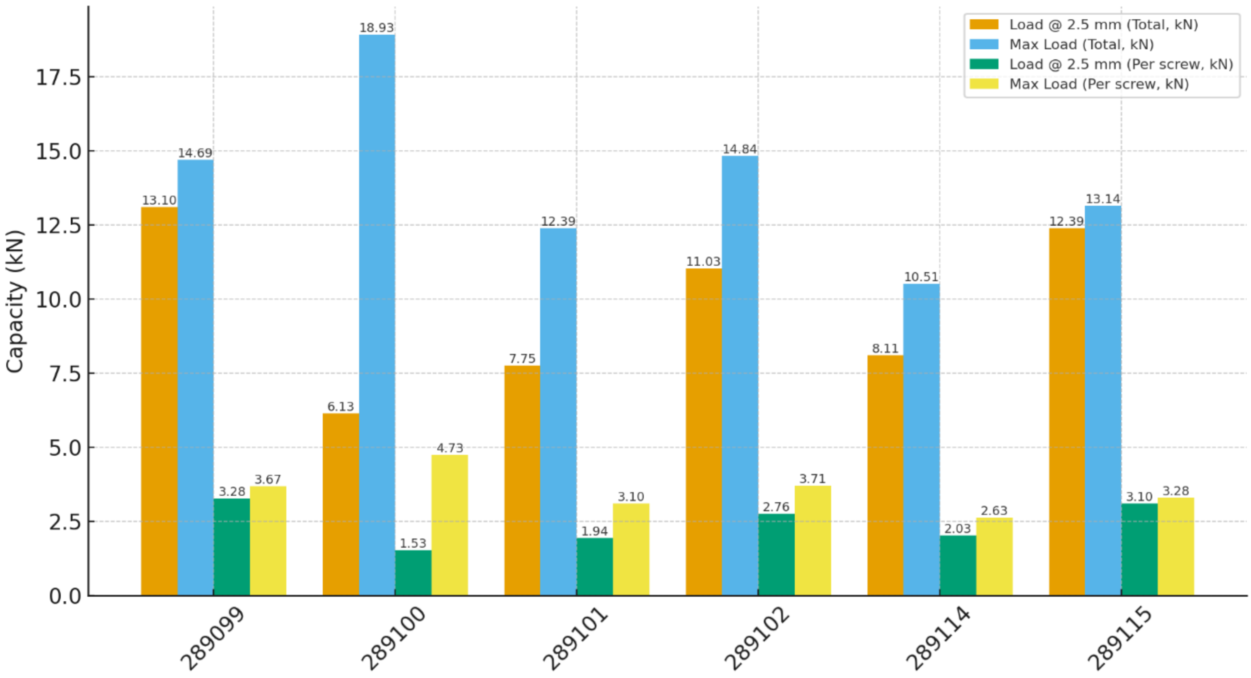

Figure 64-12g screws FRP panel fixing lateral resistance test result

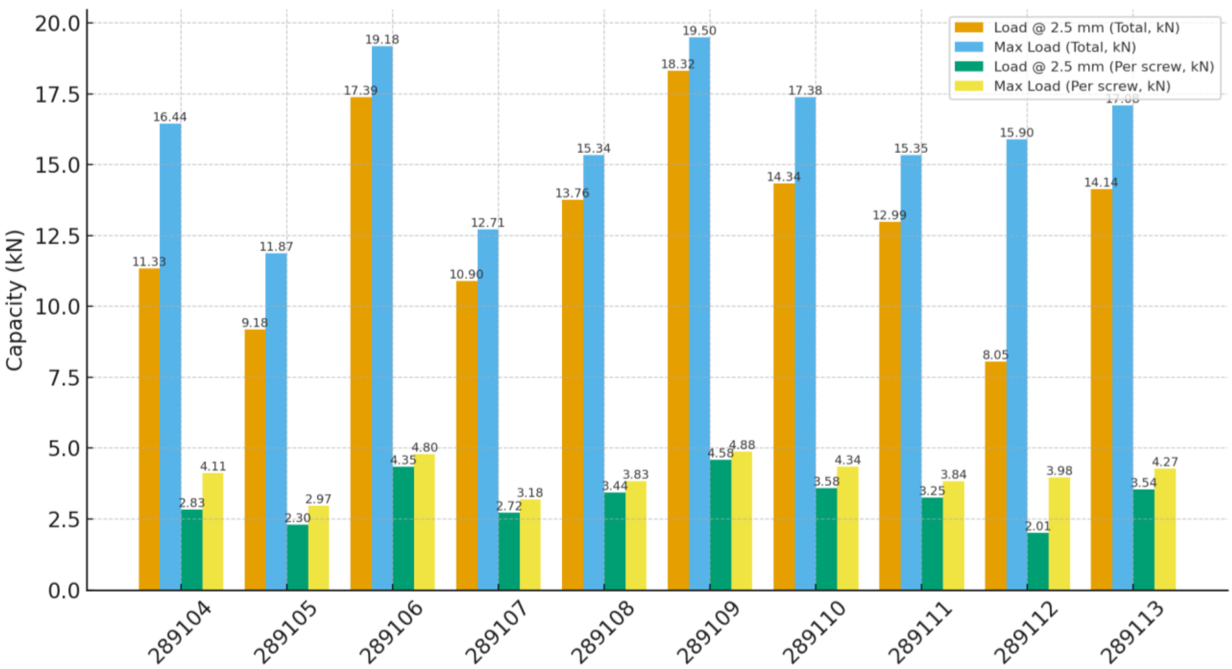

Figure 65-10g screws FRP panel fixing lateral resistance test result

Figure 66-The steel U-section on the side buckling at the bottom

Although a degree of variability was observed across specimens as reflected by the reported coefficients of variation, this behaviour is typical for fastener testing where outcomes are influenced by minor differences in embedment, local material heterogeneity, and installation conditions. It was also noted during testing that the U-section steel components were not cut perfectly square, which resulted in minor misalignment of the specimens within the test rig. Therefore, packing was required to prevent rocking of the assembly during load application. This imperfection in the test setup contributed to local instability in some specimens.

The most common failure mode was initiated by buckling of the thin steel U-section, followed by twisting of the screw under increasing lateral load. In one notable specimen (ID 389106), the U-section did not buckle, and this specimen achieved the second-highest lateral resistance recorded among the ten tests. This observation suggests that the capacity of the connection was, in several cases, governed by premature instability of the steel section rather than by the intrinsic shear resistance of the screw–FRP interface. It is therefore reasonable to conclude that the reported test results are likely conservative, and that the true lateral capacity of the screw when fixed into the FRP panel may be higher than indicated by the measured values.

7.5 Verification of Screw Fixing to the Cladding of the Case Study Building

Cladding and cavity battens are fixed directly to the external face of the FRP panel walls of the case study building as shown in Figures 61 and 62. Accordingly, the design action for the cladding fasteners can be conservatively taken as the external wind pressure alone, with a design ULS pressure 2.5 kPa as discussed in Section 7.2 above. The force acting on an individual cladding fixing was determined using the tributary area method, in which a uniformly distributed surface pressure is converted into an equivalent point load acting on an individual screw. This approach is consistent with standard structural engineering practice for the application of wind actions in accordance with AS/NZS 1170.2 [66]. Taking the 600 mm fixing spacing commonly adopted in high wind zone timber framed construction as a reference [3], a spacing of 600 mm × 600 mm is applied for the cladding fixings in this study. Accordingly, the tributary area associated with each fixing is calculated as 0.36 m².

For the purposes of convenience and consistency in structural verification calculations, the design wind pressure of 2.5 kPa is expressed as 2.5 kN/m², therefore allowing the applied wind load to be directly related to the tributary area associated with each fixing. This unit conversion facilitates a straightforward determination of the resultant force acting on individual cladding fasteners under the specified ultimate limit state condition.

On this basis, each screw within the 600 mm × 600 mm spacing designated for the cavity batten or cladding attachment will possess a lateral force resistance capacity as:

$$2.5\ \text{kN/m}^2 \times 0.36\ \text{m}^2 = 0.9\ \text{kN}$$

Based on the comparative test results, the 10-gauge screws demonstrated a consistently higher shear load capacity than the 12 gauge screws. In addition, 10 gauge screws are specified by the relevant cladding manufacturer for fixing cladding systems to steel framing [70]. Accordingly, the verification of the fixing performance in this study is based on the measured capacity of the 10-gauge screws, as this represents both the better structural capacity option and the industry recommended configuration.

In structural verification, the governing consideration is not the best performing specimen but the lowest level of performance that can be relied upon in practice. AS 1649 is explicitly concerned with the derivation of basic working loads and characteristic strengths for mechanical fasteners and connectors [66]. The characteristic strength is commonly taken to be a fifth-percentile value, representing a level of resistance that at least 95% of comparable connections are expected to exceed [66]. Furthermore, it is appropriate to adopt the load corresponding to a displacement of 2.5 mm as the representative serviceable capacity of the screw to FRP wall substrate fixings.

This distinction is particularly important for cladding fixings, where performance is not governed solely by avoidance of sudden failure, but also by the requirement to limit movement and maintain functional integrity. If relative movement at the cladding–substrate interface is not adequately controlled, undesirable serviceability issues may arise. Such movement can manifest as rattling, cracking, or fretting of the cladding around the fixings, compromise the integrity and tightness of joints, create potential pathways for moisture ingress, and lead to localised damage at the connection points between cladding and FRP interface under repeated wind loading. Accordingly, the adoption of the 2.5 mm displacement load as the basis for verification provides a rational and conservative assessment of the connection's ability to maintain both structural adequacy and serviceability under the prescribed wind actions.

In the case study building, cavity battens and, therefore, the associated cladding fixings are installed on a regular grid at 600 mm centres in both the vertical and horizontal directions. For verification purposes, each screw is assumed to support a tributary area equal to 0.36 m^2. The lowest measured lateral resistance of the 10 gauge screw at a displacement of 2.5 mm was 2.01 kN, representing the minimum proven performance recorded in the later force resistance test series. This lowest value is therefore more than twice the calculated design demand of approximately 0.90 kN imposed on a single fixing under a design differential wind pressure of 2.5 kPa at 600 mm × 600 mm spacing. Accordingly, even when the most conservative test result is adopted for verification, the screw to FRP wall fixing demonstrates a substantial margin of safety. This confirms that cavity battens and cladding fixed to the FRP wall panel system at this spacing will remain securely restrained, maintaining the stability and integrity of the cladding under extreme wind loading conditions.

8. Infield Heatflux Investigation and U-value Validation

8.1 Heat-Flux Monitoring Setup

This study focuses on heat-flux variations and derived U-values to validate the theoretically calculated R-value of the FRP wall panel system and to provide a more granular assessment of how the system's inherent configuration mitigates thermal bridging and contributes to the overall thermal performance of the building envelope.

Figure 67-The Investigated master bedroom (circled) of the case study building

Figure 67 identifies the selected case-study dwelling and the north-east-facing master bedroom chosen for experimental monitoring between October and December 2024. Dynamic thermal-performance data were collected using Greenteg heat-flux sensors and Pico data loggers to enable the calculation of in-situ thermal transmittance. The tested external wall of the master bedroom is constructed using the FRP wall-panel system, finished with black metal cladding, and complemented by lightweight steel roofing, double-glazed windows, and aluminium sliding doors. The room is formed on a concrete slab with a carpet overlay, and the ceiling is lined with gypsum board. The internal dimensions are approximately 3.1 m × 3.2 m, enclosing a volume of roughly 24 m^3.

The analysis focuses on heat transfer through the external wall, with particular attention to heat-flux patterns and the corresponding thermal transmittance (U-values) over a full diurnal cycle from 12:00 a.m. to 11:59 p.m. To maintain analytical clarity, several simplifying assumptions are introduced. First, the assessment is confined to the north-east-facing wall, which receives the greatest morning solar exposure and therefore provides a representative basis for evaluating potential overheating during the spring monitoring period. Second, the temperature and heat-flux measurements are used to examine the relationship between thermal transmittance, diurnal temperature fluctuations, and indoor thermal comfort. This methodological approach facilitates a targeted and evidence based evaluation of the FRP wall-panel system's thermal performance under real-world operating conditions.

The case study building is located in Climate Zone 2 (Hamilton, Waikato) shown in Figure 68,

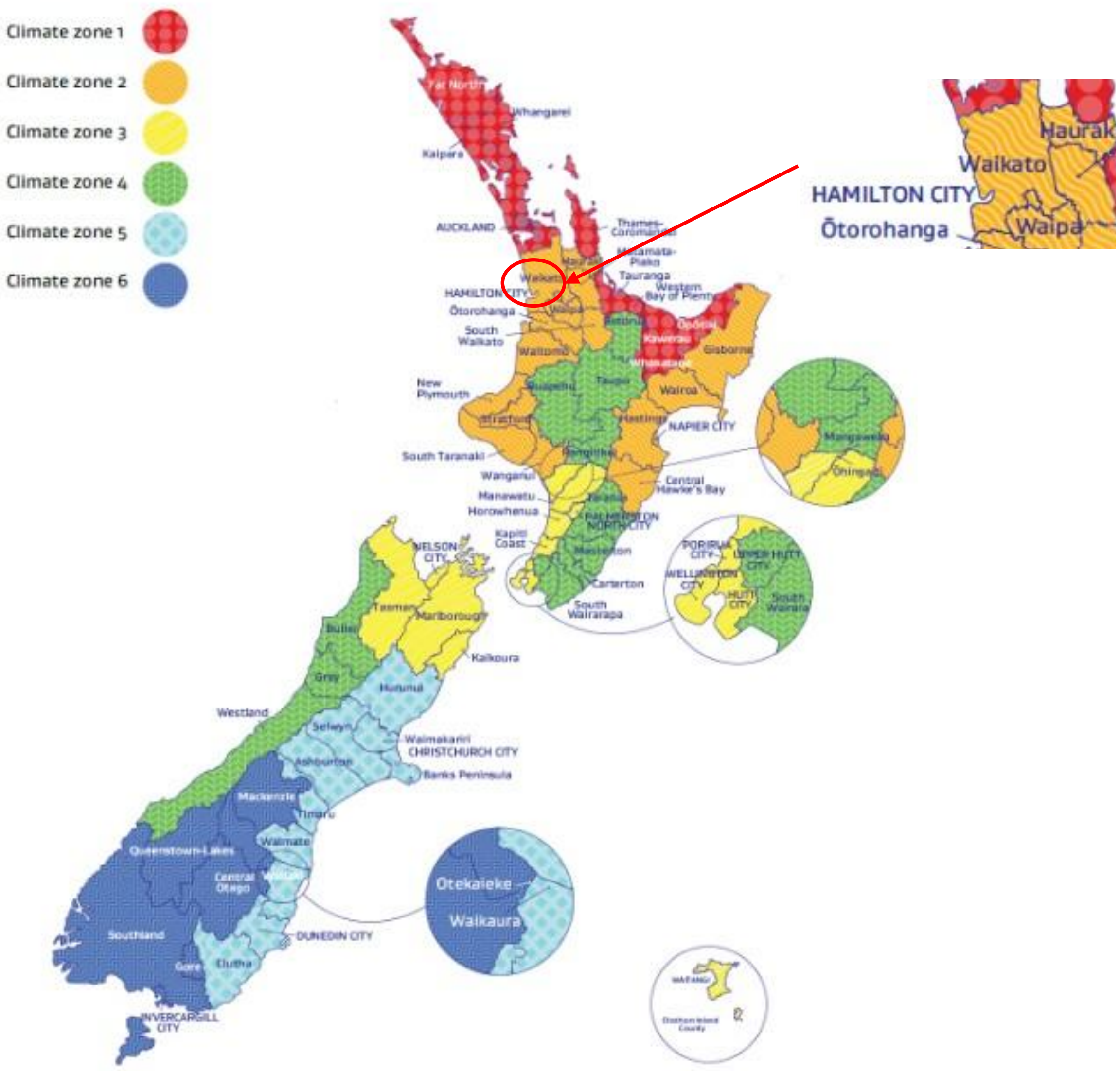

Figure 68-Map of New Zealand Climate zones [6]

Table 20 represents the average temperature in each zone of the six climate zones showing in Figure 68 from H1/AS1 [6]. The case study building is in Hamilton, which is classified as climate zone 2 as shown in the table.

Table 20-The average temperature in each zone of the six climate zones. [11]

Climate Zone	Regions	Summer Avg. (°C)	Winter Avg. (°C)	Notes
Zone 1	Northland, Auckland	18 - 22	10-14	Warmest zone, humid summers, mild winters
Zone 2	Bay of Plenty, Waikato, Gisborne	16 - 21	8-12	Moderate winters
Zone 3	Taranaki, Manawatū-Whanganui, Hawke's Bay	15 - 20	6-10	Inland areas experience cooler winters
Zone 4	Wellington, Nelson, Marlborough	14 - 19	5-9	Moderate climate, windy conditions in Wellington
Zone 5	Canterbury, Otago	12-18	3-10	Dry summers, cold winters, occasional frosts
Zone 6	Southland, West Coast, Fiordland	10-16	2-7	Wettest and coldest region, high rainfall

8.2 Investigation Procedures

This field investigation applied non-invasive methodologies to evaluate thermal performance, incorporating temperature monitoring, heat flux measurements, and thermal transmittance assessments. Data collection was conducted from 14 October to 30 December 2024, employing a Greenteg U-value kit (heat flow meter method, HFM) (Figure 69) and Pico loggers (TC-08 model) (Figure70) equipped with K-type thermocouples, in accordance with ISO 9869-1 guidelines [76]. The loggers, fitted with six calibrated thermocouples, were positioned on both the interior and exterior surfaces of the tested wall. Figure 70 shows the loggers are place on the outside of the tested wall.

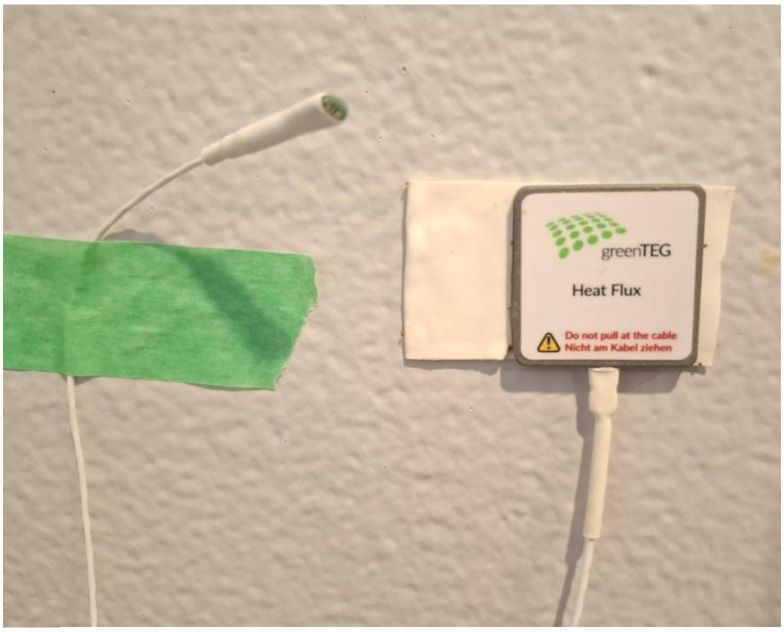

Figure 69-Heat flow meter (right) Pico logger (left)

Figure 70-The Pico loggers set up on the outside of the wall

The Greenteg kit comprised a heat flux sensor and two surface-mounted thermocouples, while the Pico loggers utilised six calibrated thermocouples (±0.5°C accuracy). Sensors were installed on a 3.0 × 2.42 m FRP wall panel system to evaluate thermal transmittance (U-value) and heat flux. During the first phase, four thermocouples and one heat flux sensor were positioned at 250 mm intervals across the wall's lower half (Figure 69). In the second phase, the configuration was expanded to six thermocouples distributed uniformly across the entire wall surface (Figure 71). All sensors were connected to a Pico logger, recording indoor and outdoor temperatures at 1-minute interval and heat flux at 10-minute intervals. The data were then averaged hourly to align with the analysis intervals.

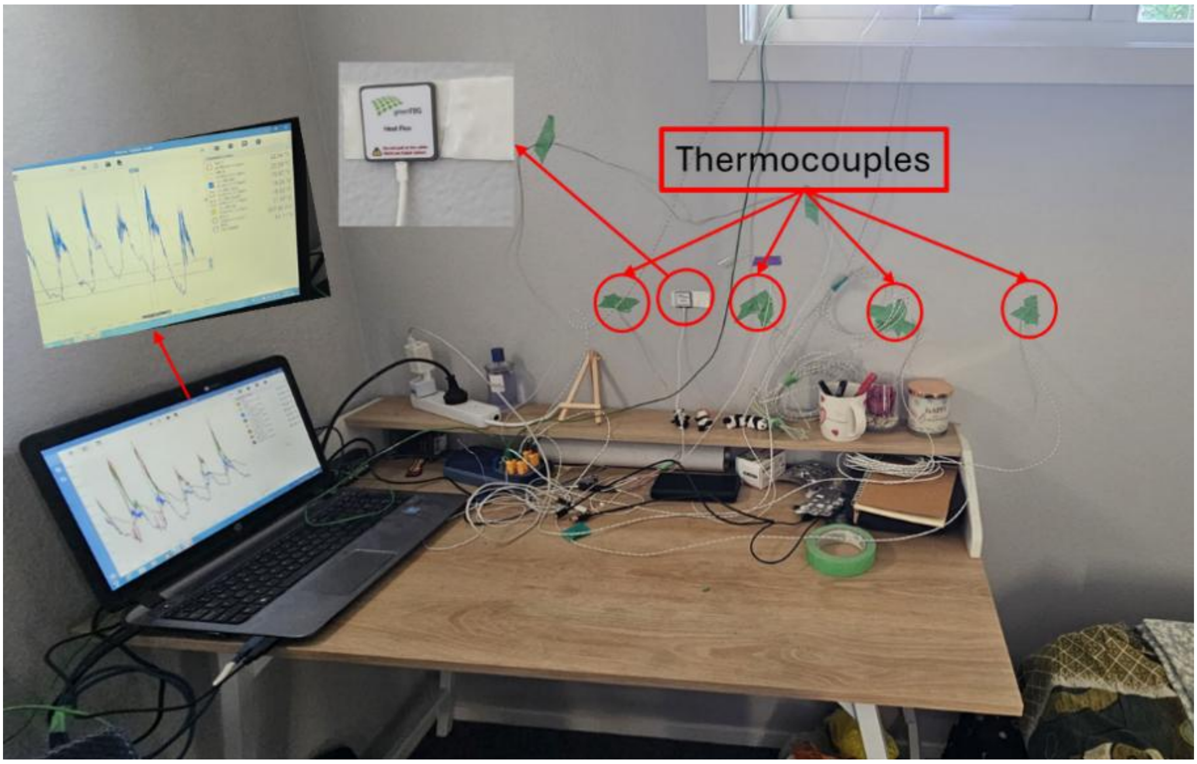

Figure 71-Overall view of the thermocouples and heat flux sensor inside of the wall

8.3 In-situ Measurements

8.3.1Temperature Measure

There are various instruments used to measure indoor and outdoor temperatures of the building, such as thermometers, sensors, thermocouples, and infrared cameras [77, 78, 79]. However, type K thermocouples are most widely used because of their cost effectiveness and reliability for temperature recording over a long period of time [79,80,84]. This research uses a Pico logger and thermocouples (type K) to measure indoors and outdoors (Table 21). The thermocouples used for research were calibrated using boiling water (99.5–100 °C) and cold water (0°C–0.5°C).

Table 21-Sensor/Datalogger details

Sensor/data logger	Model	Number	Range	Accuracy
Data logger	TC08 A0059/413	8 channels	–270 up to +1820°C	-
Thermocouple	Type K	8	–250 to +1370°C	±0.5ºC
Terminal board	Single channel	1	±70 mV	-
Humidity		1	5% to 95%	±5%

8.3.2 Thermal Transmittance and Heat Flux

The thermal performance of building walls is most effectively evaluated through their thermal transmittance (U-value). Prior research has widely applied the heat flow meter (HFM) method to determine the U-values of different wall systems [34], including studies that assessed three typologically distinct walls using in-situ heat-flux monitoring [81,82]. Other investigations have combined HFM measurements with ISO 6946 based simulation methods to analyse thermal conductivity in non-uniform assemblies such as light steel framing systems [83]. Jung et al. [84] further demonstrated the efficacy of heat-flux monitoring for quantifying the thermal transmittance of building envelopes under real operating conditions. Across these studies, experimental procedures generally conform to ISO 9869-1, which specifies data acquisition protocols for low-thermal-mass materials, including the requirement that measurements be collected from one hour after sunset until sunrise to minimise solar influences [85]. In alignment with this standard, the FRP wall-panel system characterised by its non-homogeneous composition, lightweight construction, and low thermal mass was subjected to a continuous 75-day monitoring programme. Heat-flux and temperature data were recorded using Greenteg sensors in accordance with ISO 9869-1 shown in Table 22 to ensure accurate, stable, and representative determination of the system’s in-situ thermal transmittance.

Sensor	gSKIN®-XO 67 7C (30mm x 30mm)
Logger	gSKIN® DLOG-4231
Heat Flux Range	±300 W/m²
Heat Flux Resolution	<0.22 W/m²
Temperature Accuracy	±0.5°C (-10 to +46°C)
Calibration Temperature range	-40 to 70°C
Operating Temperature	-40 to 100°C
Measurement Frequency	1/s to 1/h
Calibration Accuracy	±3%

Table 22-Greenteg U-Value kit

This research examines heat transfer, heat loss and gain, heat-flux behaviour, heat storage, and thermal transmittance through the tested external wall over the monitoring period from 14 October to 30 December 2024. During this period, the room was occupied approximately 80% of the time, providing a representative set of real-world internal thermal conditions. The selected wall is oriented toward the north-east, exposing it to substantial morning solar radiation during the spring and early summer months, thereby offering an appropriate basis for evaluating both heat-gain dynamics and potential overheating risk. In addition to in-situ monitoring, the study employs the ISO 6946 calculation method to derive theoretical thermal transmittance values for comparison with measured performance [80].

$$U = \frac{1}{R_{sout}+\sum_{i=1}^{n}\frac{S_i}{\lambda_i}+R_{sin}} \qquad \text{(Eq. 23)}$$

Additionally, the average method from ISO 9869 has been used to calculate thermal transmittance using the heat flux value obtained from U-Value kit [85].

$$U = \frac{\sum_{j=1}^{n} q_j}{\sum_{j=1}^{n}(T_{ij}-T_{ej})} \qquad \text{(Eq. 24)}$$

The thickness (si (m)) and thermal conductivity(λi [W/(m/K)]) of each wall layer are considered, while q_j represents the heat flux through the wall. T_{ij} and T_{ej} denote the indoor temperature and outdoor air temperature, respectively. *Rs,out* and *Rs,in* are the thermal resistances of the outer and inner surfaces, respectively.

To apply the overall construction R-value of 2.84 the FRP wall panel system calculated in Section 5.8 of Chapter 5, and substitute 0.09 + 2.72 + 0.03 = 2.84 m²·K/W into Equation 23 to calculate the theoretical U-value = 0.352 W/m²·K.

8.4 Summary of Findings and Discussion

For the monitored wall, measurements were averaged from two thermocouples (±0.5°C accuracy) on both the indoor and outdoor surfaces, and one thermocouple each indoors and outdoors to measure ambient temperature. Data were logged at one-minute intervals (temperature) and 10 minutes (heat-flux) intervals, then aggregated into hourly averages for seasonal trend analysis. The 10-minute interval for heat flux recording was chosen due to the FRP wall panel system’s low thermal mass, integrated 60mm phenolic foam rigid insulation (high thermal inertia), and 25 mm air gap.

According to ISO 9869 [85], accurate U-value measurement for low thermal mass materials requires data collection exclusively between sunset and sunrise. Hourly averages were first calculated to ensure accuracy, after which these values were categorised into distinct daily timeframes (Table 23).

12:30 - 8:30 a.m.	Night to Pre-sunrise
8:30 - 11:30 a.m.	Solar gain and occupancy
11:30 a.m. - 6:30 p.m.	Peak solar exposure
6:30 - 10:30 p.m.	Post-sunset cooling – Thermal lag
10:30 p.m. - 12:30 a.m.	Late-night stabilization

Table 23-Different time frames for study

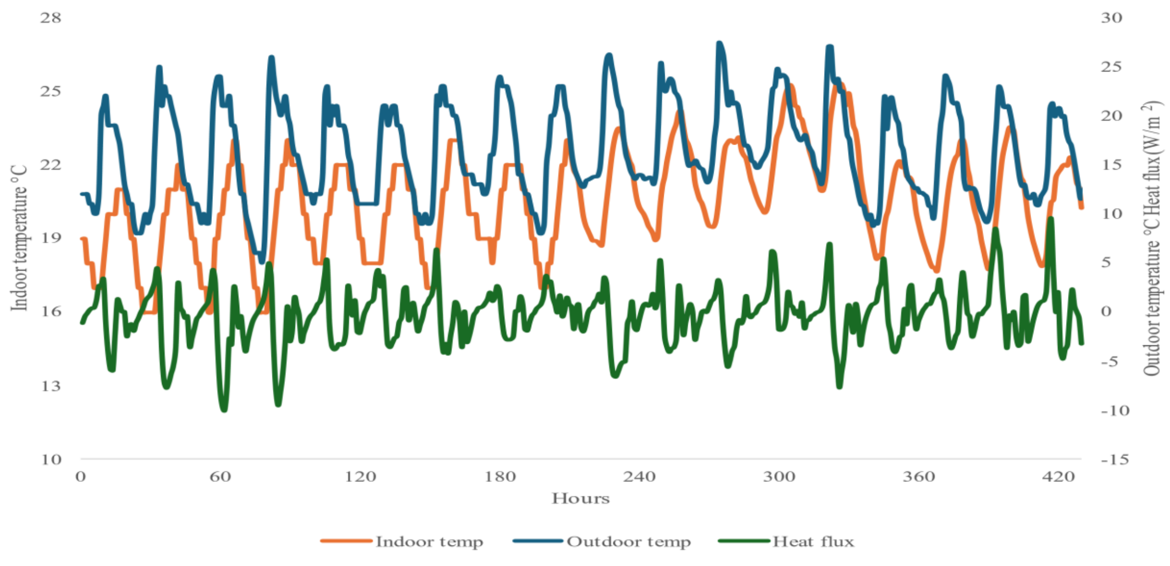

Figure 72-Outdoor temperature, indoor temperature and heat flux in October 2024

Figure 72 presents the outdoor and indoor temperature data recorded from 14 to 31 October 2024. The data indicate that the maximum hourly outdoor and indoor temperatures reached 27°C and 25°C, respectively. Throughout this period, indoor temperatures remained within the comfort range of 18°C to 25°C for 387 hours, accounting for 89.6% of the total 432 hours, which corresponds to 16 out of the 18 days. The FRP wall panel system exhibited strong performance during the spring and early summer, effectively maintaining thermal comfort despite moderate outdoor heat. Furthermore, heat flux analysis revealed that 378.51 W/m² was transferred into the wall, while 528.97 W/m² (28% higher than the amount absorbed from indoors) was released into the room from the external wall system, underscoring its capacity for thermal regulation.

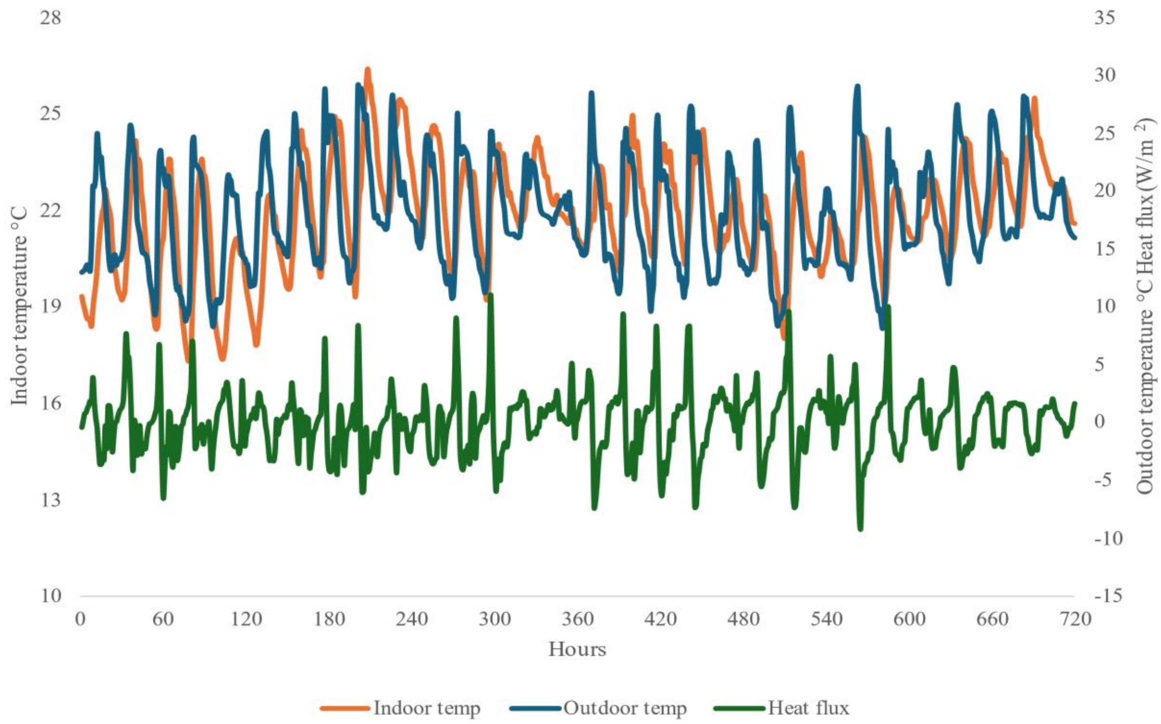

Figure 73-Outdoor temperature, indoor temperature and heat flux in November 2024

Figure 73 illustrates the temperature trends observed from 1 to 30 November 2024, with outdoor and indoor temperatures reaching 29°C and 26°C, respectively. Indoor temperatures remained within the comfort range (18°C–25°C) for 694 hours, accounting for 96.4% of the total 720 hours, which corresponds to 29 out of 30 days. Notably, heat flux measurements revealed that the wall absorbed 712.68 W/m² and released 740.59 W/m², which is 4% higher than the absorbed amount from indoors, thereby highlighting the efficiency of the FRP wall panel system under moderate thermal stress.

Figure 74 presents the temperature trends and heat flux data from 1 to 30 December 2024, during which the outdoor and indoor temperatures reached maximum values of 33°C and 28°C, respectively. Indoor conditions remained within the comfort range of 18°C to 25°C for 490 hours, accounting for 68.1% of the total 720 hours, equivalent to 20 out of 30 days. During this period, heat flux measurements indicated that 914.11 W/m² of heat was absorbed by the wall panel system, while 1013.76 W/m², which is 10% higher than the absorbed amount, was released from the system, demonstrating dynamic thermal regulation. Additionally, cumulative data from October to December 2024 indicate that indoor temperatures were within the comfort range (18°C–25°C) for 83.9% of the time, with 13.3% of the time exceeding 25°C (overheating) and 2.8% falling below 18°C (underheating).

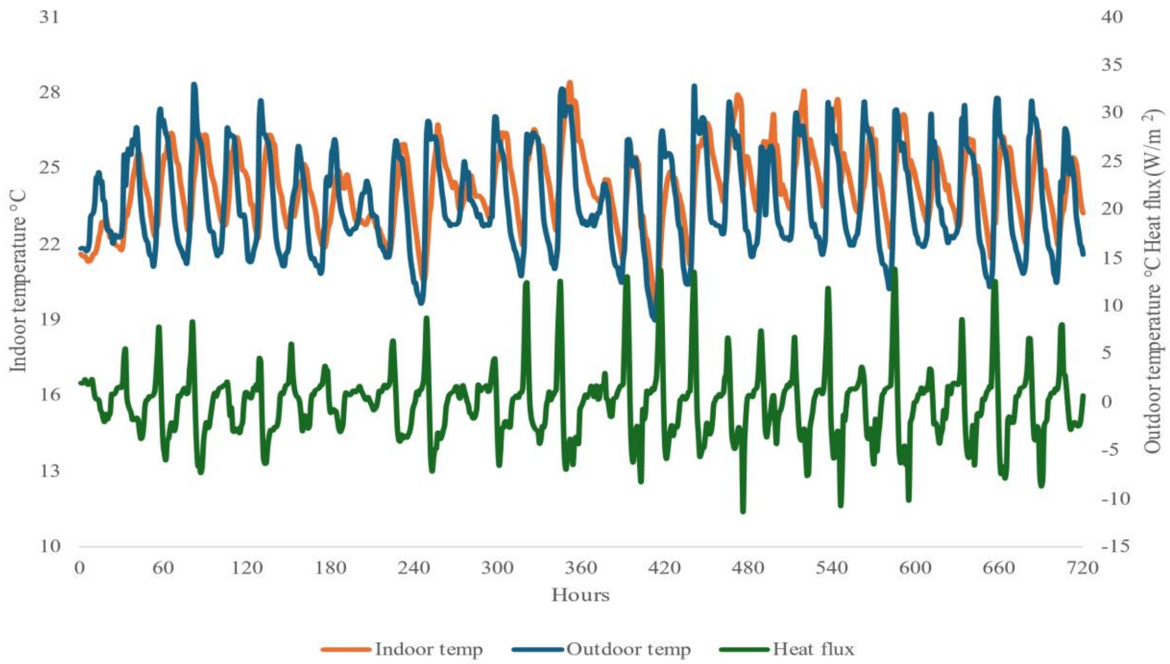

Figure 74-Outdoor temperature, indoor temperature and heat flux in December 2024

In October, the FRP wall panel system absorbed 307.41 W/m² of heat into the wall while releasing 509.20 W/m² back into the room, resulting in a net heat discharge of 201.79 W/m². This indicates that the system utilised stored thermal energy to help maintain indoor comfort during the cooler spring conditions. In contrast, the behaviour changed in November and December, when the heat absorbed by the wall (606.36 W/m² and 914.11 W/m², respectively) exceeded the heat released indoors (694.24 W/m² and 1013.76 W/m²). This pattern demonstrates the FRP wall panel system's increasing capacity to store excess thermal energy as outdoor temperatures rose and heat stress intensified. Taken together, the net heat release observed in October and the net heat absorption recorded in the following months highlight the dynamic thermal balance maintained by the building system. By alternating between thermal storage and thermal dissipation, the system contributes to stable indoor temperatures across changing seasonal and climatic conditions.

Despite the inherently low thermal mass of the FRP panels, the integrated system design, which incorporates insulation, external cladding, and an air gap, enables effective heat retention. This behaviour is evidenced by the positive heat flux directed into the wall and the negative heat flux from the wall into the indoor environment, together indicating that the system stores heat derived from both outdoor solar gains and indoor thermal loads. The subsequent gradual release of this stored heat during cooler periods contributes to the stabilisation of indoor temperatures and mitigates the occurrence of temperature extremes.

Hourly outdoor temperature, indoor temperature, and heat flux measurements for the case study room (14 October – 30 December 2024) are presented in Figure 75. The data illustrate the relationship between positive heat flux (heat flow into the wall) and negative heat flux (heat flow from the wall). In the morning (8:30 a.m. – 11:30 a.m.), predominantly positive heat fluxes indicate wall absorption of heat from the room, driven by sunrise-induced solar radiation. Conversely, in the daytime (11:30 a.m. – 6:30 p.m.), mostly negative heat flux persists, signifying heat transfer through the wall system into the room. This aligns with peak solar radiation and outdoor temperatures, driving convective and conductive heat gain.

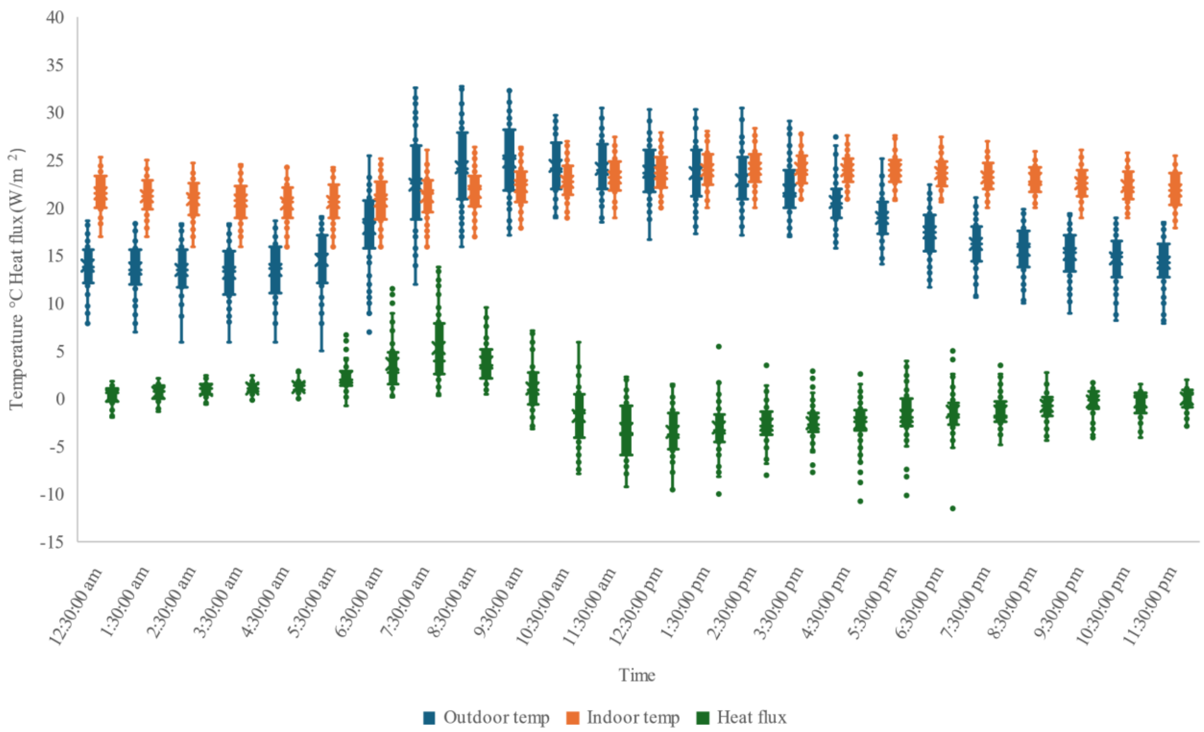

Figure 75-Outdoor temperature, indoor temperature and heat flux of different time frame October - December 2024

During the period from evening through to the following morning (6:30 p.m. to 8:30 a.m.), the recorded heat flux alternates between positive and negative values. Between 6:30 p.m. and midnight, negative heat flux dominates, reflecting the release of stored heat from the wall into the room as both outdoor and indoor temperatures decline. This behaviour demonstrates a clear diurnal cycle in which the wall system absorbs heat during warmer daytime conditions and then releases it during cooler periods, which helps moderate indoor temperature fluctuations. During the summer monitoring period (15 November to 30 December), the early morning hours (12:30 a.m. to 8:30 a.m.) show a gradual movement of heat from the room into the wall. This inward heat transfer contributes to the maintenance of stable nighttime indoor temperatures within the comfort range of 18 °C to 25 °C and limits the influence of outdoor cooling on indoor conditions.

Month	Duration	Outdoor	Indoor	U values [W/m^{2}K]
Oct	12:30 - 8:30 a.m.	16	23	0.108
Nov	12:30 - 8:30 a.m.	14	21	0.243
Dec	12:30 - 8:30 a.m.	16	23	0.246
Oct	8:30 - 11:30 a.m.	22	20	0.178
Nov	8:30 - 11:30 a.m.	23	21	0.332
Dec	8:30 - 11:30 a.m.	27	24	0.273
Oct	6:30 - 10:30 p.m.	14	22	0.086
Nov	6:30 - 10:30 p.m.	16	23	0.129
Dec	6:30 - 10:30 p.m.	19	25	0.387
Oct	10:30 p.m. - 12:30 a.m.	13	20	0.280
Nov	10:30 p.m. - 12:30 a.m.	15	22	0.151
Dec	10:30 p.m. - 12:30 a.m.	17	24	0.060

Table 24-U value during different hours October 2024 - December 2024

Table 24 presents a summary of the U-values calculated based on the data collected for indoor and outdoor temperatures in the testing room, excluding daytime hours (11:30 a.m. – 6:30 p.m.), in accordance with ISO 9869 guidelines for lightweight materials [85]. Utilizing Equation 24, the highest U-value (0.387 W/m^{2}K) was observed in December during the period from 8:30 a.m. to 11:30 a.m., whereas the lowest U-value (0.06 W/m^{2}K) was recorded in December from 10:30 p.m. to 12:30 a.m. The average U-value for the study period was 0.206 W/m^{2}K, with outdoor and indoor temperatures of 17°C and 22°C, respectively, thereby confirming the effectiveness of the FRP wall panel system in moderating heat transfer.

During monitoring, the FRP wall panel system maintained indoor temperatures within the comfort range (18–25°C) for 83.9% of the period, even when outdoor temperatures reached 33°C. Heat flux analysis revealed dynamic thermal behaviour. In October, 28% more heat was released from the wall than was absorbed, indicating thermal storage from external sources such as solar radiation. In November and December, the heat flow into the room exceeded the outflow by 4% and 10%, respectively, demonstrating the system's capacity to adaptively release heat and stabilise indoor conditions during summer. In October, indoor heating contributed to thermal stability, whereas in November and December, heat dissipation was needed to maintain comfort indicating that reduced heat flow enhances thermal comfort during warmer months.

8.5 R-value Validation

The comparison between the in-field measured U-values and the theoretically calculated U-value of the FRP wall panel system (0.352 W/m²K) demonstrates a consistent trend of superior thermal performance under real operating conditions. The in-field results, which range from 0.060 to 0.387 W/m²K with an average value of 0.206 W/m²K, are predominantly lower than the theoretical prediction. As illustrated in Table 24, eleven of the 12 measurements fall below the theoretical benchmark, with only one marginal exceedance of 0.387 W/m²K (approximately 10% higher). The substantially lower measured U-values indicate reduced heat transfer across the FRP wall assembly, reflecting the effectiveness of the system's insulation configuration, integrated air cavity, and minimised thermal bridging. The 41 percent reduction in the mean in-field U-value relative to the theoretical value shown in Table 25 suggests that the FRP wall panel system performs more efficiently in-situ than indicated by the theoretical calculation through the NZS 4214 isothermal planes method. This enhanced performance aligns with the dynamic thermal behaviour observed throughout the monitoring period and reinforces the system's suitability as a high-performing building envelope solution for New Zealand residential application.

Metric	In-field U-value	Theoretical U-value	Difference	% Difference
Minimum	0.060	0.352	–0.292	–83%
Maximum	0.387	0.352	+0.035	+10%
Average	0.206	0.352	–0.146	–41%

Table 25- The mean in-field U-value relative to the theoretical value

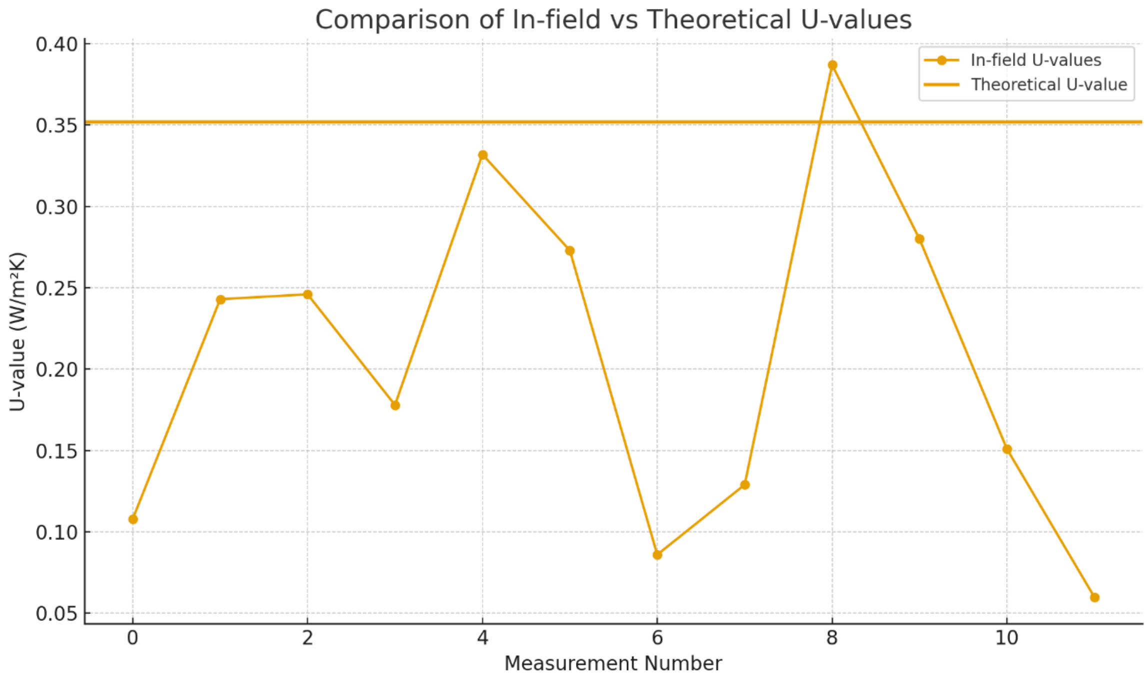

Figure 76-Comparison between the mean in-field and Theoretical U-values

The mean in-field U-value of the FRP wall panel system, derived from the twelve measurements, is 0.206 W/m²K. This corresponds to an in-situ construction R-value of approximately 4.85 m²K/W, calculated as the reciprocal of the average U-value. When compared with the theoretically derived U-value of 0.352 W/m²K (equivalent to an R-value of 2.84 m²K/W), the in-field result represents a substantial enhancement in thermal resistance (Figure 76). This finding provides strong empirical validation of the thermal-bridging calculations and supports the underlying assumption that the FRP wall panel system delivers an improved overall construction R-value relative to conventional framing-based assemblies. The elevated in-situ R-value indicates that the integrated configuration of FRP skins, phenolic foam insulation, and controlled cavity detailing effectively mitigates thermal bridging and enables the wall system to perform closer to its idealised thermal potential under real operating conditions.

The 70.8 percent improvement observed in the infield thermal resistance, compared with the theoretical R value calculated using the NZS 4214 isothermal planes method, can be explained by several factors that are not fully represented in the steady state calculation procedure. The isothermal planes method idealises the wall as a one-dimensional layered system and therefore excludes additional resistances provided by the internal gypsum lining, the carpeted concrete slab, and the internal and external air films, all of which contribute to higher effective thermal resistance in practice. The method also does not account for the external ventilated cavity created by the cavity battens, or for the localised still air regions within the FRP panel geometry that further suppress convective heat transfer. In addition, the calculation does not include the insulated corner junctions used in the case study dwelling. These corners were specifically detailed and filled with insulation to minimise thermal bridging, yet their contribution is not captured in the NZS 4214 construction R value calculation. Finally, the FRP wall system performs as a continuous insulated enclosure with minimal structural thermal bridges, and its real time behaviour, including its capacity to moderate short term temperature swings through transient heat storage, often exceeds what is predicted by steady state analytical methods. Together, these uncounted resistances and system level effects provide a coherent explanation for why the measured infield R value of 4.85 m^2K/W exceeds the theoretical value of 2.84 m^2K/W by 70.8 percent.

9 Conclusion

This study demonstrates that the novel FRP wall panel system provides a thermally superior and structurally competent alternative to conventional lightweight timber-framed construction for residential buildings in New Zealand.

Thermal-bridging calculations based on NZS 4214 show that the FRP wall panel system achieves a conservative construction R-value of R2.84 $m^2 \cdot K/W$, representing a 70–78% improvement over typical timber-framed walls with realistic framing fractions. In-field heat flux measurements further validated this advantage, with a mean measured U-value of 0.206 $W/m^2 \cdot K$ corresponding to an in-situ R-value of approximately R4.85 $m^2 \cdot K/W$, which is approximately 70.8% higher than the theoretical predictions. These results indicate that the system's integrated configuration, which combines continuous phenolic-foam insulation, controlled air cavities, and minimal structural thermal bridges, allows the FRP wall panel system to perform closer to its thermal potential under real operating conditions, whereas the performance of timber-framed walls is consistently depressed by framing density, insulation discontinuities, and workmanship variation.

Structural testing and assessments similarly confirmed the viability of the FRP wall panel system. BRANZ P21 racking evaluations showed that the FRP wall and lintel configurations satisfied or exceeded the requirements of NZBC Clause B1 and the AS/NZS 1170 suite, with acceptable ductility, displacement recovery, and system factors. Unlike timber lintel assemblies, which require trimming studs and create concentrated thermal bridge clusters, the integrated FRP lintel solution maintains structural robustness without undermining thermal continuity.

The combined findings highlight an important system-level characteristic: the FRP wall panel system is not a modification of the existing framing practice but a reconfiguration of the building envelope into a unified structural–thermal component. This integration eliminates many dual-material interfaces that drive thermal bridging and reduces the reliance on secondary thermal mitigation strategies. Consequently, the gap between the designed and as-built performance, which remains a persistent challenge for timber-framed construction, is significantly reduced.

Overall, the FRP wall-panel system exhibited consistent alignment between its theoretical, laboratory, and in-situ performance outcomes. The evidence presented in this study positions

FRP wall panel system as a credible and, in many respects, superior solution for achieving high-performance, energy-efficient housing in New Zealand’s residential sector. The results support a broader investigation of FRP wall panel system-based building envelopes, including year-round hygrothermal monitoring, comparative assessments against steel-framed systems, and evaluation of scalability across diverse architectural and climatic contexts.

10 Limitations and Future Studies

This research is subject to several limitations that should be acknowledged when interpreting the findings. The case study building is located within a single climatic region of New Zealand, and therefore the thermal performance analysis of the FRP wall panel system is limited to one representative climate zone. Broader applicability requires region specific monitoring across a wider range of New Zealand climate zones. In addition, the field investigation monitoring period covered only a single season over approximately three months, representing one quarter of the year. A full year cycle, including winter conditions, is essential to capture the complete seasonal variability of heat transfer, thermal comfort, and potential condensation risk. The analysis was also limited to heat flux and temperature measurements within a single room, with no direct assessment of other important indoor environmental parameters such as relative humidity and airflow due to instrumentation constraints. Future research should address these limitations by undertaking continuous year-round monitoring, evaluating the system's hygrothermal behaviour across different climates.

Similarly, the structural assessment is confined to one wind and seismic zone in accordance with the site-specific parameters adopted for the case study building. While these zones are representative of many residential developments in New Zealand, they do not capture the full range of design actions that may be encountered in more exposed or higher seismic-risk locations.

Moreover, the comparative analysis undertaken in this study evaluates the FRP wall panel system only against conventional timber-framed construction, which remains the dominant residential building typology in New Zealand. Steel-framed wall systems were not included in the thermal or condensation-risk modelling and therefore no direct performance comparison can currently be made between the FRP wall panel system and light steel framing in terms of thermal bridging, vapour behaviour, or condensation susceptibility. Future research should extend the comparative framework to include steel-framed assemblies and multiple climate zones to provide a more comprehensive and nationally representative evaluation of the FRP wall panel system across a broader range of environmental and regulatory conditions.

Further experimental testing is recommended to continue optimising the FRP wall panel system and to support the development of a more comprehensive and robust alternative residential building solution for application in New Zealand. Such work could include expanded thermal and hygrothermal monitoring across multiple climatic zones, extended long-term airtightness and durability assessments, and additional structural testing under a wider range of load combinations and environmental exposure conditions. Comparative testing against both timber- and steel-framed wall construction approach would enable a more complete evaluation of thermal bridging behaviour, vapour control performance, and condensation risk. Through this iterative programme of testing, modelling, and in-situ validation, the FRP wall panel system can be further refined and standardised, strengthening its potential to provide a resilient, high-performance, and code-compliant housing solution for diverse New Zealand contexts.

11 References

[1] BRANZ. Research Now Physical Characteristics of New Buildings #1; BRANZ: Porirua, New Zealand, 2020;

[2] Ryan, V., Penny, G., Cuming, J., & Riley, M. (2021). *Thermal bridging in external walls: Stage two* (BRANZ External Research Report ER64, Project LR12322). Beacon Pathway Inc. https://www.branz.co.nz/pubs/research-reports/er64/

[3] Standards New Zealand. (2011). *NZS 3604:2011 Timber-framed buildings*. Standards New Zealand.

[4] Ministry of Business, Innovation & Employment. (2021, April 6). Building Code update 2021: Consultation document – Issuing and amending acceptable solutions and verification methods. https://www.mbie.govt.nz

[5] Hindley, D. (2023). BRANZ house insulation guide (6th ed.). BRANZ Ltd.

[6] Ministry of Business, Innovation and Employment. (2022). *Building Code compliance: H1 Energy efficiency, Acceptable Solution H1/AS1 (5th edition, Amendment 1)*. Wellington:MBIE.https://www.building.govt.nz/assets/Uploads/building-code-compliance/h1-energy-efficiency/asvm/h1-energy-efficiency-as1-5th-edition-amendment-1.pdf

[7] Ministry of Business, Innovation and Employment. (2022). Building Code compliance: H1 Energy efficiency, Verification Method H1/VM1 (5th edition, Amendment 1). Wellington:MBIE.https://www.building.govt.nz/assets/Uploads/building-code-compliance/h1-energy-efficiency/asvm/h1-energy-efficiency-vm1-5th-edition-amendment-1.pdf

[8] New Zealand Government. (1992). *Building Regulations 1992, SR 1992/150*. Retrieved from https://www.legislation.govt.nz/regulation/public/1992/0150/latest/whole.html

[9] Isaacs, N., 2007. Thermal insulation. NZ Build Magazine, 102, 110–111.

[10] Thorsnes, P. (2013). The value of basic building code insulation. Energy Economics, 37(1), 68–81. https://doi.org/10.1016/j.eneco.2013.01.014

[11] Z. Jalali, A.Y. Shamseldin, A. Ghaffarianhoseini, Impact assessment of climate change on energy performance and thermal load of residential buildings in New Zealand, Build Env. 243 (2023), https://doi.org/10.1016/j.buildenv.2023.110627.

[12] Y. Kharbouch, M. Ameur, Prediction of the impact of climate change on the thermal performance of walls and roof in Morocco, Int. Rev. Appl. Sci. Eng. 13 (2) (2022) 174–184, https://doi.org/10.1556/1848.2021.00330.

[13] Standards New Zealand. (2009). *NZS 4218:2009 Thermal insulation – Housing and small buildings*. Standards New Zealand.

[14] Ministry of Business, Innovation and Employment. (2021, April 6). Consultation document: Building Code update 2021 (Issuing and amending acceptable solutions and verification methods). https://www.mbie.govt.nz

[15] Ministry of Business, Innovation and Employment. (2021). *Outcome of consultation: Building Code update 2021*. Wellington, New Zealand: MBIE. Retrieved from https://www.building.govt.nz

[16] BRANZ. (2024). *Industry insights 2024*.

[17] New Zealand legislation, "Building Act 2004 No 72 (as at 26 November 2024), Public Act 4 principles to be applied in performing functions or duties, or exercising powers, under this Act – New Zealand Legislation".

[18] BRANZ. (2022). *Industry insights 2022*

[19] BRANZ. (2021). *Doing better in residential dwelling: Going beyond code (ER27)*. BRANZ. https://www.branz.co.nz/pubs/research-reports/er27

[20] Ryan, V., Penny, G., Cuming, J., Mayes, I., & Baker, G. (2020). *Measuring the extent of thermal bridging in external timber-framed walls in New Zealand* (BRANZ External Research Report ER53, Report Wall/3). Beacon Pathway Inc. https://www.branz.co.nz/pubs/research-reports/er53/

[21] Kohler, A. (2012, January 27). *Unhealthy living*. *Architecture Now*. https://architecturenow.co.nz/articles/unhealthy-living/

[22] OECD (2017), *OECD Environmental Performance Reviews: New Zealand 2017*, OECD Publishing, Paris, pp.43, http://dx.doi.org/10.1787/9789264268203-en

[23] United Nations. (2021). *The state of the world's housing report*. United Nations Human Settlements Programme (UN-Habitat), pp.12.

[24] P. Howden-Chapman, H. Viggers, R. Chapman, K. O'Sullivan, L. Telfar Barnard, and B. Lloyd, "Tackling cold housing and fuel poverty in New Zealand: A review of policies, research, and health impacts," *Energy Policy*, vol. 49, 134–142, Oct. 2012. http://doi:10.1016/j.enpol.2011.09.044

[25] R. Ade and M. Rehm, "Home is where the health is: New Zealand responses to a 'healthy' housing crisis," *Pacific Rim Property Research Journal*, vol. 26, no. 1, 69–93, 2020. http://doi:10.1080/14445921.2020.1808278

[26] Hogan, M. (2021, June 30). *New Zealand housing often damp, cold and built to code* [Opinion]. RNZ. https://www.rnz.co.nz/news/national/445856/marcus-hogan-new-zealand-housing-often-damp-cold-and-built-to-code

[27] Trethowen, H. A. (1986). R-values that are made-to-measure. *ASHRAE Transactions*, 91(2).

[28] Thorsnes, P., & Bishop, T. (2013). *The value of basic building code insulation*. Energy Economics. https://doi.org/10.1016/j.eneco.2013.02.001

[29] O.A. Abdou, K. Murali, and A. Morsi (1996). "*Thermal performance evaluation of a prefabricated fiber-reinforced plastic building envelope system*". https://doi.org/10.1016/0378-7788(95)00967-1

[30] N. Marston, "*Study report SR172 fibre reinforced polymer composites*," 2007.

[31] P. Cherian, S. Palaniappan, D. Menon, M.P. Anumolu, *Comparative study of embodied energy of affordable houses made using GFRG and conventional building technologies in India*, Energy Build. 223 (2020), https://doi.org/10.1016/j.enbuild.2020.110138

[32] R. Reider, I.A. Meir, *Comparing the energy implications of FRP and concrete residential construction in a hot arid climate*, Energy Build. 186 (2019) 98–107, https://doi.org/10.1016/j.enbuild.2019.01.003.

[33] G. Tumminia, F. Guarino, S. Longo, M. Ferraro, M. Cellura, V. Antonucci, Life Cycle Energy Performances and Environmental Impacts of a Prefabricated Building Module, Elsevier Ltd, 2018, https://doi.org/10.1016/j.rser.2018.04.059.

[34] Velayudham, P., Roy, K., Fang, Z., Feng, C., Ghaffarianhoseini, A., & Lim, J. B. P. (2025). *Investigating the thermal performance of fibre-reinforced polymer wall panel system in Waikato, New Zealand*. Building and Environment, 282**,** 113298. https://doi.org/10.1016/j.buildenv.2025.113298

[35] Khabaz, A. (2017). *Optimum thermal performance of green wall systems and design requirements against heat transfer of conventional external walls of low-rise buildings*. Energy and Buildings, 152, 248–256. https://doi.org/10.1016/j.jobe.2023.107654y

[36] N. Aste, A. Angelotti, and M. Buzzetti, "The influence of the external walls thermal inertia on the energy performance of well insulated buildings," *Energy Build*, vol. 41, no. 11, pp. 1181–1187, Nov. 2009, https://doi: 10.1016/j.enbuild.2009.06.005

[37] B. Yesilata, H. Bulut, and P. Turgut, "Experimental study on thermal behavior of a building structure using rubberized exterior-walls," *Energy Build*, vol. 43, no. 2–3, pp. 393–399, Feb. 2011, https://doi: 10.1016/j.enbuild.2010.09.031

[38] S. D. Astarini and C. Utomo, "Performance-Based Building Design: A Review," in *Lecture Notes in Civil Engineering*, Springer Science and Business Media Deutschland GmbH, 2024, pp. 359–368. https://doi: 10.1007/978-981-99-4049-3_29

[39] Cox-Smith, I. (2009). *Thermal breaks and bridges*. Build, *16* (February/March), 16–17.

[40] Pringle, T. (2018). *A bridge too far: Comfortable indoor environments*. Build, *169*, 47–50.

[41] BRANZ. (2024). *Thermal bridges in external wall framing* (BRANZ Bulletin No. 690). BRANZ.

[42] Ministry of Business, Innovation and Employment. (2020). *Acceptable Solutions and Verification Methods for New Zealand Building Code Clause E2 External Moisture* (3rd ed., Amendment 10). https://www.building.govt.nz

[43] Ministry of Business, Innovation and Employment. (2020). *Acceptable Solutions and Verification Methods for New Zealand Building Code Clause E3 Internal Moisture* (2nd ed., Amendment 7). https://www.building.govt.nz

[44] ASTM International. (2019). *ASTM C177-19: Standard test method for steady-state heat flux measurements and thermal transmission properties by means of the guarded-hot-plate apparatus*. ASTM International. https://doi.org/10.1520/C0177-19

[45] Ministry of Business, Innovation and Employment. (2023). *Building Code compliance document: Verification method B1/VM1 – Structure*. Wellington, New Zealand. https://www.building.govt.nz/building-code-compliance/b-stability/b1-structure

[46] Standards New Zealand. (2006). *NZS 4214:2006—Methods of determining the total thermal resistance of parts of buildings*. Standards New Zealand.

[47] Standards Australia & Standards New Zealand. (2002). *AS/NZS 4859.1:2002 – Materials for the thermal insulation of buildings – General criteria and technical provisions*. Standards Australia/Standards New Zealand.

[48] Kingspan Insulation Pty Ltd. (2020). *Kingspan Kooltherm® K10 G2 soffit board: Product data sheet* (Issue 8, Sept 2020).

[49] Ministry of Business, Innovation and Employment. (n.d.). *Acceptable Solution B1/AS1 and NZS 3604:2011*. Building Performance. https://www.building.govt.nz/building-code-compliance/b-stability/b1-structure/building-structure-documents-changes-in-2011/acceptable-solution-b1as1-and-nzs-36042011

[50] Pratchett, M. (2022, September). *Using P21 tested bracing units outside the scope of NZS 3604*. Engineering New Zealand.

[51] Shelton, R. (2010). *P21: A wall bracing test and evaluation procedure* (BRANZ Technical Paper P21). BRANZ Ltd.

[52] Thurston, S. J. (2010). *BRANZ test and evaluation method EM3-V3 for bracing rating of walls to NZS 3604* (BRANZ Study Report SR 220). BRANZ Ltd, Judgeford, New Zealand.

[53] King, A. B., & Lim, K. Y. S. (1991, December). Supplement to P21: An evaluation method of P21 test results for use with NZS 3604:1990 (BRANZ Technical Recommendation No. 10). Building Research Association of New Zealand (BRANZ), Judgeford, New Zealand.

[54] Standards New Zealand. (2004). *NZS 1170.5:2004 Structural design actions—Part 5: Earthquake actions – New Zealand*. Standards New Zealand.

[55] Shelton, R. (2013). *BRANZ engineering basis of NZS 3604*. BRANZ Ltd.

[56] Liu, A. (2015). Design guidance of specifically designed bracing systems in light timber-framed residential buildings (BRANZ Study Report SR337). BRANZ Ltd.

[57] GIB® (2017). GIB EzyBrace® for light steel frame systems (March 2017 ed.). Winstone Wallboards Ltd.

[58] Ministry of Business, Innovation and Employment. (2021). *H1/AS1: Energy efficiency — Acceptable solution (Fourth edition, Amendment 3)*. MBIE.

[59] Ministry of Business, Innovation and Employment. (2021). *H1/VM1: Energy efficiency — Verification method (Fourth edition, Amendment 3)*. MBIE.

[60] Standards Australia & Standards New Zealand. (2002). AS/NZS 1170.0:2002, Structural design actions – Part 0: General principles. Sydney, Australia: Standards Australia.

[61] SkyCiv Engineering. (2023, November 25). *Tributary area and tributary width explained – with examples*. https://skyciv.com/docs/tutorials/load-tutorials/tributary-area-explained/

[62] Standards Australia & Standards New Zealand. (2010a). *AS/NZS 4063.1:2010 Timber – Stress-graded – In-grade testing – Part 1: General requirements.* Standards Australia/Standards New Zealand.

[63] Standards Australia & Standards New Zealand. (2010b). *AS/NZS 4063.2:2010 Timber – Stress-graded – In-grade testing – Part 2: Determination of MOE.* Standards Australia/Standards New Zealand.

[64] Roylance, D. (2000). *Beam displacements*. Massachusetts Institute of Technology, Cambridge, MA.

[65] SkyCiv.(2024, May 3). *Beam deflection: Definition, formula, and examples*. https://skyciv.com/docs/tutorials/beam-tutorials/what-is-deflection/

[66] Standards Australia & Standards New Zealand. (2021). *AS/NZS 1170.2:2021 Structural design actions — Part 2: Wind actions*. Sydney, NSW, Australia: Standards Australia.

[67] Shelton, R. (2009). Wind pressure 101. Build, (114), 32–33.

[68] Burn, G. (2025). Structurally fixing cavity battens for horizontal timber weatherboards. Build, (205), 31–32.

[69] Standards Australia. (2001). AS 1649:2001 Timber — Solid and engineered — Quartersawn for external use. Sydney, NSW, Australia: Standards Australia.

[70] BRANZ. (2021). PALLISIDE® cellular uPVC weatherboard cavity cladding system (Appraisal No. 491). Building Research Association of New Zealand.

[71] Overton, G. (2016). Building materials: Vapour flow and condensation risk in New Zealand wall assemblies (BRANZ Study Report SR344). BRANZ.

[72] Ministry of Business, Innovation and Employment. (2025, July 3). *Making buildings more affordable by changing Building Code insulation requirements*. https://www.building.govt.nz/about-building-performance/all-news-and-updates/making-buildings-more-affordable-by-changing-building-code-insulation-requirements

[73] Ade, R., & Rehm, M. (2020). Summertime comparative evaluation of indoor temperature and comfort in Auckland, New Zealand: A survey of green certified, code and older homes. Building Research & Information. Advance online publication. https://doi.org/10.1080/09613218.2020.1712185

[74] Figure 1. Heat loss distribution through building envelopes. Adapted from *Diffuse transmission dominant smart and advanced windows for less energy-hungry building* by A. Ghosh, 2023, *Journal of Building Engineering*, *64*, 105604, based on IEA (2019) Global Status Report for Buildings and Construction. https://doi.org/10.1016/j.jobe.2022.105604

[75] Ministry of Business, Innovation and Employment. (2025). H1 Energy efficiency: Acceptable Solution H1/AS1 (Sixth edition). https://www.building.govt.nz

[76] N. Soares, C. Martins, M. Gonçalves, P. Santos, L. S. da Silva, and J. J. Costa, “Laboratory and in-situ non-destructive methods to evaluate the thermal transmittance and behavior of walls, windows, and construction elements with innovative materials: A review”, *Renewable and Sustainable Energy Reviews, 111*, 259–286, Jan. 01, 2019. https://doi:10.1016/j.enbuild.2018.10.021

[77] D. Bienvenido-Huertas, J. Moyano, D. Marín, and R. Fresco-Contreras, “Review of in situ methods for assessing the thermal transmittance of walls,” *Renewable and Sustainable Energy Reviews, 102*, 356–371, Mar. 01, 2019. https://doi:10.1016/j.rser.2018.12.016

[78] A. Taşer, B. K. Koyunbaba, and T. Kazanasmaz, “Thermal, daylight, and energy potential of building-integrated photovoltaic (BIPV) systems: A comprehensive review of effects and developments,” *Renewable and Sustainable Energy Reviews, 172*, 113055, Feb. 01, 2023. https://doi:10.1016/j.solener.2022.12.039

[79] D. Sadhukhan et al., “Estimating surface temperature from thermal imagery of buildings for accurate thermal transmittance (U-value): A machine learning perspective,” *Journal of Building Engineering*, vol. 32, Nov. 2020. https://doi:10.1016/j.jobe.2020.101637

[80] D. Bienvenido-Huertas, J. Moyano, D. Marín, and R. Fresco-Contreras, “Review of in situ methods for assessing the thermal transmittance of walls,” Mar. 01, 2019. https://doi:10.1016/j.rser.2018.12.016

[81] J. Byun, J. Baek, J. Shim, S. Park, and D. Song, “Proposal of a correction factor for predicting the thermal transmittance of building envelopes in existing buildings accounting for aging and environmental conditions,” Build Environ, vol. 243, Sep. 2023, http://doi:10.1016/j.buildenv.2023.110658.

[82] L. Evangelisti, C. Guattari, P. Gori, and R. De Lieto Vollaro, “In situ thermal transmittance measurements for investigating differences between wall models and actual building performance,” Sustainability (Switzerland), vol. 7, no. 8, pp. 10388–10398, 2015, http://doi:10.3390/su70810388.

[83] P. Santos, M. Gonçalves, C. Martins, N. Soares, and J. J. Costa, “Thermal transmittance of lightweight steel framed walls: Experimental versus numerical and analytical approaches,” Journal of Building Engineering, vol. 25, Sep. 2019, http://doi:10.1016/j.jobe.2019.100776.

[84] D. E. Jung, D. H. Shin, J. Seo, K. H. Lee, and J. Kim, "In-situ virtual heat flow meter model for monitoring heat flux of existing building envelope," Build Environ, vol. 253, Apr. 2024, http://doi:10.1016/j.buildenv.2024.111320.

[85] International Organization for Standardization. (2014). ISO 9869-1:2014: Thermal insulation—Building elements—In-situ measurement of thermal resistance and thermal transmittance—Part 1: Heat flow meter method. https://www.iso.org/standard/59697.html